UNIVERSITY OF CALIFORNIA,
IRVINE

The Roles of Oxidative Stress, Mitochondria, and Lipid Droplets in Glutathione Deficiency and Benzo(a)pyrene-induced Germ Cell Death and Reduced Oocyte Developmental Competence

DISSERTATION

submitted in partial satisfaction of the requirements
for the degree of

DOCTOR OF PHILOSOPHY

in Environmental Health Sciences

by

Kelli F. Malott

Dissertation Committee:
Professor Ulrike Luderer, MD PhD MPH (Chair)
Adjunct Professor Michael T. Kleinman, PhD
Professor Charles Limoli, PhD
Professor Grant R. MacGregor, PhD

2022

DEDICATION

This work is dedicated to my parents, John and Terri Malott.

Your love and dedication inspire me to be the greatest version of myself.

Thank you for believing in me.

"What you do makes a difference,
and you have to decide what kind of difference you want to make."
Jane Goodall Ph.D.

"History shows us clearly that science does not provide certainty. It does not provide proof. It only provides the consensus of experts, based on the organized accumulation and scrutiny of evidence".
Naomi Oreskes Ph.D. and Erik M. Conway Ph.D., *Merchants of Doubt,* 2010

TABLE OF CONTENTS

LIST OF FIGURES

LIST OF TABLES

ACKNOWLEDGEMENTS

The cliché of a scientist sitting at her or his lab bench and computer alone is not a myth, but merely a 2-dimensional snapshot of a frequent circumstance. What is hidden from that snapshot is the manpower behind the hours of brainstorming and guidance, editing and advice on manuscripts, assistance on planning and executing experiments, the list goes on. It is not lost on me that so much work in this dissertation would not be possible without the guidance and assistance of many individuals. First and foremost, I would like to thank my advisor and mentor, Dr. Ulrike Luderer. It is hard to believe that my journey began with an email to you in 2015 expressing interest in the Environmental Health Sciences graduate program and excitement over your work. Thank you for your investment in my growth and education. I have been truly honored to have your guidance these past six years – I am a better scientist for it.

I would also like to thank my committee members, Dr. Michael Kleinman, Dr. Charles Limoli, and Dr. Grant MacGregor, your guiding questions, insightful comments, and encouragement were invaluable in the process of this project. To Dr. Kleinman, I am so grateful to have rotated in your lab – it was a crucial part of my toxicology training. Thank you for your support of my education and training at and away from the bench. To Dr. Charles Limoli, thank you for challenging me and guiding me with your questions, you have been a wonderful mentor through this process. Dr. Grant MacGregor, being your TA was transformative for how I approached communicating and teaching science, thank you being a wonderful instructor and committee member.

This project would not have been possible without the Optical Biology Core at UCI and training from Dr. Adeela Syed. Your support, technical advice, and friendship over the years have been invaluable to me. Thank you to Dr. Felix Grun whose technical expertise was invaluable in the beginning stages of my estradiol extraction project, and for allowing me the bench space in the Mass Spectrometry Facility in the later stages of that project.

I would not have been able accomplish as many aspects of this project without the assistance of my lab mates and my undergraduate research assistants. Dr. Jinhwan Lim and Laura Ortiz, thank you both for your mentorship, assistance, and friendship – the mistakes were much easier to stomach with you around to laugh with about them. To my undergraduate research assistants, Melody Lee, Jonathon Nguyen, Hong An Truong, and Edward Swanson, thank you for your support and assistance over the years, all of this work would not have been possible without each of you. Training and watching all of you grow as scientists, professionals, and individuals was truly a highlight of my training, thank you for your time and trust. I hope you learned at least as much from me as I learned from all of you.

Finally, I would like to thank my best friend and life partner, Vincent Gutierrez. I have cherished our hours-long conversations about our work, that, several times, have improved the way I interpreted the findings of this project. Your love and support over the years have been a guiding light during the darkest hours and have made the moments of celebration even more joyful.

Thank you to the greater UCI community for their continuous support.

I would also like to acknowledge the following for use of materials in this work. The text of Chapter 3 is a reprint of the material as it appears in *Particle and Fibre Toxicology.* The

co-author listed in this publication directed and supervised research which forms the basis for the thesis/dissertation. For Chapter 4, the author received prior reprint permissions through Oxford University Press.

VITA

Kelli F. Malott

Education

2022 **Ph.D. in Environmental Health Sciences**

University of California, Irvine, School of Medicine, Center for Occupational and Environmental Health

2014 **B.S. in Cellular and Molecular Biology**

University of Michigan, Ann Arbor, College of Literature, Science, and Arts

Research Experience

09/2016-Present **Graduate Student Researcher (PhD)**
Dr. Ulrike Luderer laboratory, University of California, Irvine
Project: The Roles of Oxidative Stress, Mitochondria, and Lipid Droplets in Glutathione-deficient and Benzo(a)pyrene-induced Germ Cell Death and Reduced Oocyte Developmental Competence

06/2014- 05/2016 **Post-baccalaureate Intramural Research Fellow**
Dr. Mark Mattson Laboratory of Neuroscience, National Institute on Aging, National Institutes of Health
Project: Expression of Uricase is Sufficient to Modify Cellular Respiration, Enhance Longevity and Endurance

01/2012- 05/2014 **Undergraduate Research Assistant**
Dr. Ivan Maillard laboratory, Life Sciences Institute, University of Michigan, Ann Arbor
Project: Notch Signaling Regulates T Cell Accumulation and Function in the Central Nervous System during Experimental Autoimmune Encephalomyelitis

Honors and Awards

- H&H Lee Foundation Scholarship awardee (2021)
- University of California Tobacco-Related Disease Research Program Pre-Doctoral Fellow (2019-2022)
- UCI College of Health Sciences, Bright Future highlight (October 2019)
- School of Medicine PhD Student Fellowship Bonus Award (2019-2022)
- School of Medicine PhD Student Fellowship Application Incentive Award (2019)
- School of Medicine PhD Student Travel Support (2018, 2019)

- Union of Concern Scientists: Science for Public Good Fund (2017)
    - Awarded to Science Policy Group at University of California, Irvine
- Post-Baccalaureate Intramural Research Training Fellowship Award (2014-2016)

Publications

Malott, K.F., Luderer U., (2022) The Effects of Polycyclic Aromatic Hydrocarbons on Mitochondria. *Mitochondrial Intoxication.* (In press)

Malott, K.F., Reshel S., Ortiz L., Luderer U., (2022) Glutathione Deficiency Decreases Lipid Droplet Stores and Increases Reactive Oxygen Species in Mouse Oocytes. *Biol of Reprod.* (Online ahead of print)

Luderer, U., Lim J., Ortiz L., Nguyen J.D., Shin J.H., Allen B.D., Liao L.S, **Malott K.**, et al., (2022) Exposure to Environmentally Relevant Concentrations of Ambient Fine Particulate Matter (PM2.5) Depletes the Ovarian Follice Reserve and Causes Sex-Dependent Cardiovascular Changes in Apolipoprotein E Null Mice *Part and Fibre Toxicol.* 19(5)

Malott, K.F., Luderer, U. (2021) Toxicant Effects on Mammalian Oocyte Mitochondria. *Biol of Reprod.* 104(4), 784-793.

Cutler, R.G., Camandola, S., **Malott, K.F.**, Edelhauser, M.A., Mattson, M.P. (2015) The Role of Uric Acid in the Prevention of Age-Related Neurodegenerative Disorders. *Curr Top Med Chem.* 21, 2233-2238.

Sandy, A.R., Stoolman, J., **Malott, K.**, Prongtornpipat, P., Segal, B.M., Maillard, I. (2013). Notch Signaling Regulates T Cell Accumulation and Function in the Central Nervous System during Experimental Autoimmune Encephalomyelitis. *J. Immunol*. 191, 1606-1613.

ABSTRACT OF THE DISSERTATION

The Roles of Oxidative Stress, Mitochondria, and Lipid Droplets in Glutathione Deficiency and Benzo(a)pyrene-induced Germ Cell Death and Reduced Oocyte Developmental Competence

by

Kelli F. Malott

Doctor of Philosophy in Environmental Health Sciences

University of California, Irvine, 2022

Professor Ulrike Luderer, Chair

Polycyclic aromatic hydrocarbons (PAHs) are ovotoxicants. Benzo[a]pyrene (BaP) is a PAH that depletes the ovarian reserve when females are exposed directly or *in utero*. Oocyte quality is developmental competence acquired through folliculogenesis. Among the attributes of the oocyte that determine its competence include mitochondria, lipid droplets (LDs), and small antioxidant molecules such as glutathione (GSH). Whether the developing germ cells in the embryo are more sensitive to BaP exposure during proliferation or meiosis has been unexplored. Further, how gestational BaP exposure and persistent oxidative stress impact the developmental competence of the oocyte remains unclear.

C57BL/6J female mice were mated with males and orally dosed with 0 or 2 mg/kg/day of BaP from either embryonic day (E)6.5-11.5 (proliferative phase, BaP6.5 and Oil6.5) or E12.5-17.5 (meiotic phase, BaP12.5 and Oil 12.5). F1 pubertal ovaries were examined for follicle counts and persistent oxidative stress. BaP6.5 and BaP12.5 had statistically significant depletion in primordial, primary, and secondary follicles as well as increased lipid peroxidation compared with controls. Oocytes from F1 BaP6.5 and Oil6.5

females were examined and BaP6.5 oocytes were observed to have increased levels of superoxide while significantly decreased mitochondrial membrane potential and LD volume.

We exposed female mice to concentrated air particulates at 2.5 μm or less (PM2.5) in aerodynamic diameter using a Versatile Air Concentration Enrichment System (VACES) for 6 h/ day, 5 days/ week, for 12 weeks. With our collaborators, I developed and validated an extraction and HPLC-MS/MS method to measure ovarian 17β-estradiol concentrations. The concentration of 17β-estradiol did not differ among exposure groups. However, the 17β-estradiol content of ovaries from wild-type, unexposed mice were significantly higher than either exposure group of the transgenic mouse model (*Apoe* -/-) that were used in this study.

GSH deficiency reduction mature oocyte developmental competence was explored. Using a transgenic mouse model, deleting the modifier subunit of the rate-limiting enzyme in GSH synthesis, glutamate cysteine ligase (*Gclm*), we demonstrated that *Gclm -/-* oocytes have increased levels of ROS, superoxide and decreased mitochondrial membrane potential. Additionally, *Gclm -/-* oocytes had decreased LD content compared with *Gclm +/+* oocytes. The data in this work demonstrate that the developing ovary is sensitive to BaP exposure across the entirety of its development resulting in F1 ovarian follicular depletion, and persistent F1 ovarian oxidative stress which reduces oocyte developmental competence through disrupted redox homeostasis and lipid dysregulation, and that BaP has similar effects on the ovary as PM2.5.

Chapter 1: Introduction

1.1 Dissertation Statement

Gestational BaP exposure is equally damaging across ovarian developmental windows, resulting in persistent ovarian and oocyte oxidative damage that is similar to ovarian and oocyte deficits observed in glutathione deficient mice. Both gestational BaP exposure and glutathione deficiency result in decreased fertility and shortened reproductive lifespan.

1.2 Significance

Premature ovarian failure, also known as premature menopause and primary ovarian insufficiency, is characterized by amenorrhea, hypoestrogenism, and elevated gonadotropin levels in women under the age of 40 and affects about 1% of women [1]. The length of the female reproductive lifespan is determined by the number oocytes that make up the ovarian reserve as primordial follicles. Menopause is characterized by the cessation of menses whereby the ovary is presumably no longer maturing follicles or ovulating oocytes; therefore, menopause is accompanied by the reduction in production of estrogens. Premature ovarian failure is an acceleration of this naturally occurring event, and is diagnosed when ovarian function ceases prior to 40 years of age, and early menopause is defined as occurring between 40-44 years of age [2].

Cigarette smoke and air pollution have both been reproducibly shown to be associated with negative reproductive outcomes, increased time-to-pregnancy, and increased risk of unsuccessful *in vitro* fertilization in exposed women [3–6]. One of the most abundant constituents of both cigarette and air pollution is polycyclic aromatic hydrocarbons (PAHs) – commonly associated with particulate matter less than 2.5 μm in

aerodynamic diameter (PM2.5) [7]. It is only recently that researchers have begun to examine the effects of gestational exposure on reproductive outcomes of the adult daughters; these studies are showing similar associations as the direct exposure [8–13].

A growing body of evidence demonstrates that the premature menopause can lead to long-term health consequences for women including cognitive impairment, cardiovascular, bone, and sexual health effects, as well as early mortality [2,14]. There is extensive evidence of increased risk of cardiovascular disease and loss of bone density in postmenopausal women. Moreover, there is an increasing body of evidence to show that premature ovarian failure, as well as early menopause exacerbates risk of cardiovascular disease, bone density loss and other sequelae significantly beyond that of average menopause. Women, 45-55 years, with early menopause had lower bone mass compared with age-matched women with normally occurring menopause [15]. Additionally postmenopausal women in their 40s had increased incidence of cardiovascular disease compared to age-matched premenopausal women. Women with premature ovarian insufficiency were at increased risk of cardiovascular disease and ischemia [2]. This was further supported by reports that young women with premature ovarian insufficiency had significantly impaired vascular endothelial function, and risk of heart failure was increased by 66% in women having gone through menopause earlier than 45 years [15].

A shift in societal norms has been progressing slowly over the past few decades. Couples and women are opting to delay pregnancy, likely in favor of the pursuit of higher education and secure career options for myriad of reasons. From 2007-2009, 34.2% of live births in the United States were to women aged 30-39 years, but that percentage increased

significantly by 2017-2019 when 43.6% of live births in the United States were to women of that age group [16]. Regardless of the reasons, the trend is clear. Premature ovarian failure is diagnosed in about 1% of women in the United States, and that prevalence has remained relatively unchanged from 1980 to the present.

Therefore, understanding and communicating how exposure to specific compounds in air pollution and cigarette smoke can induce germ cell death gestationally resulting in a reduced reproductive lifespan in exposed women is more important now than ever. It provides valuable information for expectations societally and at the individual level about fertility and potential health risks with aging. On the policy level, discerning this information provides more evidence for regulatory oversight and policy initiatives to ensure clean air, indoors and outdoors to ensure a healthier population.

1.3 Polycyclic Aromatic Hydrocarbons: Human Exposure

Polycyclic aromatic hydrocarbons (PAHs) are products of incomplete combustion of organic materials, most commonly found in air pollution from fossil fuel and biomass combustion, cigarette and cannabis smoke, as well as burnt and barbequed foods. Compounds of this class have molecular structures that range in size from 2 to 6 fused aromatic rings. Due to the nature of how PAHs are released into the environment, humans are generally exposed to mixtures of PAHs, often attached to other particles such as particulate matter less than 2.5 μm in aerodynamic diameter (PM2.5) or ultrafine particulates, as opposed to single compounds [7]. Humans are exposed to PAHs through inhalation and ingestion with dermal absorption as an additional route of exposure. Though exposure is variable and dependent on the individual, total daily human exposure for the

general population in United States is estimated to be 0.207 μg from air, 0.027 μg from water and 0.16-1.6 μg from food [7]. Zhang et al., modeled spatial and temporal variations in predicted daily air concentrations of PAHs in the continental United States and observed there to be significant regional and temporal variation in the predicted average monthly concentrations of PAHs. Unsurprisingly, metropolitan areas such as New York, Boston, and Los Angeles had higher concentrations above 0.4 $\mu g/m^3$ and PAH concentrations were lower in the spring and summer months, except for wildfire hotspots [17].

1.3.1 PAH Metabolism

PAHs are small compounds that range in lipid solubility. PAHs with only 2 or 3 aromatic rings are more soluble in aqueous solutions while PAHs with 5 or more rings are lipid soluble [18]. This allows the larger PAHs to traverse cellular membranes with ease. Following exposure, PAHs are absorbed through the lymphatic system, into blood circulation and distributed throughout the body. Evidence has shown that PAHs are metabolized in all tissues [7].

PAHs require metabolic activation to exert their negative effects, and in most cases, undergo oxidation to produce metabolites that interact with cellular macromolecules [19]. Oftentimes, PAH metabolites will bind to endogenous aryl hydrocarbon receptor (AhR), activating its translocation to the nucleus where it forms a complex with aryl hydrocarbon receptor nuclear translocator [20]. This complex localizes to the xenobiotic-response element to upregulate transcription of phase I oxidizing enzymes, including cytochrome P450s [20], as well as the antioxidant transcription factor NF-E2 p45-related Factor (Nrf2) [21].

During this upregulation, and as a consequence of it, PAHs are metabolized in the cell through three major pathways. The first, through cytochrome P450s (CYP450s) to eventually yield dihydrodiols after hydrolysis by epoxide hydrolases. The second is metabolism by CYP450s to produce a radical cation. The third is the formation of quinones through metabolism by dihydrodiol dehydrogenases [19]. Both the epoxides and quinones can lead to oxidative DNA damage, but only the quinone metabolites can undergo reduction and oxidation (redox) cycling [19]. The activation of NRF-2 by AhR-XRE induces the upregulation of phase II metabolizing enzymes to detoxify PAH reactive metabolites produced by phase I enzymes [21]. Phase II enzymes catalyze the conjugation of PAH reactive metabolites (e.g., glutathione conjugation) or metabolize the intermediates further (e.g., superoxide dismutase). Both pathways increase their water solubility for excretion.

1.4 Ovarian and Oocyte Biology

1.4.1 Primordial Germ Cells and Ovarian Folliculogenesis

Primordial germ cells (PGCs) are the embryonic precursors of oocytes, arising in the mouse proximal posterior epiblast at embryonic day 6.25 (E6.25), then rapidly proliferate while migrating to the gonadal ridge which they enter as gonocytes. After the ovary begins to differentiate, the gonocytes become oogonia and continue proliferation until beginning to enter meiosis at E13.5 [22–24]. By E14.5, the developing mouse ovary contains about 6,000 germ cells [25]. Now referred to as oocytes, they progress through meiosis arresting at the diplotene stage of the first meiotic prophase beginning at E17.5. At this stage, oocytes remain arrested in interconnected germ cell nests. Beginning shortly before birth, the germ cell nests begin to break down and form follicles; simultaneously oocyte apoptosis commences and

these processes continue through postnatal day 2 (PND2) [25]. Germ cell development in the fetal ovary produces a finite oocyte pool, the primary determinant of female fertility and reproductive lifespan.

The ovary is composed of functional units called follicles, that consist of an oocyte surrounded by granulosa and theca cells which are highly specialized for supporting a growing oocyte. Follicles can be classified by maturity, ranging from dormant, primordial follicles, and activated primary follicles through growing secondary and antral follicles to fully matured, preovulatory follicles. The follicle typically contains a single oocyte encompassed by a layer or multiple layers of somatic cells depending on the maturity. Primordial follicles contain a single oocyte surrounded by an incomplete layer of immature, fusiform granulosa cells while primary follicles are characterized by a single layer of mixed fusiform and mature round granulosa cells. Secondary follicles, now responsive to gonadotropin stimuli, are comprised of an oocyte surrounded by more than one layer of granulosa cells and layers of theca cells. The antral, or preovulatory follicle, is distinguished by the presence of a follicular fluid-filled antrum, a large oocyte seemingly suspended away from the rest of the follicle encased by differentiated cumulus granulosa cells, with mural granulosa cells lining the antrum and theca cells outside the basement membrane that surrounds the granulosa cells. A large fraction of follicles does not persist to this stage and is lost to a degeneration process called atresia, which occurs mainly during the antral stage [26]. It is thought that atresia is a process intended to ensure only the healthiest oocytes are ovulated for fertilization.

1.4.2 Oocyte Development and Developmental Competence

Starting from the induction of the germ cell population in the early embryonic stages, PGCs and eventually oocytes, are preparing themselves to sustain life – this is referred to as developmental competence. Developmental competence is a two-step process involving cytoplasmic maturation which occurs throughout folliculogenesis and then supports the second step, nuclear maturation, after ovulation.

Cytoplasmic maturation is characterized by the stockpiling of organelles, including endoplasmic reticula, mitochondria, and lipid droplets (LDs), as well as small molecules such as maternal RNAs, proteins, and antioxidants. PGCs have fewer than 10 mitochondria prior to migration, expanding to 100 mitochondria per cell when the cells enter the gonadal ridge, then doubling to 200 mitochondria in oogonia [27]. As the ovary and germ cells continue to develop, the mitochondrial population expands to roughly 6,000 per cell in the primordial oocyte and eventually expanding to 100,000 mitochondria per healthy, ovulated mouse oocyte. Generally, these mitochondria are quiescent, maintaining low level metabolic activity, minimizing oxidative stress, and fulfilling basic cellular functions. To produce ATP, PGCs preferentially oxidize pyruvate, as opposed to glucose [28]. Once the oocyte is packaged into follicles, the primordial follicle consumes pyruvate and glucose, however pyruvate remains the preferential substrate for the oocyte and it is largely dependent on the supportive granulosa cells throughout follicular development [29,30]. Once ovulated, the gap junctions between the oocyte and the cumulus cells break down, leaving the oocyte dependent on its own metabolic reserves to sustain and support preimplantation development [30–33]. Consequently, any deficiencies in mitochondria or their function more readily affect the oocyte after ovulation and are thought to be a predominant cause of female infertility and chromosomally abnormal conception [34].

A less well characterized, but arguably equally as important organelle to oocyte developmental competence is the lipid droplet (LD). LDs are highly dynamic organelles comprised of a monophospholipid layer encasing a triacylglycerol and sterol ester core [35]. Triacylglycerols and free fatty acids are present in the follicular fluid of several mammalian species, including mice and humans and can be taken up from the follicular fluid or broken down from endogenous cellular lipid to be stored in LDs [36,37]. Additionally, granulosa cells can import lipids to the oocyte throughout folliculogenesis [38]. LDs have been demonstrated to be sources of energy where triacylglycerols are broken down into fatty acids to undergo β-oxidation; they also supply secondary signaling molecules [38,39], phospholipids for cellular membrane maintenance [38,40], and provide lipoic acid, an important cofactor for mitochondrial dehydrogenases, that generate NADH to regulate cellular homeostasis [41]. Recent reports have shown that when ovulated, metaphase II (MII) oocytes that have been delipidated prior to *in vitro* maturation begin building their own LDs *de novo*, suggesting that LDs are of high importance to the oocyte [42]. Moreover, delipidation did not disrupt the developmental potential of oocytes. The importance of LDs was further supported, when delipidated oocytes had their LD formation inhibited through the inactivation of long-chain acyl-CoA synthetase, embryonic development was significantly disrupted and these embryos had significantly decreased LD content [42]. Further, inhibition of long-chain acyl-CoA synthetase resulted in decreased LD content over time in all oocytes. Together these data suggest that MII oocytes have a level of cellular lipolysis, can produce their own LDs *de novo*, and that LD content is important to preimplantation development [42].

Another important aspect of oocyte developmental competence is maintenance of cellular redox homeostasis by the antioxidant glutathione (GSH). GSH is produced through two ATP-dependent reactions, the rate-limiting reaction is catalyzed by glutamate cysteine ligase. This enzyme is comprised of two subunits, the catalytic subunit (Gclc) and the modifier subunit (Gclm). Knockouts of the *Gclc* subunit are embryonic lethal [43]; however, *Gclm -/-* mice live seemingly healthy lives are and capable of reproduction, despite possessing 10-20% of normal GSH levels [44]. The oocyte possesses among the highest GSH concentration of any cell type at 10 mM GSH per mature oocyte, which is important for sperm nuclear decondensation [45], pronucleus formation [46], and meiotic spindle formation in the MII oocyte [47]. When GSH synthesis is inhibited for 2 days preceding ovulation, GSH concentrations are reduced to 10% of normal levels in the mouse oocyte, demonstrating that GSH storage and production in the oocyte occurs during the final stages of folliculogenesis [45]. Others have shown the GSH is consumed as the fertilized embryo develops, that GSH levels are highest in the unfertilized MII oocyte, and that when GSH levels are depleted by the addition of tertiary-butyl hydroperoxide *in vitro*, MII oocytes' development to the blastocyst stage is significantly decreased [48]. These data were later corroborated by our group which demonstrated that *Gclm -/-* females, while producing the same number of litters as *Gclm +/+* yielded significantly fewer pups per litter [49]. This was found to be the result of increased preimplantation mortality as there were no differences in uterine resorption sites between the two genotypes, and following *in vitro* fertilization, significantly embryos from *Gclm -/-* oocytes progressed to the blastocyst stage [49]. Together the above data demonstrate that oocyte developmental competence is highly dependent on mitochondria, LDs, GSH, and cellular redox homeostasis.

1.4.3 Oxidative Stress, Premature Ovarian Failure, and Ovarian Aging

Ovarian aging is a natural process defined by the age-specific decline in the functional ovarian reserve leading to menopause. Premature ovarian failure, also known as premature menopause or premature ovarian insufficiency, is characterized by amenorrhea, hypoestrogenism, and elevated gonadotropin levels in women under the age of 40 [1]. Premature ovarian failure is a common cause of infertility in women and current estimates show that 1% of women under the age of 40 are affected [1]. While there is limited evidence to suggest that premature ovarian failure is becoming more prevalent, ovarian aging is of increasing concern as shifts in societal norms are delaying individuals' decisions to have children until later in life. Only a few causes have been definitively linked to premature ovarian failure including familial genetic causes, X chromosome abnormalities, autoimmune conditions, as well as chemotherapy, cigarette smoking and malnutrition [50–52].

Above, I discussed three important components of oocyte developmental competence that are acquired through folliculogenesis. These same components, mitochondria, lipids, and GSH all play a role in cellular and ovarian aging. It has been well-documented that imbalance in cellular redox homeostasis exacerbates cellular aging [53]. We have demonstrated that *Gclm -/-* females, deficient in GSH, undergo accelerated age-related ovarian reserve decline compared with *Gclm +/+* females [54,55]. *Gclm -/-* females show a significant decrease in total number of healthy follicles beginning at 3 months age, primarily observed as a decline in number of primordial follicles [54]. Further, the rate of decline in number of follicles was significantly more rapid than *Gclm +/+* [54] .

As a cell ages, increased reactive oxygen species (ROS) are produced and cells have a decreased ability to neutralize and metabolize these ROS. The marked increase in ROS with age is directly tied to the mitochondria. These organelles are the primary oxygen consumer in the cell and convert 0.2-2% of a cell's oxygen into ROS [56]. The majority of ROS in the oocyte are generated through metabolism by dysfunctional mitochondria [57]. Maternal age-associated oocyte mitochondrial morphological abnormalities observed in human oocytes include mitochondrial swelling, vacuolization, and cristae alterations [58]. In mouse oocytes, several morphological and ultrastructural changes have been observed in the oocytes derived from older females, including altered matrix density and ooplasmic fraction of vacuoles. [59]. Mitochondrial activity in the human [60] and mouse [61] oocyte has been observed to decrease with maternal age and is crucial to global redox regulation and energy production within the oocyte [62].

Other mechanisms through which mitochondria contribute to ovarian aging include mitochondrial DNA (mtDNA) mutations, impaired fission and fusion, altered mitochondrial membrane potential ($\Delta\Psi m$), altered metabolism, and defective electron transport chain [63]. Oocyte-specific knockout of the gene Mitofusin1, a part of the mitochondrial machinery that regulates mitochondrial fusion, results in accelerated ovarian aging [64]. Further, aged oocytes have been shown to have decreased Drp1-dependent mitochondrial fission [59], and oocyte-specific deletion of Drp1 leads to decreased oocyte quality [63]. In a transcriptomic analysis of gene expression comparing oocytes from 5-6 week old mice and 42-45 week old mice, surprisingly of 5% of 11,000 detected transcripts show significantly different expression levels [65]. Interestingly, electron transport chain-associated genes, were more highly expressed in old oocytes, while nuclear genome encoded genes associated with

"energy pathways" and mitochondrial function were more highly expressed in young oocytes [65]. Recent studies have observed age-related differences among key markers of mitochondrial function and redox homeostasis among germinal vesicle (GV), meiosis I (MI), and meiosis II (MII) oocytes. When comparing GV and MII oocytes from 8-week-old and 52-56-week-old mice, mtDNA copy number in GV oocytes were unchanged, but mtDNA copy number decreased with age in MII oocytes, as did ΔΨm; and *Gclc* expression was significantly reduced [66]. Similar age-associated differences in ΔΨm were observed in human oocytes [66]. Others have shown that mitochondrial superoxide was increased in GV oocytes when comparing 1-month and 12-month old oocytes, while no differences were observed in MII oocytes [67]. However, ΔΨm was decreased in MI oocytes from 12-month-old mice, but no age-related differences among MII oocytes at this age were observed. At 18 months of age MII oocytes had significantly decreased ΔΨm compared with MII oocytes from 1-month-old mice [67]. These age-related effects were rescued by antioxidant supplementation, demonstrating a major role for ROS and redox homeostasis in oocyte mitochondrial dysfunction with aging.

It is clear that lipid homeostasis becomes imbalanced through the aging process and that lipid peroxidation is an important indicator of aging [68]. One of the more well-established endpoints is the expression of the lipid peroxyradical, 4-hydroxynonenal (4-HNE), an electrophilic aldehyde generated as a secondary product of the peroxidation cycle. 4-HNE has been implicated in normal ovarian aging as well as ovarian aging accelerated by radiation exposure in adult mice [69,70]. PND21 *Gclm -/-* ovaries, have significantly increased production of 4-HNE in the granulosa and theca cells compared with *Gclm +/+* ovaries [54]. 4-HNE has also been shown to have significantly increased prevalence in GV

and MII oocytes derived from 14 month-old mice compared with 1 month-old oocytes [71]. The formation of 4-HNE can further propagate ROS-generation and mitochondrial dysfunction through the formation of stable and covalent Michael and Schiff base adducts to nucleophilic functional groups in proteins such as cysteine-rich side chains [72]. Mitochondrial proteins contain cysteine-rich side chains making them especially vulnerable to increase 4-HNE propagation. These covalent modifications can cause premature electron transfer to oxygen which, in turn, dissipates $\Delta\Psi m$ and further propagates redox dysregulation [57]. However, the role of lipids in ovarian aging goes beyond 4-HNE generation.

Follicular fluid composition has come under increasing scrutiny over the past couple decades. There have been several studies correlating follicular fluid lipid levels and ovarian aging [73–76]. Interestingly, all these studies reported differing results, though it is worth noting that several studies did not perform meta-analyses on lipidomics data, most of them report on clinical endpoints such as LDL, cholesterol, and HDL – which are correlated in the plasma with ovarian aging. The most interesting study was performed on a relatively small patient population of only 12 women over the age of 35 years and 17 women were 35 or younger. Lipidomics was performed on follicular fluid from each of these women and the authors reported distinct lipid populations in the follicular fluid based on age [76]. These results are corroborated by Knauff et al., (2008) which used follicular fluid from women with premature ovarian failure and compared with age-matched controls [75]. Together these data demonstrate that redox homeostasis, involving mitochondria, LDs, and GSH in the ovary and oocytes contribute to the reproductive aging process and that imbalances in this homeostasis cause oxidative stress and hasten age-associated reproductive decline.

1.5 PAHs induction of Ovarian and Oocyte Toxicity

1.5.1 Epidemiological Studies of Air Pollution and Female Fertility

Associating the environmental exposure to PAHs and their impact on female fertility is difficult due to the myriad of potential PAH sources, inexact dosage estimation, and confounding due to exposures to other reproductive toxicants such as plasticizers, pesticides, and heavy metals. Epidemiological studies have examined the impacts of occupational exposure, cigarette smoking, traffic-related air pollution, with many focusing on assisted reproductive technologies (ART) study populations. Consequently, these studies have several limitations and must be supplemented with animal studies to assess direct exposure and interrogate mechanisms.

Boulet and colleagues did a retrospective analysis of ambient air pollution exposure and *in vitro* fertilization (IVF) outcomes for 270, 898 patients in the United States between 2010 and 2012 [77]. PM2.5 concentration was estimated at the county level at three time periods during IVF: cycle start to oocyte retrieval, oocyte retrieval to embryo transfer, and embryo transfer plus 14 days. Associations of PM2.5 exposure with implantation rate, pregnancy, and live birth were assessed, and no association between PM2.5 concentration and reproductive outcomes was found [77]. However, this was a biased sample population across a relatively short time period.

In 2016, Mahalingaiah et al., published a prospective cohort study on 36, 294 female nurses enrolled in the Nurses' Health Study II cohort, from September 1989 to December 2003, assessing adult air pollution exposure and infertility risk in this population [3]. In this study, infertility was defined as attempted conception for greater than 12 months without

success, and air pollution exposure was estimated using residential addresses to assess proximity to major roadways, as well as PM10, PM2.5-10, and PM2.5 exposure, modeled using publicly available spatiotemporal models from filter-based monitors through the United States Environmental Protection Agency. In this study, of over 213,416 person-years, 2508 incidents of infertility were observed, and there was a small, but statistically significant increase in infertility associated with living closer to major roadways [3]. Others have reported a positive association between PM2.5 exposure and reduced fecundity in women [4], a decrease in clinical pregnancy rate associated with higher recorded PM2.5 levels [5], and a statistically significant decrease in fertility rates with increased traffic-related air pollution exposure in women in Barcelona [6].

Each of the epidemiological studies cited thus far assessed adult air pollution exposure and female fertility – not gestational exposure. Associating gestational PAH exposure and reproductive outcomes of daughters exposed *in utero* is considerably more difficult, as the determination of exposure often relies on reporting by either the daughter or the mother. Additionally, analyzing a direct correlation to PAHs poses the same difficulties as previously discussed. To this end, investigators rely on parameters such as PM2.5 concentration, traffic-related air pollution, and cigarette smoking – all of which are complex mixtures that contain PAHs but are not solely constituted of PAHs. To date there have been comparatively few studies that attempted to analyze this association. One study focused on gestational air pollution exposure and biomarkers of oxidative damage in the newborn. Oxidative DNA damage marker 8-Oxo-2'-deoxyguanosine and lipid peroxidation marker 15-F2t-isoprostane were measured in urine and blood of nonsmoking mothers and newborns and compared with gestational PM2.5 exposure [8]. PM2.5 concentrations were estimated

based on city of residence over two seasons; summer and winter. Concentration was higher across the two cities of interest in the winter and was consistently higher in the city of Karvina, Czech Republic compared to Ceske Budejovice, Czech Republic. Lipid peroxidation markers were higher in the newborns gestationally exposed in winter compared with summer across both cities while markers of DNA damage differed only in cohorts gestationally exposed during the winter, being significantly higher in newborns exposed to higher concentrations of PM2.5 [8]. In 2010, Ye et al., published on findings from the Norwegian Mother and Child Cohort Study based on 90,190 pregnancies recruited from 1999 to 2007 [9]. Of these pregnancies, 59,917 women with planned pregnancies were included in this analysis. Among these women, there was a slight association between time-to-pregnancy and *in utero* cigarette smoke exposure with a slightly higher proportion of exposed women taking longer than 12 months to conceive compared to those who reported no exposure. Given that the increase in percentage was small (12% exposed vs 11% unexposed) the authors did note that this difference could be attributed to other confounding factors [9].

In 1989, investigators from the National Institute of Environmental Health Sciences published an analysis on a small cohort of 230 women recruited from communities around Research Triangle Park, North Carolina from 1983-1985 [10]. They reported a strong negative association between fecundity and prenatal exposure to cigarette smoking as reported by the daughter. These results were supported by Jensen et al., which published reduced fecundity in nonsmoking women who reported cigarette exposure *in utero* in an analysis of 430 Danish couples [11]. This reduction in fecundity was further exacerbated in smoking women who were exposed to cigarette smoke *in utero*.

Weinberg et al., also observed in the 1989 publication no association with *in utero* cigarette smoke exposure and age at onset of menarche [10]. These findings are discordant with another report in 2015. Zhang and colleagues performed a retrospective analysis of 751 students 8 to 20 years old in Shanghai, China [12]. In this analysis the investigators reported that daughters with maternal tobacco smoke exposure experienced a relatively earlier onset of menarche and had shorter cycle lengths [12]. A more recent assessment comparing age at onset of menarche and maternal smoking exposure in two different cohorts suggests that there is likely an interaction between maternal smoke exposure and rapid weight gain that contribute to acceleration at age of menarche [13]. In an *in vitro* study, human fetal ovaries from terminated pregnancies in the 1st and 2nd trimesters were cultured with dimethylbenzanthracene metabolite 9,10-dimenthylbenz(a)anthrene-3,4-diyhydrodiol (DMBA-DHD) for 7 days. Exposure significantly decreased the number of proliferating germ cells in the fetal ovary, but slightly increased the number of germ cells [78]. In a follow-up by the same group, ovaries collected from normal progressing pregnancies that were voluntarily terminated in the 2nd trimester compared ovaries that were exposed to cigarette smoke to those that were not. This study reported increased density of primordial follicles in the smoke exposed ovaries and an increase in VASA-positive germ cells [79]. Together these human data demonstrate that gestational cigarette smoke or air pollution exposure, and likely PAHs specifically, dysregulates primordial follicle formation in the human female embryo, accelerates onset of menarche, and reduces female fertility.

1.5.2 Animal Studies on PAH Ovarian Toxicity and Antioxidant Involvement

The use of animal models has allowed for toxicological research to provide a more detailed and mechanistic assessment of how exposure to PAHs and sources of PAHs can impact the mammalian ovary. C57BL/6J mice exposed to the equivalent of 2 cigarettes/day, 5 days a week for 6 weeks through nose-only exposure had decreased ovarian volume and decreased total follicle counts, driven by a significantly decreased number of primordial and transitional (primordial to primary) follicles [80]. PND4 ovaries exposed *in vitro* to cigarette smoke extract have decreased Bcl-2 expression, an anti-apoptosis protein, and increased ratio of Bax to Bcl-2 after 24 h [80]. Gannon and colleagues later corroborated these observations. They exposed C57BL/6J mice to cigarette smoke 2 times a day for 50 minutes per exposure 5 days a week for 8 weeks using a whole body smoke exposure system [81]. Ovaries were assessed for autophagy and mitochondrial dysfunction, and results showed that cigarette smoke decreased Bcl-2 protein, and increased LC3, a marker for autophagy, in ovarian homogenates [81]. Others have shown similar results following a similar cigarette smoke exposure paradigm in which exposed mice had decreased ovarian weights and follicle counts compared with controls, driven by significant decreases in primordial and primary follicle numbers [82]. Microarrays of exposed and control ovaries revealed 154 differentially expressed genes, several of which were associated with lipid metabolism [82].

Several studies have demonstrated PAHs to be ovotoxicants using direct exposure. Mice exposed to a single dose of 80 mg/kg of benzo(a)pyrene (BaP), 3-methylcolanthrene, or 7,12-dimethyl-benz(a)anthrene (DMBA) had significantly fewer primordial follicles compared with controls when sacrificed 40 h [83] or 6 days after exposure [84]. These mice were exposed using i.p. injection which is not truly translational to human exposure. More recently, adults rats were exposed to 0, 50, 75, or 100 μg/m^3 of BaP 4 h/day for 14 days using

nose-only inhalation [85]. Females exposed to the highest concentration of BaP had significantly decreased ovulation rates and pups compared to controls and females expose to 50 or 75 μg/m^3. BaP metabolites, such as BaP-7,8,-diol and BaP-3,6-dione, were significantly increased in the ovaries of exposed mice [85]. Though it was not statistically analyzed, it is interesting to note that of the three organs that were assayed for BaP metabolites (lung, liver, and ovary), the ovary was observed to have the highest reported average concentrations of BaP metabolites (BaP-7,8-diol: 12±1.6, ovary, 1.3 ±0.08, lung, 3.4 ±0.2, liver and BaP-3,6-dione: 9.3±0.75, ovary, 1.2±0.01, lung, 3±0.32, liver) [85]. The ovaries of neonatal mice exposed to 0, 1.5, or 3 mg/kg/day of BaP for 7 days by oral pipette had significantly altered transcriptome [86]. Specifically, genes involved in homologous recombination, AhR signaling, and nitric oxide and ROS production were observed to be significantly differentially expressed in exposed ovaries compared with controls. BaP also induced primordial follicle activation in exposed ovaries and increased apoptosis in primary and secondary follicles [86]. Together these data demonstrate the sensitivity of the adult and prepubertal ovary to PAH exposure. Specifically, they show that the exposed adult ovary is capable of metabolizing PAHs, which results in dysregulation of folliculogenesis and increased apoptosis.

Further, the embryonic ovary has been shown to be especially sensitive to PAHs. E13.5 ovaries exposed to the DMBA-DHD for 24-72 h *in vitro* had dose-dependently decreased total germ cells. However, when ovaries were exposed to DMBA-DHD in the presence of aryl hydrocarbon receptor (AhR) antagonist, ANF, there was no difference in in germ cell number compared with unexposed controls, indicating that the deleterious effect of DMBA-DHD was mediated through AhR activation [87]. Additionally, DMBA-DHD

exposure increased BAX expression in E13.5 ovaries exposed *in vitro* and F1 mice exposed to gestational DMBA of *Bax-/-* mice did not have decreased primordial follicles counts whereas *Bax +/+* mice did, implicating the involvement of the mitochondrial apoptosis pathway in PAH-mediated germ cell death [87].

Our group has confirmed and expanded on these results using BaP [88,89]. E13.5 ovaries exposed *in vitro* to 0, 1, 5, 10, 100, 500, or 1000 ng/mL of BaP for 6, 24, 48, or 72 h showed a dose-dependent increased in cleaved-caspase-3 and -9 expression in germ cells after 24 h of exposure [88]. Caspase-9 is a part of the caspase cascade associated with the mitochondrial apoptosis pathway; this pathway is induced by the activation of BAX proteins to form channels in the outer mitochondrial membrane. The formation of BAX pores allows cytochrome c to be released into the cytosol leading to the cleavage of caspase 9 [90]. After 6 h of exposure, BAX expression was significantly increased in germ cells of E13.5 ovaries exposed to 1000 ng/mL of BaP [88]. Further exploration of ovarian sensitivity to BaP showed that the antioxidant glutathione (GSH) is imperative to ovarian detoxification of BaP. *Gclm -/-* E13.5 ovaries had increased germ cell apoptosis after 24 h exposure to BaP *in vitro* compared to *Gclm +/-* and *Gclm +/+* ovaries exposed to the same concentration [89]. Together these data show ovotoxicity of PAHs against the embryonic ovary and demonstrate a role for oxidative stress and mitochondrial apoptosis pathway in the F1 ovary.

One of the earliest reports to demonstrate a causal relationship between gestational PAHs exposure and decreased fertility in F1 animals exposed CD-1 mice to 0, 10, 40, or 160 mg/kg/day BaP from gestational day 7-16 [91]. Gestational exposure to 40 or 160 mg/kg/day of BaP resulted in total sterility of 97% of F1 animals that were exposed. F1

females exposed to 10 mg/kg/day BaP were still fertile; however, their litters were significantly smaller than the litter sizes of F1 controls and had significantly fewer pups over their reproductive lifespan [91]. Our group's work has expanded on these observations. Using the GSH-deficient, transgenic *Gclm* mouse model we characterized the ovotoxicity of BaP and the role of GSH. *Gclm +/-* females were time mated and exposed to 0, 2, or 10 mg/kg/day of BaP from gestational day 7-16 and the estrous cycles, fertility, and ovarian follicles were assessed in F1 females [92]. In the fertility study, BaP had a dose-dependent effect in the cumulative number of litters and of pups regardless of genotype. Within treatment group, *Gclm -/-* had reduced cumulative litters and offspring compared to *Gclm +/+* in the 2 mg/kg/day treatment group showing an interaction between GSH deficiency and BaP exposure. F1 females exposed to 2 mg/kg/day had predominantly leukocytic estrous cycles compared with 0 mg/kg/day and the number of leukocytic to cornified transitions over a 14-day observation period decreased with BaP dose. Further, ovarian histomorphometry showed a dose-dependent decrease in PND35 healthy follicle counts was observed in *Gclm +/-* F1 females. At 7.5 months of age an interaction between genotype and BaP dose was observed, with *Gclm -/-* F1 females having greater relative BaP-induced follicle depletion than *Gclm +/+* littermates [92].

Most recently, we demonstrated that embryos exposed to gestational BaP are capable metabolizing the PAH [93]. Wildtype C57BL/6J mice were time-mated and exposed to 0, 0.2, or 2 mg/kg/day from E6.5-11.5. BaP metabolites were observed in both the embryos and placentas of exposed dams in a dose-dependent manner with female embryos and placentas possessing significantly more BaP metabolites compared to male embryos and respective placentas [93]. The most abundant BaP metabolites in both male and female embryos were

BaP-7,8-diol and 3(OH)BaP, and both BaP-6,12-quinone and BaP-3,6-quinone were more abundant in embryos than placentas, with female embryos having higher concentrations of quinone metabolites than male embryos at both doses. To assess gonadal gene expression following gestational BaP exposure, time-mated wildtype dams were exposed to 0 or 3.33 mg/kg/day of BaP from E9.5-11.5 and RNA-seq was performed on whole E13.5 gonads [93]. *Cyp1b1* was expressed in both the testes and ovaries and was significantly decreased in BaP-exposed ovaries. Additionally, there were significant sex differences in other Phase I and Phase II enzymes, but their expression was not altered by BaP exposure [93]. Together, the above data demonstrate that cigarette smoke, and specifically PAHs, are ovotoxicants and that the embryonic ovary is especially sensitive to PAH-induced germ cell destruction through mitochondrial apoptosis, resulting in a depletion in the ovarian reserve at birth, and that the antioxidant GSH is protective. What has been left unexplored was whether there is a specific ovarian developmental window that is more sensitive to PAH-induced germ cell death.

1.5.3 Animal Studies on PAH Oocyte Toxicity

There is accumulating evidence that damage from maternal or direct exposure to PAHs, or PM2.5, persists in the MII oocyte. Studies focused directly on the impact on MII oocytes are few and far between; however, there has been increased interest in recent years. Germinal vesicle stage oocytes collected from ICR mice and *in vitro* matured to MII stage in the presence of 25, 50, 100, 200, and 400 μM of benzo(ghi)perylene exhibited a dose-dependent decrease in polar body extrusion and oocyte maturation, as well as increased incidence of spindle abnormalities and misaligned chromosomes [94]. Further exploration

revealed that exposure to benzo(ghi)perylene resulted in a less homogenous distribution of mitochondria throughout the oocyte and exposed oocytes exhibited a higher level of perinuclear mitochondrial clustering and increased ROS production [94]. Similar results have been observed using the PAH benzo(b)fluoranthene [95] and the PAH containing mixture PM10 [96]. Germinal vesicle oocytes exposed to 0, 8, 20, or 40 μM of benzo(b)fluoranthene during *in vitro* maturation, exhibited no differences in the rate of progression to MII oocytes; however, oocytes exposed to 20 and 40 μM had a significantly increased rate of misaligned chromosomes and increased DNA damage compared to controls [95]. Analysis of mitochondrial content revealed that oocytes exposed to 8, 20, and 40 μM had significantly decreased mitochondrial content, supported by decreased expression of transcription factor A, mitochondrial (TFAM). Benzo(b)fluoranthene dose-dependently decreased ΔΨm and increased BAX expression in exposed oocytes compared with controls [95]. Similarly, GV oocytes *in vitro* matured with 0, 1, 5, or 10 mg/mL PM10 demonstrated a dose-dependent inhibition of oocyte maturation, likely driven by the observed decreased expression of CyclinB1 throughout maturation in exposed oocytes [96]. Additionally, exposed oocytes had increased incidence of spindle abnormalities, phosphorylation of histone protein 2AX (γH2AX) expression, and mRNA expression of the antioxidant enzymes catalase and glutathione peroxidase 1 compared with controls. Exposed oocytes also showed increased ROS and superoxide alongside decreased GSH content and ΔΨm compared with control oocytes [96].

Similar results were observed by another study assessing *in vivo* exposure to BaP [97]. Female 4-6-week-old ICR mice were orally dosed with 0, 10, 20, or 40 mg/kg/day of BaP in corn oil for 10 days. Oocytes derived from mice exposed to 40 mg/kg/day had

increased levels of ROS, increased incidence of spindle abnormalities and misaligned chromosomes, and a significantly decreased fertilization rate compared with oocytes derived from unexposed controls [97]. An interesting publication reported on *in vivo* exposure to 0 or 13 mg/kg/day and DNA damage in ovulated MII oocytes that were exposed in antral, early antral, large secondary, primary, or primordial follicles [98]. This group reported that only the oocytes exposed to BaP as early antral or large secondary follicles had significantly increased DNA damage compared with controls, not oocytes exposed in primary or primordial follicles [98]. These findings are interesting but not surprising considering that homologous recombination DNA repair is highly active in primordial and growing oocytes [99].

Others have assessed exposure to cigarette smoke 2 times/day 5 days/week for 60 min/exposure, for 12-18 weeks and observed that oocytes derived from mice exposed to cigarette smoke ovulated significantly fewer oocytes than controls and the oocytes of exposed females had significantly increased superoxide and lipid peroxidation [82]. In 2020, a study focused on inhalation exposure to PM2.5 8 h/day, 6 days/week, for 12 weeks total and the impact on MII oocyte redox homeostasis and embryo viability [100]. This group reported that females exposed to PM2.5 ovulated fewer oocytes on average than the females that were exposed to filtered air. Further, the oocytes that were ovulated had increased levels of cellular ROS in PM2.5 exposed compared with controls. Transcriptomics performed on ovulated oocytes showed significant differences in gene expression patterns, notably, of the differentially expressed genes, a few genes belonging to the electron transport chain were significantly down-regulated in PM2.5-exposed oocytes, NADH:ubiquinone oxidoreductase subunits 5 and 7 (Complex I) , LYR motif containing 7 (Complex III), as well

as ubiquinol-cytochrome c reductase, complex III subunit [100]. It is notable that all four of these downregulated genes belong to either Complexes I or III of the electron transport chain and are the primary sources of superoxide in the mitochondria.

Oocyte mitochondria are especially sensitive to detrimental effects of PAHs [86,97,101,102]. The high lipid content of mitochondria facilitates the accumulation of lipophilic compounds such as PAHs [103]. One of the primary metabolism pathways for PAHs is oxidative metabolism through cytochrome P450s, of which some isoforms are located on the inner mitochondrial membrane, yielding reactive metabolites which then react with other macromolecules generating ROS [19,104–108]. This was demonstrated by Sobinoff et al., 2012, who administered 0, 1.5, or 3 mg/kg/day of BaP for 7 consecutive days by i.p. injection of PND4 female Swiss neonatal mice. At 6 weeks of age, oocytes were observed to have a BaP dose-dependent increase in mitochondrial superoxide production and increased lipid peroxidation levels, compared with controls [86]. These results are consistent with persistent oxidized environment, initiated by the BaP exposure.

Moreover, mouse zygotes exposed *in vitro* to 5 and 50 nM BaP, for up to 96 h, demonstrated a concentration-dependent increase in ROS production and a significant reduction in blastocyst formation [101]. These findings support a recent study from Sui et al., which observed that maternal exposure of 40 mg/kg/day BaP for 10 days preconception decreased polar body extrusion and increased incidence of aberrant meiotic spindle assembly in F1 oocytes [109]. In this same study, oocytes from maternally exposed F1 females had decreased mitochondrial content, ATP production, and decreased ROS generation although it is not clear whether the unit of statistical analysis was the F0 mother,

F1 female, or the number of oocytes [109]. These data together suggest that BaP, a representative PAH, is metabolized in the oocyte and imbalances redox homeostasis by increasing lipid peroxidation and disrupting mitochondrial function, which leads to dysregulated meiotic spindle formation, polar body formation, and ability to support fertilization. However, left unaddressed was whether gestational PAH exposure results in persistent oxidative damage to the F1-derived oocyte.

1.6 Hypothesis

I hypothesized that the developing ovary has increased sensitivity to BaP-induced germ cell death during the proliferative phase as opposed to the meiotic phase of ovarian development and that gestational BaP exposure results in significantly decreased follicle numbers, driven by mitochondria- mediated apoptosis, and persistent oxidative damage to the pubertal F1 ovary and oocyte. I further hypothesized that these effects are multi- and transgenerational.

1.7 Dissertation Contribution

- Delineation of a susceptibility of a developmental window to BaP-induced germ cell death.
- Exploration of multi- and transgenerational ovarian toxicity to BaP.
- Evidence to support that gestational BaP exposure results in persistent DNA damage and oxidative lipid in the ovaries of F1 mice.
- Observation that gestational BaP exposure results in diminished oocyte competence.
    - Increased mitochondrial oxidative stress in the ovulated oocyte.
    - Decreased $\Delta\Psi m$, but no difference in overall mitochondria content.
    - Decreased LD content resulting in overall smaller individual LD volume.

    - Decreased percentage of mitochondria colocalized with LDs.
- Confirmation that BaP exposure *in vitro* induces the mitochondrial apoptosis pathway using structure illumination microscopy to resolve fluorescent signal from cytochrome c to 60 nm for localization to the cytosol.
- Development and validation of a method to extract, derivatize, and measure 17β-estradiol using UPHLC-MS/MS.
- Provided evidence to ascertain the characteristics of GSH-deficient oocytes from *Gclm -/-* females that increase their incidence of preimplantation mortality and contribute to our understanding of the crucial role GSH maintenance of reproductive health.
    - *Gclm -/-* oocytes have increased mitochondrial superoxide and decreased ΔΨm compared to *Gclm +/+* oocytes.
    - Mitochondria of *Gclm -/-* oocytes have decreased percentage of clustered mitochondria volume in the subcortical region.
    - *Gclm -/-* oocytes have decreased LD content but show no differences in mitochondria content or mitochondria and LD colocalization.

1.8 Conclusion

Proliferative and meiotic germ cell developmental windows are equally sensitive to gestational BaP-induced germ cell death, likely mediated by mitochondrial apoptosis. This exposure resulted in persistent oxidative damage and oxidative stress in the F1 ovary and oocyte and dysregulation of oocyte lipid content. This is supported by similar observations of MII oocytes in the *Gclm -/-* model. However, the effects of gestational BaP exposure were not inherited in multi- or transgenerational manner.

Chapter 2

In this chapter, I focus on a primary component of air pollution, cigarette smoke, and other mixtures resulting from incomplete combustion of organic materials. Polycyclic aromatic hydrocarbons (PAHs) are well established reproductive toxicants. Previously, we demonstrated that the embryonic ovary is more sensitive to BaP-induced germ cell depletion compared to the embryonic testis [88]. These data strongly suggested a role for the mitochondrial apoptosis pathway in driving germ cell loss. We have also shown that gestational BaP exposure during ovarian development depletes ovarian follicle numbers in pubertal animals in a dose-dependent manner [92,110]. More recently, our group showed that BaP is metabolized by the embryos and the placentae of exposed pregnant dams, resulting in the formation of reactive dihydrodiol and quinone metabolites, which were more abundant in the female embryos and accompanying placentae than in male embryos and placentae [93]. Left unaddressed in these inquiries was whether the embryonic ovary was more sensitive to gestational BaP exposure during a discrete developmental window and if this exposure resulted in persistent oxidative stress in the pubertal ovaries and compromised the developmental competence of mature oocytes.

To address this question, wildtype females were timed-mated and exposed to either 0 or 2 mg/kg/day of BaP in oil across two developmental windows. These windows were chosen to target the window of germ cell proliferation and migration from embryonic day 6.5 to 11.5 (E6.5-11.5, BaP6.5) or the initiation and progression of meiosis from E12.5-17.5 (BaP12.5). F1 females were used for ovarian histology, estrous cycle monitoring, mature oocyte collection and generation of subsequent F2 generation. Breeding was carried out

using non-littermate males of the same treatment group to generate the F2 and F3 generations. The following manuscript demonstrates that gestational BaP exposure resulted in induction of the mitochondrial apoptosis pathway for oocytes in the E13.5 ovary, yielding F1 females born with a smaller ovarian reserve. Our data further showed that the proliferative and meiotic developmental windows are equally sensitive, with both demonstrating equivalent loss of primordial, primary, and secondary follicles, as well as equal persistence of oxidative stress. Intriguingly, granulosa cells and oocytes of secondary follicles from the BaP12.5 exposure were more sensitive to induction of DNA double strand breaks as observed through the phosphorylation of histone 2AX. Together these results showed that gestational BaP resulted in persistent ovarian oxidative stress and may impact ovulated oocyte quality.

To elucidate this, we explored markers of oxidative stress and oocyte developmental competence in the BaP6.5 and Oil6.5 F1 females. We found that gestational BaP exposure resulted in a borderline statistically significant increase in mitochondrial superoxide production in F1 oocytes as well as a significantly decreased oocyte $\Delta\Psi m$- both of which suggest that the ovulated oocyte has increased levels of oxidative stress. However, we did not observe a difference in lipid peroxidation levels in exposed oocytes, which is likely attributable to the dysregulation of oocytes LDs we observed. BaP6.5 oocytes had smaller LDs in comparison to Oil6.5 oocytes and a smaller percentage of mitochondria were colocalized with LDs in BaP6.5 oocytes. These results suggest that gestational BaP exposure results in persistent oxidative stress in the ovulated oocyte, which may have a role in the compromised fertility and preimplantation development reported by our group and others [86,92,109].

We carried out our breeding to generate F2 and F3 females from all four treatment groups to assess potential multigenerational and transgenerational effects of gestational and ancestral exposure to BaP. Contrary to our preliminary results, we observed that BaP had no impact on the ovarian reserve for the F2 or F3 generations. This may be a result of the shortened exposure windows- as our previous study employed an exposure paradigm that included both proliferative and meiotic windows of development (E6.5-17.5).

Primary Research Article

Gestational Benzo[a]pyrene Exposure Destroys F1 Ovarian Germ Cells through Mitochondrial Apoptosis Pathway and Diminishes Surviving Oocyte Quality

Kelli F. Malott[1,2], Kathleen Leon Parada[3], Melody Lee[4], Edward Swanson[4], Ulrike Luderer [1,2,3,4,5]

[1]Environmental Health Sciences Graduate Program, [2]Department of Environmental and Occupational Health, [3] Department of Developmental and Cell Biology, [4]Department of Medicine, University of California, Irvine, Irvine, Ca 92617

[5]Correspondence: Dr. Ulrike Luderer

Center for Occupational and Environmental Health

100 Theory Drive, Suite 100

Irvine, CA 92617

U.S.A

Tel: 949-824-8641

Email: uluderer@uci.edu

Running head: Gestational benzo[a]pyrene and F1 oocyte competence

Keywords: oocyte, mitochondria, lipid droplets, polycyclic aromatic hydrocarbons, oxidative stress, benzo[a]pyrene

Abstract

Polycyclic aromatic hydrocarbons (PAHs), including benzo[a]pyrene (BaP), are products of incomplete combustion. Primordial germ cells (PGCs) arise in the mouse at embryonic day 5.5 (E5.5), proliferate before and after arriving at the gonadal ridge E10.5, and begin entering meiosis at E13.5. Now oocytes, they arrest in the first meiotic prophase beginning at E17.5. We previously reported dose-dependent depletion of ovarian follicles in female mice exposed to 2 or 10 mg/kg-day BaP E6.5-15.5. We hypothesized that embryonic ovaries are more sensitive to gestational BaP exposure during the mitotic developmental window, and that this exposure results in persistent oxidative stress in the F1 ovary and oocyte. We orally dosed timed-pregnant female mice with 0 or 2 mg/kg-day BaP in oil from E6.5-11.5 (mitotic window) or E12.5-17.5 (meiotic window). Cultured E13.5 ovaries were utilized to investigate the mechanism of BaP-induced germ cell death. We observed statistically significant follicle depletion and increased ovarian lipid peroxidation in F1 pubertal ovaries following BaP exposure during either prenatal window. Culture of E13.5 ovaries with BaP induced germ cell DNA damage and release of cytochrome c from the mitochondria in oocytes, confirming that BaP exposure induced apoptosis via the mitochondrial pathway. Mitochondrial membrane potential, oocyte lipid droplet volume, and mitochondrial-lipid droplet colocalization were decreased and mitochondrial superoxide levels were increased in the MII oocytes of F1 females exposed gestationally to BaP. Results demonstrate similar sensitivity to germ cell depletion and persistent oxidative stress in F1 ovaries and oocytes following gestational BaP exposure during mitotic or meiotic windows.

Introduction

Polycyclic aromatic hydrocarbons (PAHs), such as benzo[a]pyrene (BaP), are products of incomplete combustion of organic materials. BaP is a known ovotoxicant that depletes ovarian follicles in rodents at all ages when exposed (Gulyas and Mattison, 1979; Lim *et al.*, 2013; Mattison and Thorgeirsson, 1979; Mattison, 1980; Matikainen *et al.*, 2002). PAHs require metabolic activation to exert their negative effects, and in most cases, undergo oxidation to produce metabolites that interact with cellular macromolecules (Xue and Warshawsky, 2005). Metabolism of BaP occurs through several well-known pathways; oxidation by cytochrome P450 enzymes (CYP450) to produce dihydrodiol epoxides, the formation of a BaP radical cation by CYP450 peroxidases, and dihydrodiol-dehydrogenase oxidation to eventually lead to the formation of *o*-quinones through an NADP+-dependent mechanism (Xue and Warshawsky, 2005). An ancillary pathway for BaP metabolism occurs via prostaglandin endoperoxide synthase 2 using it as a very weak reducing co-substrate, resulting in the formation of quinones (Eling *et al.*, 1990). Of the above pathways for BaP metabolism, the pathways resulting in the formation of quinones are capable of reduction-oxidation (redox) cycling, in the presence of superoxide, producing reactive oxygen species (ROS) (Xue and Warshawsky, 2005). ROS are highly reactive compounds that can act as intracellular signaling molecules, but in high concentrations, can be detrimental to the cell through oxidation of DNA, proteins, and lipids, causing irreparable damage and eventually cell death (Penning *et al.*, 1996).

Primordial germ cells (PGCs) are the embryonic precursors of oocytes, arising in the mouse proximal epiblast at embryonic day 6.5 (E6.5). These proliferate and begin to migrate to the gonadal ridge arriving starting at ~ E9.5. In the female embryo, the gonocytes continue to proliferate becoming oogonia in the differentiating ovary, then enter meiosis to form oocytes beginning at ~E13.5 (Wear *et al.*, 2016). The oocytes progress through meiosis arresting at the diplotene stage of the first meiotic prophase beginning at ~E17.5. Germ cell development in the fetal ovary produces a finite oocyte pool, the primary determinant of female fertility and reproductive lifespan. The

developing ovary is particularly sensitive to germ cell and follicle destruction by PAHs, and exposure to BaP during germ cell development diminishes the number of oocytes in the ovary (Lim *et al.*, 2016, 2013; Lim and Luderer, 2018; Matikainen *et al.*, 2002).

In mice, germ cell nest breakdown and follicular organization in the embryonic ovary begins shortly before birth (Wear *et al.*, 2016; Pepling and Spradling, 2001). Oocytes are organized into follicles, surrounded by a few squamous granulosa cells, these primordial follicles constitute the ovarian reserve (Pepling, 2012; Pepling *et al.*, 2007). Folliculogenesis supports the growth and maturation of a healthy, developmentally competent oocyte. As the oocyte grows in volume throughout folliculogenesis, with the help of supportive granulosa cells, it is stockpiles maternal mRNAs, proteins, metabolites, antioxidants, and lipids in the form of lipid droplets (LDs) (Paczkowski *et al.*, 2014; Valsangkar and Downs, 2013). Many of the metabolites and the lipids are derived from the follicular fluid by the granulosa cells, imported into the oocyte for storage, and the oocyte can also build its lipid through *de novo* lipogenesis (Aizawa *et al.*, 2019; Zhang *et al.*, 2020; Prates *et al.*, 2014). Additionally, the oocyte expands its organelle population, particularly the mitochondria and LDs, both of which are crucial to the developmental competence of an oocyte (Ramalho-Santos and Amaral, 2013; Coticchio *et al.*, 2004; Bradley and Swann, 2019). The fully mature, healthy ovulated mouse oocyte contains roughly 100,000 mitochondria (Adhikari *et al.*, 2022; Chiaratti *et al.*, 2018).

Mitochondria are a primary source of ROS in the cell, converting 0.2-2% of oxygen taken up by the cell into ROS (Ramalho-Santos *et al.*, 2009). Electrons moving along the electron transport chain can react directly with oxygen, or other electron acceptors, creating free radicals. These free radicals can then be sequestered by antioxidants or react with macromolecules (lipids, DNA, proteins) in the cell causing damage. As outlined previously, the formation of BaP metabolites, such as quinones, can be particularly damaging as they are a class of redox cycling molecules, producing excess ROS, including superoxide, hydrogen peroxides, and hydroxyl radicals (Forman *et al.*, 2009). LDs are monophospholipid organelles that contain a neutral lipid core consisting of triacylglycerol

and cholesterol (Walther and Farese, 2009, 2012). The oxidation of lipids through fatty acid β-oxidation has been shown to be important to preimplantation development (Dunning *et al.*, 2010); additionally they are believed to play several other important roles crucial to oocyte competence and preimplantation development, from supplying lipoic acid as a cofactor for metabolism (Jarc and Petan, 2019) to secondary signaling molecules (Prates *et al.*, 2014).

The redox state of a cell refers to the relative concentrations of oxidized versus reduced intracellular components. Additionally, the balance between ROS and antioxidants has a significant role in determining this state (Devine *et al.*, 2012). Oxidative stress occurs when the balance between ROS and antioxidant systems shifts in favor of ROS (Devine *et al.*, 2012). When a cell is under oxidative stress for an extended period, BAX proteins oligomerize and insert into the mitochondrial membrane, creating a channel releasing cytochrome c, resulting in activation of the effector caspase-3, which drives intrinsic apoptosis (Orrenius *et al.*, 2007). Mitochondrial apoptosis seems to be involved in postnatal decline in female germ cell populations (Matikainen *et al.*, 2002). However, cells can exist for extended periods of time in a more oxidized state, without the induction of apoptosis (Devine *et al.*, 2012). This persistent oxidative stress is still harmful to the cell, often resulting in oxidation of macromolecules such as proteins, DNA, and lipids (Devine *et al.*, 2012). We can visualize the peroxidation of lipids in cells using the marker 4-hydroxynonenal (4-HNE), which is generated from the oxidation of lipids such as arachidonic and linoleic acids (Zhong and Yin, 2015).

Previously, we demonstrated that treatment of pregnant mice with BaP from E6.5-15.5 dose-dependently decreases fertility and results in fewer follicles in peripubertal and adult female offspring, with female *Gclm* null mice, deficient in GSH, being more sensitive to prenatal BaP exposure (Lim *et al.*, 2013). These data suggest that fetal ovaries exposed *in utero* to BaP during PGC development were subject to BaP-induced PGC death. To understand the mechanism of BaP-induced germ cell death, we demonstrated that BaP exposure of cultured E13.5 ovaries concentration-dependently induced germ cell death through increased expression of BAX protein at 6 h and

increased activation of caspases-9 and -3 at 24 h of exposure, without affecting PGC proliferation (Lim *et al.*, 2016). We further demonstrated that BaP exposure resulted in concentration-dependent decreases in PGC number after 48 h exposure (Lim *et al.*, 2016). While these findings provide strong evidence of mitochondrial involvement in BaP-induced germ cell death, this pathway has yet to be fully characterized.

In this study, we hypothesize that F1 germ cells are more sensitive to BaP-induced depletion during proliferation compared with meiosis, that BaP-induced depletion is mediated through increased oxidative stress leading to mitochondrial-driven apoptosis in the embryonic ovary, and that gestational BaP exposure reduces the development competence of oocytes by reducing their lipid stores, thus altering their oxidative state.

Materials and Methods

Animals

8-week-old C57BL/6J females and males were purchased from Jackson Laboratories and acclimated for 2 weeks. Mice for these experiments were housed in an American Association for the Accreditation of Laboratory Animal Care-accredited facility at the University of California Irvine (UC Irvine), with free access to deionized water and soy-free laboratory chow (Harlan Teklad, 2919), on a 14:10h light-dark cycle. Temperature was maintained at 21–23°C. The experimental protocols were carried out in accordance with the Guide for the Care and Use of Laboratory Animals and were approved by the Institutional Animal Care and Use Committee at UC Irvine (NRC, 2011).

BaP Exposure

Females were singly housed and estrous cycles were assessed once a day at 10:00 am by light microscopic examination of vaginal lavage fluid with 0.9% sodium chloride (Lim *et al.*, 2013). Females were caged with males on the afternoon of proestrus and the next morning pregnancy was confirmed by the presence of a vaginal plug and designated as embryonic day 0.5 (E0.5). Dams were

treated by oral pipet dosing into the cheek pouch (Lim *et al.*, 2022) with 0 or 2 mg/kg/day of BaP in sesame oil from either E6.5-11.5 (Oil6.5 and BaP6.5) or E12.5-17.5 (Oil12.5 and BaP12.5), roughly corresponding to either entirely proliferative or mostly meiotic phases of germ cell development, respectively. F0 dams were allowed to give birth to the F1 generation (Figure 2.1A).

Embryonic Ovary Culture

Female C57BL/6J mice were mated, upon confirmation of proestrus, with a C57BL/6J male. The following morning was designated E0.5 upon confirmation of a vaginal plug. One pregnant female was humanely euthanized on E13.5 using CO_2 overdose, and embryos dissected per experimental day. The uteri and embryos were quickly removed, and the ovaries, with attached mesonephros (hereafter referred to as ovaries) from each female embryo were harvested for culture (Figure 2.1B).

Each ovary was assigned to a treatment group, taking care that the individual ovaries from embryos of the same pregnant dam were distributed across exposure groups and no two ovaries from one embryo were allocated to the same exposure group. Ovaries were assigned to four concentration groups: uncultured, 0, 500, and 1000 ng/mL BaP dissolved in 0.005% DMSO (UC, DMSO, 500 ng/mL, and 1000 ng/mL, respectively). Ovaries were cultured on 0.4 μm Millicell-CM biopore membranes floating on culture medium at 37°C in 95% air and 5% CO2 as previously described (Lim *et al.*, 2016; Lim and Luderer, 2018). E13.5 ovaries were cultured for 6 h then fixed in Bouin's fixative (Ricca chemical, 1120-16) for 90 min prior to storing in optimal cutting temperature (OCT) compound (Sakura, 4583) at -80°C.

Puberty Onset and Ovarian Histomorphometry

F1 females were followed daily for vaginal opening, an indicator of the onset of puberty, beginning at weaning on PND 21, followed by daily vaginal cytology until the first day with cornified vaginal cytology typical of estrus, considered to be the best indicator of puberty in female mice (Safranski *et al.*, 1993). Vaginal lavage was performed with 0.9% sodium chloride. Lavage fluid was

immediately examined using a light microscope, and predominant cell types were recorded (Cooper *et al.*, 1992). One female per F1 litter was sacrificed via CO_2 overdose and cervical dislocation on the morning of her first estrus. One ovary per female was fixed in Bouin's fixative overnight at 4°C. After fixation, ovaries were washed three times with 70% ethanol. Ovaries were embedded in glycol methacrylate resin (Technovit 8100, EMS, 14654) and sectioned at 20 μm for follicle counting. The second ovary was fixed overnight in 4% paraformaldehyde at 4°C then incubated in 30% sucrose at 4°C for at least 90 minutes and embedded in OCT compound.

Follicles were enumerated using StereoInvestigator software (MBF Biosciences) and an Olympus BX40 light microscope equipped with a motorized stage and 40X oil immersion objective. Small follicle counts were assessed by an investigator blind to experimental group using methods previously described (Myers *et al.*, 2004; Luderer *et al.*, 2022). Briefly, small (primordial and primary) follicles were counted in every 5th section from the start of the ovarian tissue, giving sampling fraction 1 (f1) = 1/5. For the second sampling fraction, the counting frame (measuring 175 ・175 μm) was superimposed over the section with a sampling grid (measuring 250・250 μm), giving (f2) = 30625/62500. For the final sampling fraction, 10 μm within the section, with an original thickness of 20 μm was the sample thickness counted; it is important to note that section thickness shrinks slightly with tissue staining, and the average section thickness across all sections measured came to 17.76 μm. The final sampling fraction is determined by the software after bringing the sample into focus: f(3) = 10/average section thickness. Total counts were multiplied by the reciprocals of the sampling fractions $Q^{-}_{(follicle)}$ ・(1/f1) ・(1/f2) ・(1/f3) to arrive at a total estimated number of follicles per ovary. Only follicles with a visible oocyte nucleus within the 10 μm sampling height were counted. Primordial follicles were characterized by the presence of a single layer of flattened granulosa cells with no more than one cuboidal granulosa cell. A follicle was primary if two or more granulosa cells were cuboidal, and the oocyte was surrounded by 4 or more granulosa cells in total. To assess large follicles, every section was counted using an Olympus BX60 brightfield microscope. A follicle was

classified as secondary if the oocyte was surrounded by more than one layer of cuboidal granulosa cells, and an antral follicle was characterized by the presence of an antral cavity or several fluid-filled vesicles.

Immunohistochemistry

We previously validated antibodies for lipid peroxidation marker 4-hydroxynonenal (4-HNE) (Alpha Diagnostics, HNE11-S) and phosphorylated histone 2AX (ɣH2AX) (Cell Signaling Technologies, S139) (Lim and Luderer, 2018; Mishra *et al.*, 2016). Paraformaldehyde-fixed F1 pubertal ovaries and Bouin's-fixed E13.5 ovaries were embedded in OCT, sectioned at 10 μm, and stored at -80°C. Slides underwent antigen retrieval in 10 mM sodium citrate with 0.05% Tween-20 for 15 or 25 minutes, dependent on the antigen, at 95°C, followed by blocking with avidin and biotin (Vector Laboratories, SP-2001) and normal goat serum, then incubated with primary antibodies for 4-HNE (1:300, F1 ovaries only), ɣH2AX (1:500, E13.5 and F1 ovaries), or PUMA (1:200, E13.5 ovaries only) (Abcam, AB9643) raised in rabbit. Then slides were incubated with secondary anti-rabbit IgG, blocked with 0.3% H_2O_2, incubated with ABC reagent (Vector laboratories, PK-4001), and immunostaining was visualized with diaminobenzidine substrate in peroxide buffer. Sections were counterstained with hematoxylin. The following controls were used for each experimental run (i) -/- control for background (ii) +/- control for primary antibody (iii) -/+ control for secondary antibody (iv) IgG/+ control.

Scoring for immunostaining was performed by an investigator blind to experimental group. Three independent experimental runs were performed with one slide per ovary and 4 sections per slide were performed for each end point. 4-HNE staining was assessed using ImageJ FIJI (NIH). Images underwent a color-balance correction, then 4-HNE signal was measured over the total ovarian section and reported as reciprocal intensity per ovarian section area. For ɣH2AX staining in F1 pubertal ovaries, the percentages of primary, secondary, and antral follicles with positive

granulosa cells or oocyte were counted per ovary section and averaged per ovary. For E13.5 ovaries, the percentages of positive ɣH2AX oocytes per ovary section were counted and assigned to meiosis stage, determined by the chromatin morphology (Láscarez-Lagunas *et al.*, 2020), then averaged per ovary. PUMA is ubiquitously expressed in the E13.5 ovary (Myers *et al.*, 2014). Therefore total reciprocal intensity per ovarian section area was used to assess PUMA expression in E13.5 ovaries.

Immunofluorescence

Bouin's-fixed E13.5 ovaries, were embedded in OCT and sectioned at 10 μm. Slides were incubated for 15 minutes in 10 mM sodium citrate with 0.05% Tween-20 for 15 minutes at 95°C for antigen retrieval, then incubated with avidin and biotin, and M.O.M blocking reagent (Vector Laboratories, FMK-2201). Ovaries were stained with mouse anti - cytochrome c (1:200) (Santa Cruz, SC-13156) and rabbit anti – germ cell nuclear antigen (GCNA) (1:200) (Abcam, AB82527) in M.O.M diluent (Vector Laboratories, FMK-2201) overnight at 4°C. The next day, slides were washed with 1X phosphate buffered saline (PBS), incubated with anti-mouse Alex Fluor 555 (Invitrogen, A21424) and anti-rabbit Alexa Fluor 647 (Invitrogen, A21247) for 1 h, and then coverslips were mounted with Prolong Gold (Invitrogen, P36934).

Ovary sections were imaged using an Elyra 7 with Lattice SIM (Carl Zeiss). Z-stack images were taken with 12 slices per image. Three images per ovarian section were taken at least 50 μm distance apart. Images were processed using standard fixed sample SIM^2 processing applied to each image. Images were analyzed for release of cytochrome c from the mitochondria of oocytes using Imaris Imaging Software (Bitplane). Cytochrome c and GCNA fluorescence was used to generate 3-dimensional volumes. Cytochrome c volumes in close proximity to GCNA volumes (about 1 μm) were considered to be within the oocyte and were selected for analysis, while cytochrome c volumes further away from GCNA volumes were assumed to be somatic cells and were filtered out. Cytochrome c volumes proximal to GCNA surfaces were further filtered to distinguish between

punctate vs diffuse staining, with diffuse staining determined to be indicative of release of cytochrome c into the germ cell cytosol (Feng *et al.*, 2012; Liu *et al.*, 2003). Diffuse cytochrome c volumes were defined as volumes greater than 1.73 μm^3 (Motta *et al.*, 2000).

Superovulation

Postnatal day (PND) 35-45 F1 females, exposed *in utero* to 0 or 2 mg/kg/day BaP from E6.5-11.5 were primed by i.p. injection with 5 IU equine chorionic gonadotropin (eCG) (Prospec Protein Specialists, Israel, HOR-272) at 1800 h; 46 hours later superovulation was induced by an i.p. injection with 5 IU human chorionic gonadotropin (hCG) (Sigma Aldrich, CG10) (Figure 2.1C). Cumulus-oocyte-complexes were harvested from the ampullae of the oviducts 14 hours later following CO_2 euthanasia into flushing and holding medium (FHM) (Neta Scientific, MR-122-D). Oocytes were dissociated from the cumulus clouds by incubation in 0.3 mg/ml of hyaluronidase (Thermo Fisher Scientific) for no more than 5 minutes, then immediately transferred to FHM under mineral oil (Sigma-Aldrich, M8410) for assessment. Only healthy, morphologically normal oocytes were chosen. Morphologically healthy oocytes were defined as having clear, granular cytoplasm; small perivitelline space; first polar body; colorless zona pellucida; not fragmented.

Oocyte staining and imaging

To measure the ratio of oxidized:unoxidized lipids, healthy oocytes were incubated in 10 μM BODIPY 581/591 C11 (ThermoFisher, D3861) at 37ºC and 5% CO_2 for 30 minutes under mineral oil, then subsequently washed through three droplets of FHM. Oocytes were imaged in glass-bottomed petri dishes in 50 μL droplets of FHM without phenol red under mineral oil. BODIPY 581/591 C11 colocalizes with fatty acids inside the cell, upon oxidation of the polyunsaturated butadienyl portion, the fluorescence emission peak shifts from ~590 nm to ~510 nm, this red-to-green fluorescence shift allows for the use of green:red ratio reporting of oxidized lipids.

To measure the total neutral lipid content, mature oocytes were fixed with 4% paraformaldehyde for 1 h at room temperature, then washed through three droplets of 1X PBS with 3 mg/mL of polyvinylpyrrolidone (PVP) (Sigma Aldrich, P0930). Fixed oocytes were incubated in 3.82 μM of BODIPY 493/503 (4,4-difluoro-1, 3, 5, 7, 8-pentamethyl-4-bora-3a,4a-diaz-s-indacene) (ThermoFisher, D3922) for 1 h at room temperature under mineral oil, washed through three droplets of 1X PBS with 3 mg/mL PVP then imaged in glass-bottomed petri dishes in 50 μL droplets of 1X PBS under mineral oil. BODIPY 493/503 is a nonpolar lipid stain. Total lipid droplet content per oocyte was estimated by the sum fluorescence of lipid droplets per cell. This was calculated by totaling the mean fluorescence intensity of LDs per cell estimated by Imaris Imaging Software (Bitplane). Average LD volume was estimated by creating 3D volumes using Imaris Imaging Software.

To assess mitochondrial membrane potential (ΔΨm), we used the JC-1 (5,5',6,6'-tetrachloro-1,1',3,3'-tetraethyl-benzimidazolylcarbocyanine iodide) probe (ThermoFisher, T3168). Healthy oocytes were incubated in 5 μM of JC-1 for 15 minutes at 37ºC and 5% CO_2 under mineral oil, subsequently washed through three consecutive droplets of FHM, prior to imaging on a glass-bottomed petri dish in 50 μL droplet of FHM under mineral oil. Positive control oocytes were incubated in 1 μM of CCCP (carbonyl cyanide 3-chlorophenylhydrazon) (Millipore Sigma, C2759) under mineral oil for 15 minutes at 37ºC, with atmosphere of 95% air, 5% CO_2. CCCP is a known mitochondrial uncoupler, which breaks down the ΔΨm by transporting protons across the inner mitochondrial membrane (Kasianowicz *et al.*, 1984). JC-1 is a cationic carbocyanine dye that accumulates in the mitochondria. In low concentrations, the dye stays in its j-monomer form and will fluoresce green, however in high concentrations the dye will form j-aggregates that fluoresce red. Due to its cationic nature, the concentration of JC-1 per organelle is dependent on the ΔΨm, thus, under lower ΔΨm it will fluoresce green and under high ΔΨm, red. Total ΔΨm per oocyte is reported as the total sum fluorescence ratio of red:green.

MitoSOX (ThermoFisher, M36008) was used to assess mitochondrial superoxide production in live oocytes. Healthy oocytes were incubated in 5 μM of MitoSOX for 30 minutes at 37°C and 5% CO_2 under mineral oil, then washed through three droplets of FHM prior to imaging on a glass-bottomed petri dish in 50 μL droplet of FHM under mineral oil. MitoSOX is a fluorogenic dye specifically targeted to the mitochondria where it is immediately oxidized by superoxide specifically, if present, emitting red fluorescence. Mitochondrial superoxide production was estimated by total red fluorescence per oocyte. To measure oocyte GSH content, healthy oocytes were incubated in 1.5 μM of monochlorobimane for 15 minutes at 37°C and 5% CO_2 under mineral oil, then washed through three droplets of FHM prior to imaging on a glass-bottomed petri dish in 50 μL droplet of FHM under mineral oil. Oocyte GSH was estimated by total blue fluorescence per oocyte.

For colocalization of mitochondria and LDs, oocytes were incubated in 300 nM of MitoTracker Deep Red (ThermoFisher, M22426) at 37° C, with atmosphere of 95% air, 5% CO_2 for 30 minutes under mineral oil, then fixed in 4% paraformaldehyde at room temperature for 1 h, in darkness. Following fixation, oocytes were washed through three small droplets of 1X PBS with 3 mg/mL PVP then incubated in 3.82 μM BODIPY 493/503 under mineral oil for 1 h at room temperature in darkness. Following that incubation, oocytes were washed through three small droplets of 1X PBS with 3 mg/mL PVP. Oocyte mitochondria were immediately imaged using confocal microscopy at 644/665 (ex/em) and oocyte LDs were visualized using 493/503 (ex/em).

Oocyte images were taken in z-stacks, using 63X oil objective on a Zeiss two-photon laser scanning microscope (LSM) 780 (ZEISS Research Microscopy Solutions), and all imaging analysis was performed using Imaris imaging software (Bitplane) or FIJI ImageJ (NIH). Analysis of ΔΨm, mitochondria, and LDs were performed in Imaris Imaging Software by using the raw fluorescence to render volumes specific to the fluorescence wavelength. Unless otherwise specified, the mean fluorescence of each individual surface was calculated and the sum fluorescence for the whole oocyte was calculated. Mitosox fluorescence was analyzed in FIJI by compressing the z-stack, subtracting

background fluorescence, then measuring the fluorescence in a region of interest encompassing the oocyte.

Statistical Analyses

Data are displayed as means +/- SEM unless otherwise noted. Effects of BaP exposure on ovarian histological endpoints were analyzed using two-way ANOVA. Effects of prenatal BaP exposure on age at puberty onset were analyzed using Generalized Estimating Equations (GEE), a form of General Linear Model, to account for litter effects. The effects of BaP exposure on oocyte endpoints were analyzed using GEE to account for repeated measures within animals (the same endpoint was measured in multiple oocytes from the same mouse). GEE models utilized exchangeable correlation matrices. In cases when the Hessian matrix did not converge for a GEE model, ANOVA with a random effect variable to account for multiple measurements within an animal was used. IBM SPSS Statistics 25 for Macintosh was used for statistical analyses.

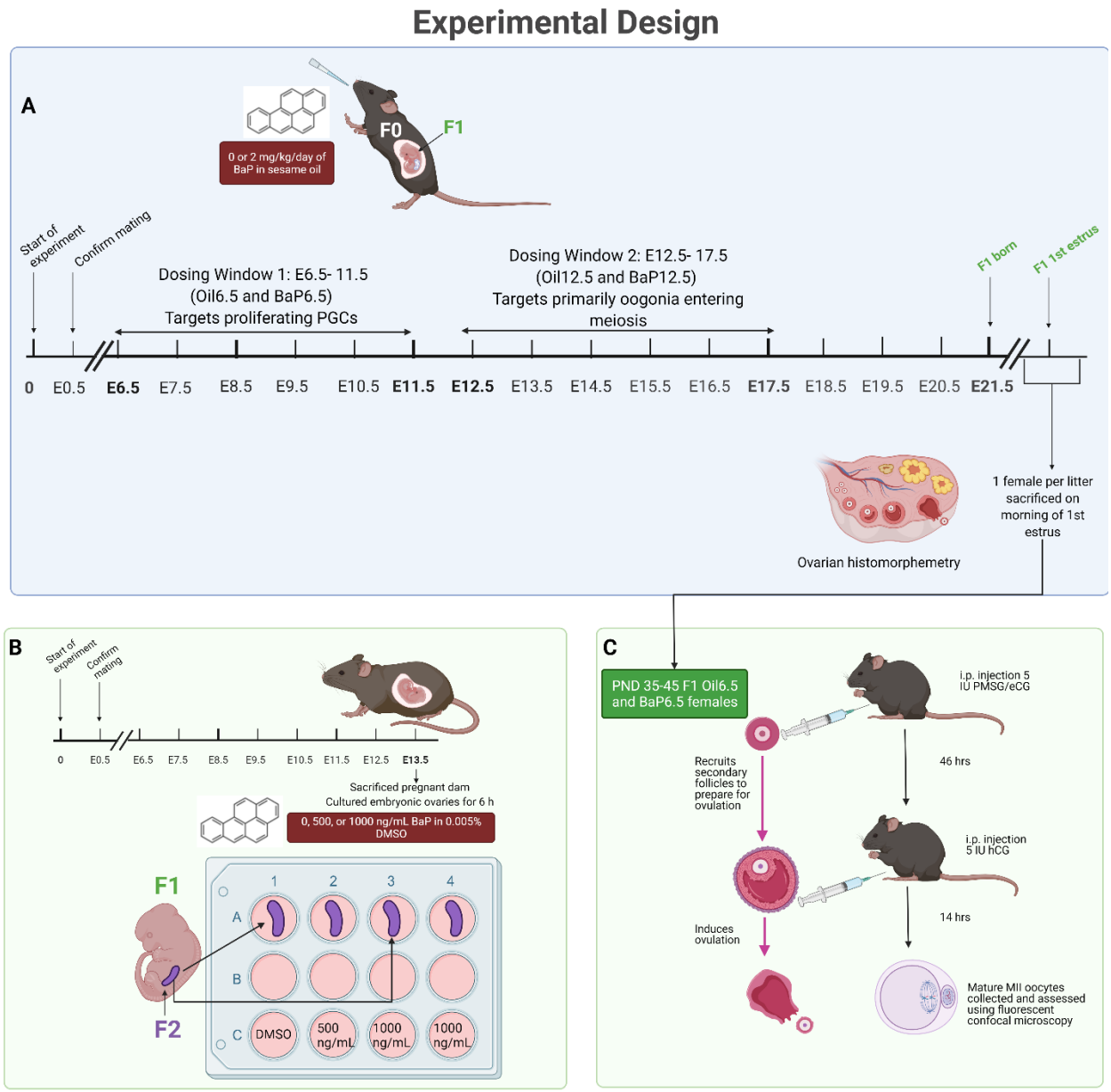

Figure 2.1: A) Experimental design for *gestational* BaP exposure and assessment of F1 ovarian effects during two critical windows of ovarian development. **B)** Experimental design for *in vitro* BaP exposure and assessment of induction of mitochondrial apoptosis pathway. **C)** Experimental design for F1 gestational BaP exposure and assessment of F1-derived MII oocyte oxidative stress and developmental competence. All details of each exposure and endpoint are described in detail in the materials and methods. Figure was created with the help of Biorender.com.

Results

BaP-induced germ cell death in F1 embryonic ovaries is driven by mitochondrial-mediated apoptosis.

BaP metabolism results in the generation of various reactive metabolites, some of which directly react with DNA, forming bulky adducts and resultant DNA damage, while others redox cycle, generate reactive oxygen species and cause oxidative DNA damage (Xue and Warshawsky, 2005; Penning *et al.*, 1996). To detect DNA damage in exposed germ cells, we cultured E13.5 ovaries in 0, 500, and 1000 ng/mL of BaP in 0.005% DMSO for 6 h and tested whether BaP exposure led to increased DNA damage. Phosphorylation of histone H2AX (ɣH2AX) occurs rapidly adjacent to DNA double strand breaks (Kinner *et al.*, 2008). We observed that both concentrations of BaP (500 and 1000 ng/mL) resulted in statistically significant increases in the percentage of ɣH2AX-positive germ cells compared with DMSO and uncultured controls (P=0.002, effect of experimental group by Kruskal Wallis test, Figure 2.2A). Further, when positive germ cells were assessed for meiosis stage, to account for DNA DSBs that occur during meiosis, exposed ovaries had statistically significant increases in ɣH2AX-positive germ cells compared with DMSO and uncultured controls during interphase and leptotene, the meiotic stages when DSBs are normally not present (P=0.007 and P=0.009, respectively, by Krukal Wallis test, Figure 2.2B), demonstrating that BaP metabolism leads to increased DNA damage in embryonic ovaries.

p53-upregulated modulator of apoptosis (PUMA), a BH3 domain only BCL2 family pro-apoptosis regulator, is ubiquitously expressed in E13.5 ovaries (Myers *et al.*, 2014). It is thought to regulate germ cell loss shortly after the conclusion of the migratory phase of germ cell development, but not during germ cell nest breakdown (Myers *et al.*, 2014). DNA damage has been shown to trigger the mitochondrial apoptosis pathway through induction of PUMA. To further characterize this mechanism of cell death, we observed that *in vitro* BaP-exposure slightly, though not statistically significantly, increased PUMA expression in the whole embryonic ovary at 6 h (Figure 2.3A, B).

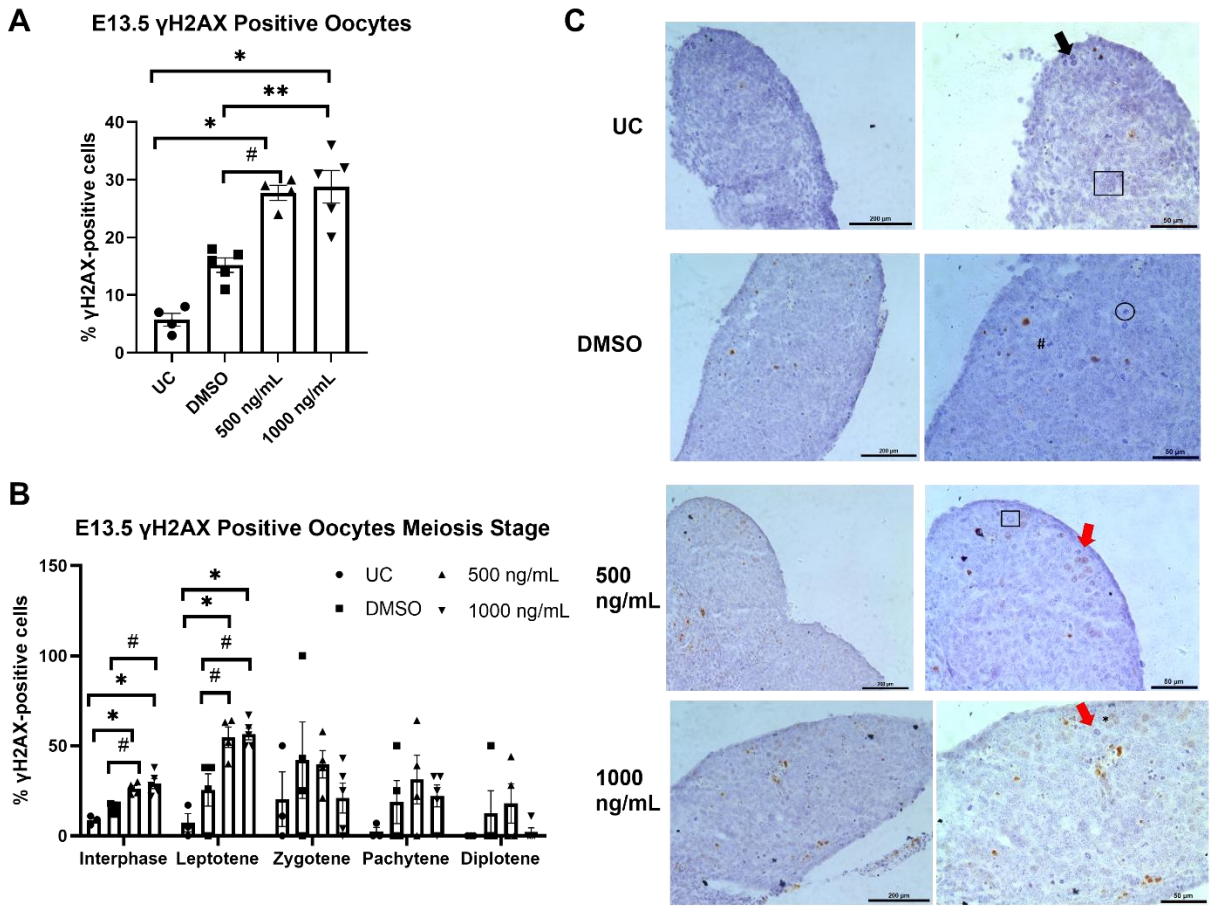

Figure 2.2: *In vitro* BaP exposure concentration-dependently increases γH2AX in germ cells of embryonic ovaries A) Total percent γH2AX-positive germ cells per E13.5 ovary increased with BaP concentration following exposure for 6 h (N=3, UC (uncultured); N=4, DMSO, 500 ng/mL; N= 5, 1000 ng/mL. P=0.002, effect of experimental group by Kruskal Wallis test. *P≤0.05, compared to uncultured, #P≤0.014 and **P≤0.009, compared to DMSO) **B)** Percent γH2AX-positive oocytes by meiotic stage per E13.5 ovary increased with BaP dose only in interphase and leptotene oocytes following exposure for 6 h (N=3, UC (uncultured); N=4, DMSO, 500 ng/mL: N= 5, 1000 ng/mL. P≤0.009 by Kruskal Wallis test, effect of experimental group. *P≤0.05, compared to uncultured; #P≤0.05 compared to DMSO) **C)** Representative images of γH2AX immunohistochemistry. Asterisks (*) point to γH2AX-positive oocytes, (square) shows interphase, (black arrow) shows leptotene, (red arrow) shows zygotene, (circle) shows pachytene, and (#) shows diplotene chromosomes. Left panel scale bars = 200 µm. Right panel scale bars = 50 µm.

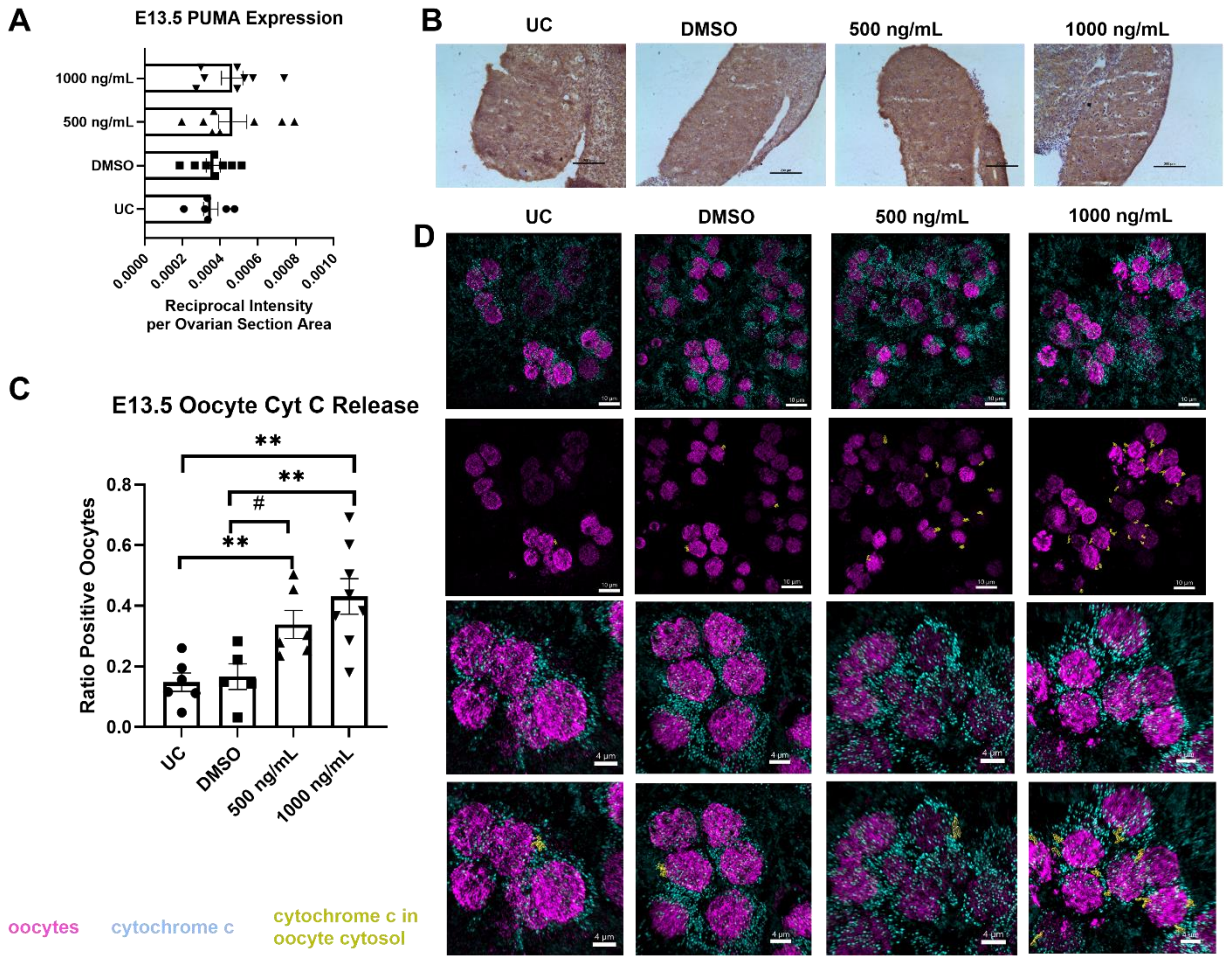

Figure 2.3: *In vitro* BaP exposure for 6h had no effect on PUMA protein expression but dose-dependently increased cytochrome c release in exposed ovaries A) Reciprocal intensity per ovarian section area was estimated in E13.5 ovaries and showed a slight, but not statistically significant, increase in PUMA immunostaining in the whole ovary (N= 6, UC (uncultured); N=8, DMSO, 500 ng/mL, 1000 ng/mL). **B)** Representative images of PUMA immunohistochemistry show ubiquitous and similar expression regardless of exposure. **C)** Cytochrome C release from the mitochondria in germ cells following BaP exposure was measured using immunofluorescence. Methods for analysis of images to estimate the ratio of oocytes positive for cytochrome c release are detailed in the Materials and Methods. These results show a dose-dependent increase in the ratio of positive oocytes (N=6, UC; N=5, DMSO; N=6, 500 ng/mL; N=8, 1000 ng/mL. P=0.001, effect of experimental group, Kruskal Wallis test. *P≤0.004, compared to uncultured; **P<0.01, compared to DMSO or uncultured; #P≤0.045 compared to DMSO, Mann Whitney test). **D)** Representative images of immunofluorescence. Top row shows germ cell-specific marker GCNA (magenta) and cytochrome c (cyan blue). Second row shows Imaris analysis with GCNA (magenta) and cytochrome c in oocyte cytosol (yellow), scale bars = 10 µm. Third row and fourth rows show same as top and second rows, respectively zoomed in, scale bars = 4 µm.

Release of cytochrome c from the mitochondria to the cytosol, where it combines with Apoptotic protease activating factor 1 (APAF1) to form the apoptosome, is a key event of the mitochondrial apoptosis pathway (Ferraro *et al.*, 2003). To confirm the activation of the mitochondrial apoptosis pathway, cytochrome c in germ cells was assessed. After 6 h of culture with 500 or 1000 ng/mL BaP, we observed statistically significant increases in the percentages of germ cells with diffuse cytochrome c immunofluorescence, indicative of release into the cytosol, as opposed to punctate, which would indicate mitochondria-localized cytochrome c (P=0.001, effect of experimental group by Kruskal Wallis test; Figure 2.3C, D). Together these data support and expand on our previous findings to demonstrate that a primary mechanism of BaP-induced germ cell death in the embryonic ovary occurs through DNA damage and subsequent initiation of mitochondrial-mediated apoptosis, resulting in the F1 females being born with fewer oocytes. However, the E13.5 ovary is heterogenous with some oocytes entering meiosis; this led us to question if there is a more sensitive developmental window for exposure to BaP.

Gestational BaP exposure hastened onset of puberty in F1 females and induced equivalent germ cell depletion following exposure during germ cell proliferation or meiosis windows

F1 females were followed for onset of puberty by assessing vaginal opening and first estrus by vaginal cytology, with onset of puberty being defined as first estrus (Safranski *et al.*, 1993). The results for onset of puberty and estrous cyclicity are in Table 2.1. We observed that females exposed to BaP during either developmental window had about 2-day earlier onset of puberty than control females (P=0.005, effect of BaP by GEE); however, we observed no statistically significant effects on body weight or estrous cyclicity. These data demonstrate that 5-day gestational BaP exposure from E6.5-11.5 or E12.5-17.5 hastens the onset of puberty.

Table 2.1 Effects of Gestational BaP on F1 Age at Puberty and Estrous Cyclicity

Treatment	N	Avg age at onset of puberty (PND)*	Avg bodyweight at onset of puberty (g)	# Not Cycling (N of group)	Mean SEM cycle length (days)	Mean SEM % days with leukocytic cytology	Mean SEM % days with cornified cytology
Oil 6.5	8	36.5	29.4		4.3	50.52	28.48
Oil 12.5	5	38.6	27.5		6.2	38.2	42.24
BaP 6.5	9	35.9	27.7		5.8	38.98	43.18
BaP 12.5	12	35.4	28.8		4.9	40.66	38.5

*P=0.005, effect of BaP, GEE. N refers to the number of F0 dams per treatment.

To determine if gestational BaP exposure depletes germ cells differentially during proliferative or meiotic windows, one female pup per F0 dam was sacrificed on the day of first estrus, and their ovaries were prepared for histomorphometry. A blinded investigator assessed small follicle counts every fifth section using stereology methods previously described (Myers *et al.*, 2004; Luderer *et al.*, 2022) and large follicles were counted in every section. We observed that gestational BaP exposure resulted in equivalent depletion of primordial (Oil6.5: 2803 533, Oil12.5: 3055 886, BaP6.5: 1138 336, BaP12.5: 1266 274; P<0.001, effect of BaP by 2-way ANOVA), primary (Oil6.5: 366 55, Oil12.5: 546 163, BaP6.5: 247 67, BaP12.5: 289 44; P=0.018, effect of BaP by 2-way ANOVA), and secondary follicles (Oil6.5: 99 11, Oil12.5: 107 12, BaP6.5: 58 9, BaP12.5: 62 11; P<0.001, effect of BaP by 2-way ANOVA), but not antral follicles (Oil6.5: 11 2, Oil12.5: 11 1.5, BaP6.5: 8 1.6, BaP12.5: 10 1.7) regardless of exposure window (Figure 2.4). Additionally, we observed no difference in atretic follicle numbers (data not shown). Although there was a slight decrease in healthy antral follicle numbers, it was not statistically significant. This is likely because pubertal ovaries have fewer antral follicles on average, and it is possible that we would see a difference in adult ovaries. These data show that proliferative and meiotic germ cell developmental windows are equally sensitive to BaP-induced germ cell death during F1 ovarian development.

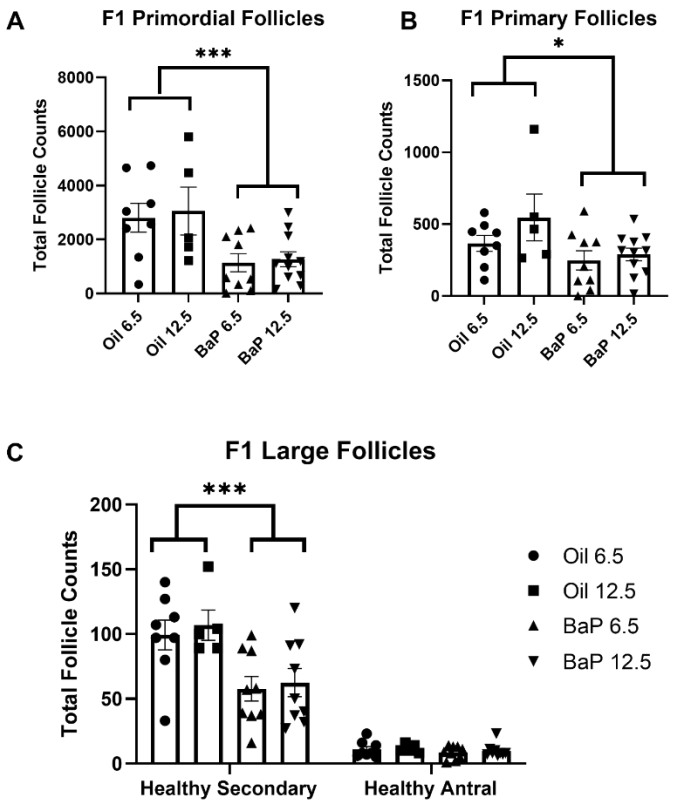

Figure 2.4: Gestational BaP exposure decreased primordial, primary, and secondary follicles in F1 pubertal ovary regardless of exposure window (E6.5-11.5 or E12.5-17.5). Total number of primordial **(A)**, primary **(B)**, and secondary **(C)** follicles in the F1 ovaries on 1st estrus were significantly decreased following BaP exposure during both developmental windows, but no difference in the total number of antral follicles **(C)** was observed. (N= 8 F0 dams, Oil6.5; N=5 Oil12.5; N=9, BaP6.5; N=10, BaP12.5, ***P<0.001, *P<0.05, effect of BaP treatment by two-way ANOVA).

Gestational BaP oxidatively damages DNA and lipids in pubertal ovaries and oocytes

We have demonstrated that BaP gestational and *in vitro* exposure depletes germ cells in F1 pubertal ovaries. To characterize if gestational BaP exposure leads to persistent oxidative damage in F1 pubertal ovaries we assessed ovarian sections for presence of ovarian histone 2A phosphorylation (γH2AX) and lipid peroxidation indicated by presence of 4-hydroxynonenal (4-HNE). 4-HNE is the product from the oxidation of lipids containing polyunsaturated omega-6 acyl groups and is a reliable marker for lipid peroxidation (Dalleau *et al.*, 2013).

We observed borderline statistically significant effects on ovarian histone 2A phosphorylation in the primordial, primary, and secondary follicle oocytes and in primary follicle granulosa cells from exposed females compared to control females (P=0.099, P=0.046, P=0.068, and P=0.097, respectively by Kruskal-Wallis nonparametric test, Table 2.2, Figure 2.5). Intergroup comparisons revealed that the fraction of ɣH2AX-positive primordial and primary follicle oocytes was decreased in the BaP12.5 compared to Oil12.5 ovaries (P=0.010, P=0.035, respectively, Mann Whitney test), and the fraction of ɣH2AX-positive primary follicle oocytes was decreased in the BaP6.5 compared to Oil6.5 ovaries (P=0.033, Mann Whitney test). Intergroup comparisons revealed that the fraction of primary follicles with ɣH2AX-positive granulosa cells was decreased in Bap12.5 compared to Oil12.5 (P=0.035, Mann Whitney test). We observed no effect of prenatal BaP on ɣH2AX in antral follicles.

Table 2.2 Effects of gestational BaP exposure on ovarian γH2AX immunostaining at puberty

	% Follicles with positive granulosa cells:			% Positive Oocytes			
	Primary ± SEM[a]	**Secondary ± SEM**	**Antral ± SEM**	**Primordial ± SEM[b]**	**Primary ± SEM[c]**	**Secondary ± SEM[d]**	**Antral ± SEM**
Oil 6.5	11 ± 5	72 ± 5	50 ± 29	60 ± 6	82 ± 6	74 ± 5	50 ± 29
Oil 12.5	22 ± 7	47 ± 14	57 ± 8	64 ± 3	84 ± 10	35 ± 9	37 ± 12
BaP 6.5	8 ± 3	47 ± 10	64 ± 11	46 ± 10	45 ± 15*	50 ± 12	51 ± 13
BaP 12.5	4 ± 3*	63 ± 7	47 ± 18	47 ± 4*	61 ± 9*	62 ± 11	33 ± 17

N=4, Oil6.5; N=5, Oil12.5; N=6, BaP6.5 and BaP12.5. [a]P=0.097, [b]P=0.099, [c]P= 0.046, [d]P=0.068, effect of experimental group, Kruskal-Wallis, *P<0.05 versus Oil same dosing window, Mann Whitney test.

In addition to oxidative DNA damage, lipid peroxidation is another form of oxidative damage. To test whether BaP exposure *in utero* results in persistent oxidative damage in the ovary we performed immunostaining with an antibody against 4-HNE and found that prenatal BaP exposure during both exposure windows increased lipid peroxidation levels in pubertal ovaries (P<0.05, effect of BaP, GEE; Figure 2.6A, B). However, we saw no change in the neutral lipid content across all

treatment groups (Figure 2.6C, D). These data show that gestational BaP exposure results in persistent oxidative damage in F1 ovaries in the form of ovarian lipid peroxidation regardless of exposure window.

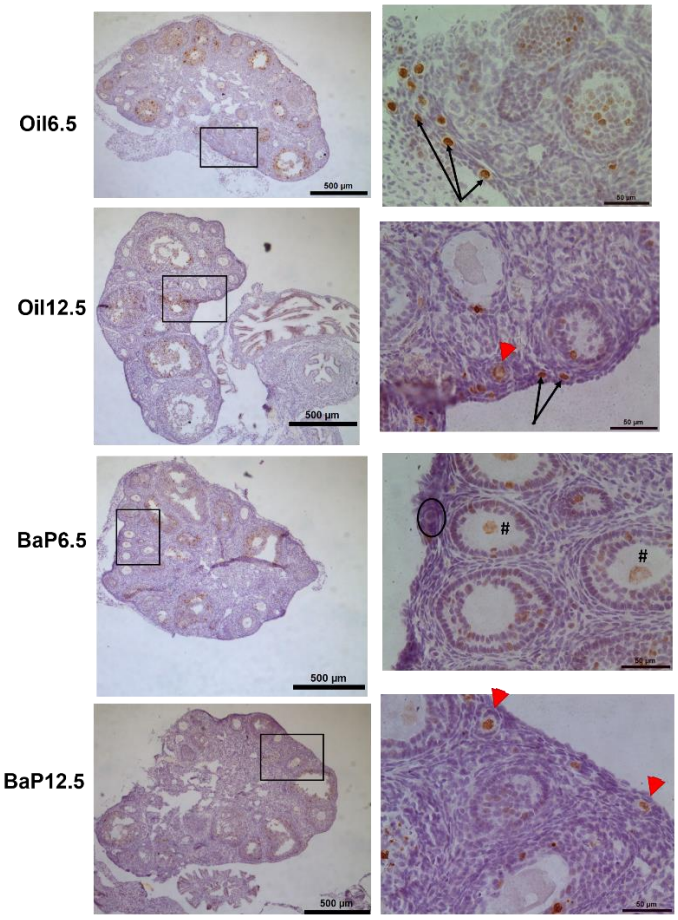

Figure 2.5: Representative images of γH2AX IHC in F1 pubertal ovaries. γH2AX is the brown staining. Left panel image taken at with a 10X objective. Right panel image taken with a 40X objective. Black arrows point to positive primordial oocytes, red arrowheads points to positive primary oocyte, circle encompasses a negative primordial follicle, (#) shows positive secondary follicle and oocyte. Left panel scale bar = 200 µm. Right panel scale bar 50 µm.

Gestational BaP exposure alters mature F1 oocyte quality through increased oxidative stress and decreased lipid droplet content

Previous studies have shown that lipids, more specifically LDs, and their metabolism play a significant role in determining mature oocyte quality (Paczkowski *et al.*, 2014; Valsangkar and

Downs, 2013) and that oocyte LD content is regulated by the surrounding granulosa and cumulus cells, as well as the follicular fluid (Zhang *et al.*, 2020). We were interested in exploring how the increased lipid peroxidation in BaP6.5 ovaries affected mature oocyte LD content and ovulated oocyte oxidative state. The BaP6.5 window was chosen because we had observed no differences in effects on ovarian follicle counts or oxidative lipid damage between the two exposure windows.

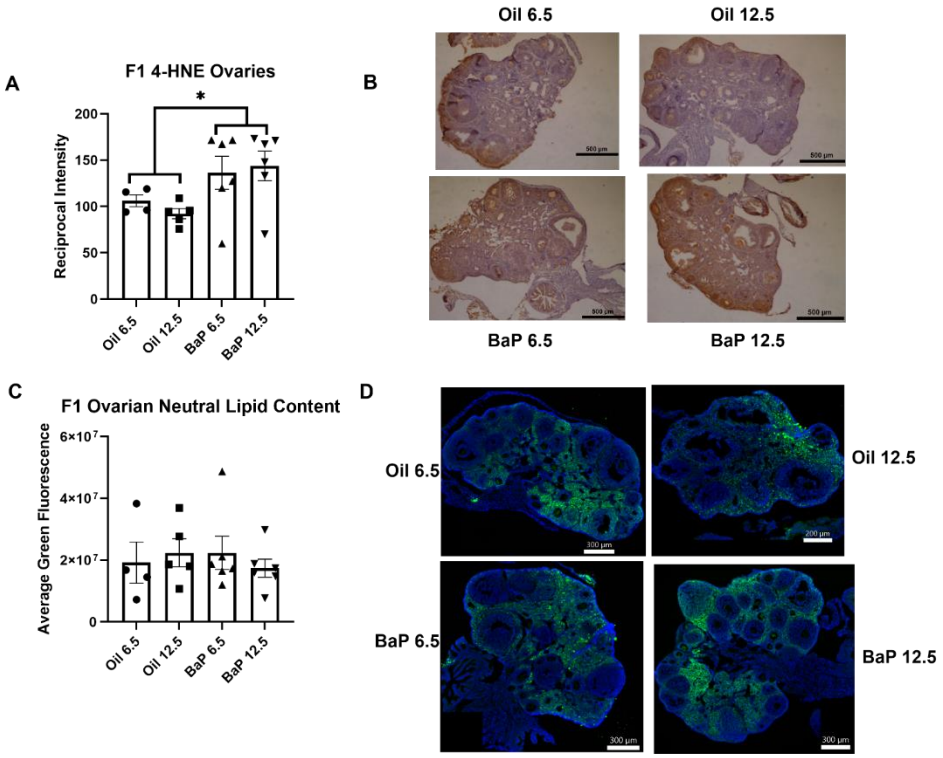

Figure 2.6: Gestational BaP exposure results in persistent oxidative stress in F1 ovaries but has no effect on ovarian neutral lipid content. A) 4-HNE immunostaining intensity estimated per total ovarian section area using reciprocal intensity shows persistently increased lipid peroxidation following gestational exposure regardless of exposure window (N=4-5 F0 dams, oil treatment; N=6 F0 dams, BaP treatment, *P<0.05, effect of BaP by two-way ANOVA). **B)** Representative 4-HNE immunostaining (brown color). **C)** Quantification of neutral lipid content in ovarian sections stained with BODIPY 493/503 showed no treatment or exposure window related differences in neutral lipid content. **D)** Representative images of BODIPY 493/503 sections, counterstained with DAPI. Neutral lipids fluoresce green.

BaP6.5 and Oil6.5 pubertal females were superovulated and their morphologically healthy, mature oocytes were assessed for indications of oxidative stress. There were no statistically significant differences in number of healthy MII oocytes ovulated between treatment groups (Oil6.5:

13.7 ± 2.5, BaP6.5: 10.9 ± 2.7 N=9 litters/treatment). We measured mitochondrial superoxide production using MitoSOX and we observed a significant increase in superoxide production in oocytes of BaP6.5 females compared with Oil6.5 (P=0.006, GEE, Figure 2.7A). Intriguingly, discordant with the increase in lipid peroxidation in BaP6.5 ovaries, we observed no difference in lipid peroxidation in the mature oocytes between treatment groups, measured as oxidized: unoxidized lipid ratio (Oil6.5: 2.05 ± 0.05, BaP6.5: 1.92 ± 0.37, N=3 females/treatment). Nor did we observe differences in whole oocyte GSH levels between treatment groups, measured by monochlorobimane fluorescence (Oil6.5: 57705.7 ± 4572.9, BaP6.5: 56945.01 ± 771.1, N=3 females/treatment). Together these data suggest that gestational BaP exposure results in persistent oxidative stress in the mitochondria but has no effect on the oxidation state of lipids in the mature oocyte.

To further explore indicators of mitochondrial oxidative stress, we assessed mitochondrial membrane potential ($\Delta\Psi m$) in the whole oocyte. Using the fluorescent probe, JC-1, we observed a statistically significant decrease in $\Delta\Psi m$ in BaP6.5 oocytes compared with Oil6.5 (P=0.04, GEE; Figure 2.7B, C). Membrane potential in the mitochondria is created by the pumping of protons across the inner membrane by the Complexes I, III, and IV of the electron transport chain. Complexes I and III are primary sources of superoxide; therefore, decreased $\Delta\Psi m$ further supports that gestational BaP exposure resulted in increased mitochondrial oxidative stress. Additionally, we observed no difference in oocyte mitochondrial content between the two treatments (Figure 2.7D), affirming that any changes in $\Delta\Psi m$ did not result from a decrease in mitochondria following exposure. Additionally, we interrogated differences in mitochondrial clustering patterns in BaP-exposed and control oocytes to further our understanding of the oocyte oxidative stress response. We observed no significant effect of BaP on mitochondrial clustering (Figure 2.7E).

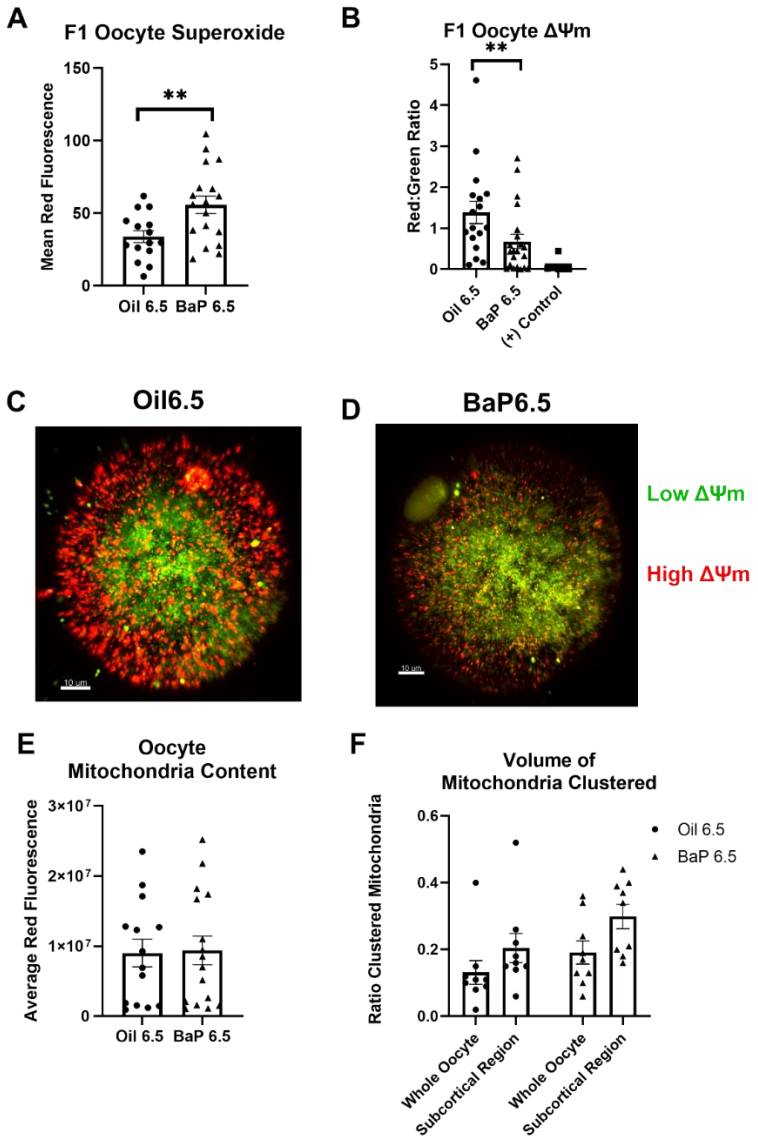

Figure 2.7: Gestational BaP exposure results in persistent oxidative stress in F1-derived superovulated MII oocytes A) Mean red fluorescence intensity of MitoSOX demonstrates increased mitochondrial superoxide anion in oocytes of females exposed to BaP during the proliferative developmental window from E6.5-11.5 (N=9, F0 dams per oil and N=8, F0 dams per BaP; **P=0.006, effect of BaP by GEE). **B)** Mitochondrial membrane potential (ΔΨm), measured using JC-1 shows that oocytes of females exposed to gestational BaP during the proliferative, developmental window have reduced ΔΨm compared to oocytes from oil control females. Positive control oocytes were exposed to 1 μM of CCCP (carbonyl cyanide 3-chlorophenylhydrazon), a known mitochondrial uncoupler, which breaks down the ΔΨm (N=8 F0 dams, oil; N=9 F0 dams, BaP; N=5; positive control; *P=0.04, effect of BaP by GEE). **C and D)** Representative images of ΔΨm from control (C) and BaP (D) exposed mice (red= high ΔΨm, green= low ΔΨm, scale bar= 10 μm). **E)** Mitochondrial content of MII oocytes estimated by red fluorescence of Mitotracker Deep Red was not affected by prenatal BaP treatment (P=0.17, effect of BaP, ANOVA with oocyte as random effect. **F)** Ratio of clustered mitochondrial volume in whole oocyte and subcortical region was not affected by prenatal BaP treatment (N=9 F0 dams/treatment, P>0.50, effect of BaP, GEE). Individual data points for **(A), (B), (E),** and **(F)** represent measurements from individual oocytes.

ROS, including superoxide, react stochastically with the first molecules they contact, thus oxidizing them. Mitochondria are often found to be colocalized with LDs (Benador *et al.*, 2018, 2019), therefore we found it curious that despite increased superoxide production and decreased ΔΨm, there were no observable changes in lipid peroxidation in BaP6.5 oocytes. To this end, we assessed neutral lipid content and mitochondria:LD colocalization in these oocytes. Using the neutral lipid stain, BODIPY 493, we observed that average LD volume in BaP6.5 oocytes was significantly smaller compared with Oil6.5 ($P<0.001$, effect of BaP, GEE; Figure 2.8A, C). To characterize mitochondria:LD colocalization, we used Mitotracker Deep Red and BODIPY 493. We observed that even though there was no difference in mitochondria content between BaP and control oocytes (Figure 2.7D), BaP6.5 oocytes had borderline significantly decreased proportion of mitochondria colocalized with LDs compared with Oil6.5 ($P=0.075$, GEE; Figure 2.8B, C), and the LDs colocalized with the mitochondria were statistically significantly smaller in volume in exposed oocytes ($P<0.001$, GEE; Figure 2.8A, C). Together, these data show that BaP exposure *in utero* increases mitochondrial oxidative stress and decreases LD content in mature F1-derived oocytes.

Discussion

We observed a significant increase in γH2AX-positive oocytes, a non-significant increase in ovarian PUMA expression, and a significant increase in oocytes positive for cytochrome c release in E13.5 ovaries cultured with BaP. Exposure to gestational BaP at 2 mg/kg/day hastened the onset of puberty in F1 females and resulted in equivalent depletion of healthy primordial, primary, and secondary follicles regardless of prenatal mitotic or meiotic exposure window. Expression of the lipid peroxidation marker 4-HNE was also significantly increased in both BaP6.5 and BaP12.5 F1 pubertal ovaries compared with Oil controls. Interestingly, in contrast to the E13.5 ovary, F1 pubertal ovaries had significantly (primordial follicle oocytes) or borderline significantly decreased γH2AX-positive primary follicle granulosa cells and oocytes, as well as primordial follicle oocytes. Gestational BaP exposure during the mitotic window resulted in oocytes with decreased average LD volume,

mitochondria:LD colocalization, and ΔΨm and increased mitochondrial superoxide levels compared with control oocytes.

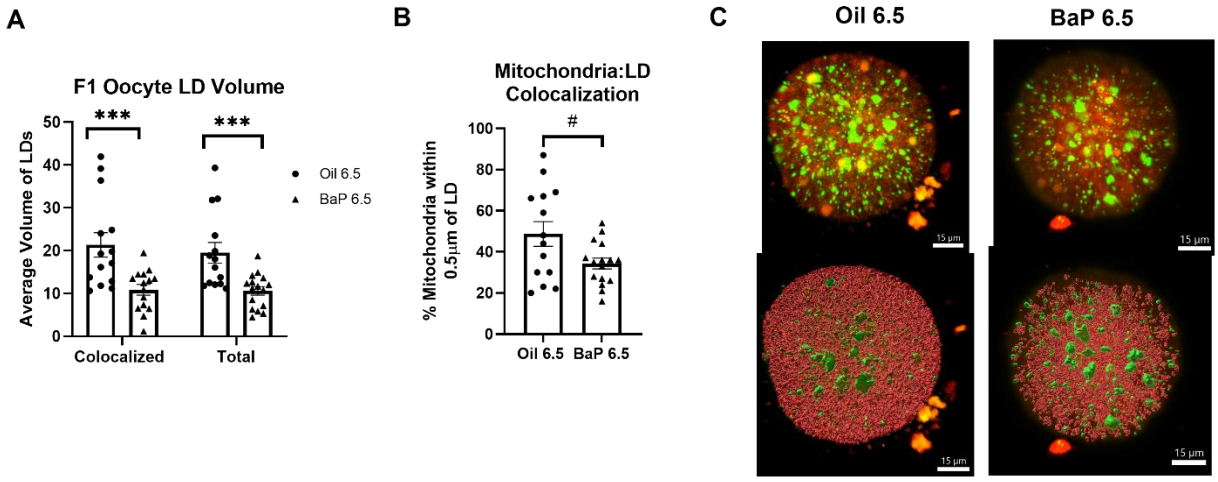

Figure 2.8: Gestational BaP exposure significantly decreases oocyte LD content A). Average volume of a single LD in the whole oocyte and in the subpopulation colocalized with mitochondria, estimated using Imaris imaging software to build 3D volumes from 3D rendered z-stack images, is significantly decreased in oocytes from females exposed to BaP during E6.5-11.5 (N=9 F0 dams/group, ***P<0.001, effect of BaP by GEE). **B)** Estimation of the percent of mitochondria colocalized with LDs estimated using Imaris to generate 3D volumes. Mitochondrial volumes within 0.5 µm of an LD volume were considered to be colocalized with LDs. Colocalization of mitochondria with LDs is decreased in gestationally exposed oocytes (N=9 F0 dams/ treatment #P= 0.075, effect of BaP by GEE). Individual data points for **(A), (B)** represent measurements from individual oocytes. **C)** Representative images of Mitotracker Deep Red and BODIPY 493/503 co-staining in oocytes (top panel). Representative images of Imaris volume renderings (bottom panel).

Together with our previously published data (Lim *et al.*, 2016; Lim and Luderer, 2018), the current data demonstrate that BaP-induced germ cell death in the developing ovary is mediated through the mitochondrial apoptosis pathway. A myriad of signals can induce activation of this pathway including, but not limited to, oxidative stress and DNA damage. In the present study, we observed an increase in the marker for DNA DSBs, γH2AX, in the germ cells of E13.5 ovaries cultured with BaP for 6 h (Figure 2.2). Some oogonia begin to progressively enter meiosis at E13.5, after completing their migration to the gonadal ridge; therefore, each γH2AX-positive oocyte was categorized by meiosis stage. Chromosomal crossover occurs during the pachytene stage of meiosis

I; we observed no differences in the percentages of γH2AX-positive oocytes among any of the treatment groups in the pachytene stage. Instead, a significant increase in γH2AX-positive oocytes in interphase and leptotene stages was observed (Figure 2.2B). These data show that BaP significantly increases DNA DSBs in oocytes, possibly due to increased oxidative stress. DNA damage is known to induce the mitochondrial apoptosis pathway. Our previous work showed that embryonic ovaries were more sensitive than the embryonic testis to BaP-induced germ cell death and that this cell death was likely mediated through the mitochondria with a concentration-dependent increase in BAX at 6 h and cleaved caspase -9 and -3 at 24 h in culture (Lim *et al.*, 2016). Additionally, in a subsequent study we observed that cultured embryonic ovaries deficient in the antioxidant glutathione were more sensitive to BaP-induced oocyte death than wildtype embryonic ovaries (Lim and Luderer, 2018).

In the current study we assessed E13.5 ovaries for PUMA (also known as BCL2-binding component 3, BBC3) protein expression. PUMA protein is diffusely present in the E13.5 ovary, and its deletion increases the size of the germ cell pool at E13.5 and of the primordial follicle pool at postnatal day 10 (Myers *et al.*, 2014). As a pro-apoptotic BH3-only BCL2 family protein, PUMA inhibits the anti-apoptosis regulator BCL-2, thus allowing for the formation of BAX pores in the mitochondria, which triggers the release of cytochrome c into the cytosol (Han *et al.*, 2001; Nakano and Vousden, 2001). PUMA is required for induction of germ cell apoptosis in the post-natal day 5 mouse ovary by ionizing radiation exposure (Kerr *et al.*, 2012); therefore, we hypothesized that it might play a role in BaP-induced germ cell apoptosis in the prenatal ovary. BaP exposure slightly increased the expression of PUMA regardless of dose after 6 h (Figure 2.3A, B). The observation of a slight, but non-significant, increase in PUMA expression in BaP-exposed ovaries could be attributed to the timing of exposure; it is possible that an earlier timepoint could have captured a significant increase in PUMA expression in response to BaP exposure. BAX-dependent cytochrome c release is primarily dependent on the concentration of BAX and not on time. Release of cytochrome c has been

detected as early as 5 minutes after BAX channel formation (Eskes *et al.*, 1998). To confirm that BaP exposure does lead to mitochondrial-mediated apoptosis, we performed immunofluorescence to assess cytochrome c release in germ cells. We observed a statistically significant, dose-dependent increase in the percentage of germ cells positive for cytochrome c release, determined by diffuse as opposed to punctate fluorescence signal (Feng *et al.*, 2012; Liu *et al.*, 2003), in E13.5 ovaries exposed to both 1000 and 500 ng/mL of BaP for 6 h compared with DMSO and uncultured controls (Figure 2.3C, D). Together, these data extend previous findings (Lim *et al.*, 2016; Lim and Luderer, 2018; Matikainen *et al.*, 2002), with compelling evidence, that a primary driver of BaP-induced germ cell death is DNA damage, resulting in activation of mitochondrial apoptosis in the embryonic ovary.

We previously showed that exposure *in utero* to 2 mg/kg/day of BaP from E6.5-15.5 hastened the onset of puberty by about 5 days, determined by age at first estrus in comparison to oil controls (Luderer *et al.*, 2017). Additionally, BaP exposure *in utero* during this same developmental window decreased primordial, primary, and secondary follicles in F1 females exposed to 2 and 10 mg/kg/day (Lim *et al.*, 2013; Luderer *et al.*, 2017). This gestational exposure window includes two very distinct germ cell populations. From E7 to E11.5, germ cells proliferate rapidly before and while migrating along the hindgut mesentery to reach the bipotential gonadal ridge. The germ cells continue their rapid proliferation until entering meiosis, beginning at E13.5 (Wear *et al.*, 2016; Findlay *et al.*, 2015). Recently we have shown that both the mouse embryo and placenta are capable of metabolizing BaP, in a sex and dose-dependent manner with female embryos and placentas generating higher metabolite concentrations (ng/g) compared to male embryos following gestational exposure from E6.5-11.5 or 0, 0.2, or 2 mg/kg/day (Lim *et al.*, 2022). What was not explored in the previous studies, was whether one of these distinct germ cell populations was more sensitive to BaP-induced germ cell death than the other. To assess this, we broke up the previous exposure windows into two developmental windows, E6.5-11.5 (proliferative) and E12.5-17.5 (meiotic). Our data show that BaP exposure during either developmental window, proliferative or meiotic, hasten the onset of puberty

(Table 2.1). Additionally, we observed that gestational BaP exposure, regardless of exposure window, decreased primordial, primary, and secondary follicle numbers, but had no effect on antral or atretic follicles at first estrus (Figure 2.4 and data not shown).

Contrary to our hypothesis, we observed decreased granulosa cell and/or oocyte histone 2AX phosphorylation, a marker for DNA DSBs, in primordial and primary follicles of mice exposed *in utero* to BaP at first estrus compared to controls (Table 2.2, Figure 2.5). A recent study using ɣ-irradiated wildtype and apoptosis-deficient mice, found primordial oocytes were highly efficient in repair of DNA DSBs preferentially relying on homologous recombination, reporting a statistically significant increase in ɣH2AX positive primordial oocytes following ɣ-irradiation of PND 10 females at 0.1, 0.2, 0.45, 4.5, or 7 Gy (Stringer *et al.*, 2020). This same study also reported a statistically significant increase in pATM and RAD51 in primordial oocytes following irradiation (Stringer *et al.*, 2020). Our group has shown that heavy ion irradiation increased ovarian 4-HNE, PUMA, and activated caspase 3, resulting in follicle depletion in adult mice (Mishra *et al.*, 2016, 2017), as well as (Mishra *et al.*, 2017). Both studies also documented that irradiation induced DNA DSBs and increased ɣH2AX at 6 h post-exposure (Mishra *et al.*, 2016, 2017). In the present work, we observed a similar increase in ɣH2AX-positive germ cells in embryonic ovaries cultured for 6 h with BaP but decreases in ɣH2AX-positive follicles at puberty. We postulate that a combination of prenatal BaP-induced apoptotic clearance of damaged germ cells combined with induction of DNA repair resulted in the decreased percentages of ɣH2AX-positive oocytes in primordial and primary follicles observed at the pubertal time point.

We observed a statistically significant increase in the lipid peroxidation marker 4-HNE in F1 pubertal ovaries, following exposure during both windows (Figure 2.6A, B). We have previously shown that glutathione-deficient mice show an accelerated age-related decline in ovarian follicles and increased lipid peroxidation measured as immunostaining for 4-HNE compared to their wildtype littermates (Lim *et al.*, 2015). We were surprised to observe equivalent effects of BaP during both

exposure windows, but it is worth addressing that developing germ cells progressively begin to enter meiosis starting on E13.5 while many germ cells are still proliferating (Wear *et al.*, 2016; Findlay *et al.*, 2015). Progressive entry into meiosis in response to retinoic acid signaling from the mesonephros creates a heterogenous population of meiotic and proliferative germ cells (Koubova *et al.*, 2006), making it virtually impossible to fully distinguish exclusively mitotic and exclusively meiotic germ cell populations by exposure window. Therefore, it is possible that the equivalent effect of BaP on lipid peroxidation and follicle depletion during both exposure windows is due to BaP affecting primarily proliferating germ cells during both windows.

Lastly, we explored whether gestational BaP exposure altered oocyte developmental competence in F1 females. Other groups have characterized oxidative stress in the oocytes of female mice following maternal (Sui *et al.*, 2020) and neonatal (Sobinoff *et al.*, 2012) BaP exposure. Sui et al., orally dosed F0 females with 0 or 40 mg/kg/day of BaP in corn oil for 10 days prior to mating. F1 females were superovulated for mature oocytes. They observed that BaP significantly reduced germinal vesicle break down and polar body extrusion (Sui *et al.*, 2020). Further they reported significantly decreased fluorescence intensity of Mitotracker staining, decreased ATP production, and increased ROS production in exposed oocytes. We observed a significant decrease of ΔΨm in oocytes of females exposed to BaP from E6.5-11.5 (Figure 2.7B, C), accompanied by a significant increase in mitochondrial superoxide production (Figure 2.7A) compared with oocytes from control females. Oxidative phosphorylation and the electron transport chain are the primary sources of superoxide and ROS in the cell (Guérin *et al.*, 2001). Complexes I, III, and IV pump protons into the inner membrane space as they transfer electrons from electron donors to acceptors thus creating ΔΨm. Complexes I and III are sources of mitochondrial superoxide. Together these data suggest that gestational BaP exposure induces mitochondrial oxidative stress in the F1-derived oocytes thus leading to a decrease in ΔΨm in a compensatory manner to avoid further ROS generation. In contrast to Sui and colleagues, we did not observe a difference in fluorescence intensity of Mitotracker in the

oocytes derived from females exposed to BaP from E6.5-11.5 (Figure 2.7D). This is likely the result of using a much lower dose and different dosing window compared with Sui et al., who used a dose 20 times higher than the one in the current study with preconception dosing.

Sobinoff et al., exposed PND 4 females to dosing regimen more comparable to ours of 0, 1.5, and 3 mg/kg/day of BaP in sesame oil for 7 days and superovulated the F1 females at 6-weeks-old (Sobinoff *et al.*, 2012). They observed a significant increase in mitochondrial superoxide and lipid peroxidation in oocytes at both 1.5 and 3 mg/kg/day (Sobinoff *et al.*, 2012). Our data shows that gestational BaP exposure increases mitochondrial superoxide, while having no effect on lipid peroxidation. The doses used in these studies are comparable. However, our study used a gestational dosing paradigm, while the Sobinoff et al. study exposed neonatal mice (Sobinoff *et al.*, 2012), leading us to conclude that timing of BaP exposure may modulate the impact of BaP on lipid peroxidation in mature oocytes. We have previously shown that prenatal BaP exposure accelerates age-related ovarian decline (Lim *et al.*, 2013) and others have demonstrated that oocytes exposed to BaP *in vitro* and *in vivo* show signs of decreased developmental competence such as increased incidence of meiotic spindle abnormalities (Zhang *et al.*, 2018), increased ROS (Sui *et al.*, 2020), decreased sperm fusibility (Sobinoff *et al.*, 2012), and increased incidence of aneuploidy (Li *et al.*, 2019) – all of which are accepted signs of aged oocytes (Kushnir *et al.*, 2012; Bianchi *et al.*, 2015). Therefore, it is possible that following gestational exposure the lipids in an oocyte will slowly undergo peroxidation as the female ages, due to persistent oxidative stress in the ovary and oocyte, as evidenced by increased 4-HNE and mitochondrial superoxide, respectively.

We previously reported that glutathione-deficient oocytes have increased oxidative stress, but not increased lipid peroxidation (Malott *et al.*, 2022). We concluded that a possible reason for this was the observed decreased LD content in glutathione-deficient oocytes (Malott *et al.*, 2022). Interestingly, we observed a similar effect of gestational BaP exposure on average LD volume in oocytes (Figure 2.8A, C), with oocytes of females exposed to BaP from E6.5-11.5 possessing smaller

LDs by volume compared with oocytes of control females. LDs have been shown to be of great importance to preimplantation embryonic development (Bradley and Swann, 2019; Dunning *et al.*, 2010; Collado-Fernandez *et al.*, 2012). Delipidated mature oocytes begin producing new LDs through de novo lipogenesis almost immediately, further supporting the significant role that LDs play in oocyte competence (Aizawa *et al.*, 2019). Lipids in the oocytes are stored throughout oogenesis from a combination of sources including de novo synthesis (Aizawa *et al.*, 2019), from granulosa cells (Dunning *et al.*, 2014), and from the follicular fluid which is supplied predominantly from serum (Zhang *et al.*, 2020). BaP exposure has previously been shown to alter lipid metabolism in mice. In a study by Li et al., a single 5 μL dose at 5 mg/mL of BaP in corn oil was administered to mice at the bronchial bifurcation through tracheal instillation (Li *et al.*, 2020). Liver homogenates were analyzed from mice 1, 3, 7, and 21 days post -dosing using UHPLC-HRMS and it was observed that BaP exposure significantly altered hepatic lipid classes with decreased phosphotidylethanolamines, lysophospholipids, free fatty acids, and eicosanoids, and increased phosphotidylinositols, phosphotidylcholines, and triacylgycerols (Li *et al.*, 2020). Triacylglycerols were reported to be the most sensitive to BaP exposure, with their hepatic content increasing 2.2-fold in the first day following exposure, suggesting that BaP exposure significantly increases hepatic triacyglycerol synthesis (Li *et al.*, 2020). Other studies have demonstrated that activation of the aryl-hydrocarbon receptor induces differential regulation of lipid synthesis following exposure (Hu, Pan, *et al.*, 2016; Hu, Wang, *et al.*, 2016; Neuschäfer-rube *et al.*, 2015). These data collectively support the dysregulation of LD storage in the oocyte following gestational BaP exposure.

To further understand the interplay between oocyte mitochondrial oxidative stress and LDs in the oocyte, we analyzed mitochondria: LD colocalization. In the current study we observed that gestational BaP exposure decreased, approaching statistical significance, the percentage of mitochondria that were colocalized with LDs and further, the colocalized LDs were smaller by volume (Figure 2.8A, C). There is still much to discover about the role of LDs in all cell types, especially in

oocytes. Mitochondria colocalized with LDs are referred to as peridroplet mitochondria and depending on the cell type, it is accepted that peridroplet mitochondria can either be lipid consuming (fatty acid β-oxidation) or lipid synthesizing (lipogenesis) (Benador *et al.*, 2018, 2019). It is currently not well understood which category peridroplet mitochondria in mature oocytes fall under; therefore, the implications of the present findings remain unclear. Mature oocytes are predominantly dependent on fatty acid β-oxidation and pyruvate oxidation to produce ATP post-ovulation up until the compacted morula commences glycolysis (Bradley and Swann, 2019). Both processes depend on endogenous lipid stores. Lipoic acid is an important cofactor of several mitochondrial enzymes including pyruvate dehydrogenase (Nowinski *et al.*, 2018). These important roles of lipids in oocytes, likely underly why otherwise healthy but delipidated oocytes are so efficient at de novo lipid synthesis (Aizawa *et al.*, 2019). Together with our observation in the current study that BaP exposure increased mitochondrial superoxide and decreased ΔΨm in mature oocytes (Figure 2.7), these data support that gestational BaP exposure results in persistent oxidative stress in mature, ovulated oocytes, ultimately reducing developmental competence.

This study reported an in-depth characterization of BaP toxicity on oocytes from the embryonic to postnatal ovary and explored persistent effects of gestational BaP on the F1 ovary and mature F1 oocytes. We confirm, using novel immunofluorescence microscopy, that *in vitro* BaP exposure induces cytochrome c release in the E13.5 ovary, mediating mitochondrial apoptosis. Further we report that both windows of embryonic ovarian development are equally sensitive to BaP-induced germ cell death and induction of persistent oxidative damage in the ovary. To our knowledge, we are the first to characterize and report on persistent oxidative stress following gestational BaP exposure, resulting in ovarian damage and reduced developmental competence. In this current study we were unable to fully characterize the metabolic profile of BaP-exposed oocytes. Future studies should perform a detailed analysis of metabolic endpoints of oocytes exposed to gestational BaP, including oxygen consumption rate of oocytes and embryos.

Acknowledgements

This research would not have been possible without the University of California, Irvine Optical Biology Core for providing training on and access to the LSM780 confocal microscope used to image live and fixed oocytes, Elyra 7 confocal microscope for imaging E13.5 cytochrome C immunofluorescence, and for Imaris imaging software. We thank Laura Ortiz, Jinhwan Lim, and Jana Chen for assistance with dosing and vaginal cytology.

Funding Statement

Grant Support: National Institutes of Health (NIH) R01ES020454 and R21HD097541 to U.L. Tobacco Related Diseases Research Program Predoctoral Fellowship T30DT0816 to K.F.M. UC Irvine Summer Undergraduate Research Program fellowship to M.L. NIH Initiative for Minority Success GM055246 to K.L.P. The authors wish to acknowledge the support of the UC Irvine Chao Family Comprehensive Cancer Center Optical Biology Shared Resource, supported by the National Cancer Institute of the NIH under award number P30CA062203.

The content is solely the responsibility of the authors and does not necessarily represent the official views of the National Institutes of Health.

Conflicts of Interest

The authors have no conflicts of interest to declare.

Author Contributions

KFM obtained funding, designed, and performed experiments, analyzed data, drafted manuscript. KL, ML, and ES performed experiments, analyzed data. UL conceived of overall idea, obtained funding, analyzed data, edited the manuscript.

Data Availability

The data underlying this article will be shared on reasonable request to the corresponding author.

References

Adhikari, D. *et al.* (2022) Oocyte mitochondria—key regulators of oocyte function and potential therapeutic targets for improving fertility. *Biol. Reprod.*, **106**, 366–377.

Aizawa, R. *et al.* (2019) Synthesis and maintenance of lipid droplets are essential for mouse preimplantation embryonic development. *Development*, **146**.

Benador, I.Y. *et al.* (2018) Mitochondria Bound to Lipid Droplets Have Unique Bioenergetics, Composition, and Dynamics that Support Lipid Droplet Expansion. *Cell Metab.*, **27**, 869-885.e6.

Benador, I.Y. *et al.* (2019) Review Mitochondria Bound to Lipid Droplets : Where Mitochondrial Dynamics Regulate Lipid Storage and Utilization. *Cell Metab.*, **29**, 827–835.

Bianchi, S. *et al.* (2015) Ultrastructural markers of quality are impaired in human metaphase II aged oocytes: a comparison between reproductive and in vitro aging. *J. Assist. Reprod. Genet.*, **32**, 1343–1358.

Bradley, J. and Swann, K. (2019) Mitochondria and lipid metabolism in mammalian oocytes and early embryos. *Int. J. Dev. Biol.*, **63**, 93–103.

Chiaratti, M.R. *et al.* (2018) The role of mitochondria in the female germline: Implications to fertility and inheritance of mitochondrial diseases. *Cell Biol. Int.*, **42**, 711–724.

Collado-Fernandez, E. *et al.* (2012) Metabolism throughout follicle and oocyte development in mammals. *Int. J. Dev. Biol.*, **56**, 799–808.

Cooper, R.L. *et al.* (1993) Monitoring of the Estrous Cycle in the Laboratory Rodent by Vaginal Lavage. Heindel JJ, Chapin RE eds. *Female Reproductive Toxicology.* San Diego: Academic Press, Inc; 45-55.

Coticchio, G. *et al.* (2004) What Criteria for the Definition of Oocyte Quality? *Ann. N.Y. Acad. Sci.* **144**, 132–144.

Dalleau, S. *et al.* (2013) Cell death and diseases related to oxidative stress:4-hydroxynonenal (HNE) in the balance. *Cell Death Differ.*, **20**, 1615–1630.

Devine, P.J. *et al.* (2012) Roles of Reactive Oxygen Species and Antioxidants in Ovarian Toxicity1. *Biol. Reprod.*, **86**, 1–10.

Dunning, K.R. *et al.* (2010) Beta-Oxidation Is Essential for Mouse Oocyte Developmental Competence and Early Embryo Development. *Biol. Reprod.*, **83**, 909–918.

Dunning, K.R. *et al.* (2014) Lipids and oocyte developmental competence: the role of fatty acids and β-oxidation. *Reproduction*, **148**, R15–R27.

Eling, T.E. *et al.* (1990) Prostaglandin h synthase and xenobiotic oxidation. *Annu. Rev. Pharmacol. Toxicol.*, **30**, 1–45.

Eskes, R. *et al.* (1998) Bax-induced cytochrome C release from mitochondria is independent of the permeability transition pore but highly dependent on Mg^{2+} ions. *J. Cell Biol.*, **143**, 217–224.

Feng, R. *et al.* (2012) Apaf-1 deficiency confers resistance to ultraviolet-induced apoptosis in mouse embryonic fibroblasts by disrupting reactive oxygen species amplification production and mitochondrial pathway. *Free Radic. Biol. Med.*, **52**, 889–897.

Ferraro, E. *et al.* (2003) Physiological and pathological roles of Apaf1 and the apoptosome. *J. Cell. Mol. Med.*, **7**, 21–34.

Findlay, J.K. *et al.* (2015) How is the number of primordial follicles in the ovarian reserve established?. *Biol. Reprod.*, **93**, 1–7.

Forman, H.J. *et al.* (2009) Glutathione: Overview of its protective roles, measurement, and biosynthesis. *Mol Asp. Med*, **30**, 1–12.

Guérin, P. *et al.* (2001) Oxidative stress and protection against reactive oxygen species in the pre-implantation embryo and its surroundings. *Hum. Reprod. Update*, **7**, 175–189.

Gulyas, B.J. and Mattison, D.R. (1979) Degeneration of mouse oocytes in response to polycyclic aromatic hydrocarbons. *Anat. Rec.*, **193**, 863–881.

Han, J. *et al.* (2001) Expression of bbc3 , a pro-apoptotic BH3-only gene , is regulated by diverse cell death and survival signals. *Proc. Natl. Acad. Sci.*, **98**, 11318–11323.

Hu, T., Wang, D., *et al.* (2016) Aryl hydrocarbon receptor negatively regulates lipid synthesis and involves in

cell differentiation of SZ95 sebocytes in vitro. *Chem. Biol. Interact.*, **258**, 52–58.

Hu, T., Pan, Z., *et al.* (2016) Benzo(a)pyrene induces interleukin (IL) -6 production and reduces lipid synthesis in human SZ95 sebocytes via the aryl hydrocarbon receptor signaling pathway. *Environ. Toxicol. Pharmacol.*, **43**, 54–60.

Jarc, E. and Petan, T. (2019) Lipid droplets and the management of cellular stress. *Yale J. Biol. Med.*, **92**, 435–452.

Kasianowicz, J. *et al.* (1984) The kinetic mechanism by which CCCP (carbonyl cyanide m-chlorophenylhydrazone) transports protons across membranes. *J. Membr. Biol.*, **82**, 179–190.

Kerr, J.B. *et al.* (2012) DNA damage-induced primordial follicle oocyte apoptosis and loss of fertility require TAp63-mediated inducation of Puma and Noxa. *Mol Cell.*, **48**, 343–352.

Kinner, A. *et al.* (2008) Gamma-H2AX in recognition and signaling of DNA double-strand breaks in the context of chromatin. *Nucleic Acids Res.*, **36**, 5678–5694.

Koubova, J. *et al.* (2006) Retinoic acid regulates sex-specific timing of meiotic initiation in mice. *Proc. Natl. Acad. Sci.*, **103**, 2474–2479.

Kushnir, V.A. *et al.* (2012) Reproductive aging is associated with decreased mitochondrial abundance and altered structure in murine oocytes. *J. Assist. Reprod. Genet.*, **29**, 637–642.

Láscarez-Lagunas, L. *et al.* (2020) SnapShot: Meiosis – Prophase I. *Cell*, **181**, 1442-1442.e1.

Li, F. *et al.* (2020) Hepatotoxic effects of inhalation exposure to polycyclic aromatic hydrocarbons on lipid metabolism of C57BL/6 mice. *Environ. Int.*, **134**, 105000.

Li, W.D. *et al.* (2019) Melatonin defends mouse oocyte quality from benzo[ghi]perylene-induced deterioration. *J. Cell. Physiol.*, **234**, 6220–6229.

Lim, J. *et al.* (2015) Glutamate cysteine ligase modifier subunit (Gclm) null mice have increased ovarian oxidative stress and accelerated age-related ovarian failure. *Endocrinology*, **156**, 3329–3343.

Lim, J. *et al.* (2013) Glutathione-deficient mice have increased sensitivity to transplacental benzo[a]pyrene-

induced premature ovarian failure and ovarian tumorigenesis. *Cancer Res.*, **73**, 908–917.

Lim, J. *et al.* (2022) Sex differences in embryonic gonad transcriptomes and benzo[a]pyrene metabolite levels after transplacental exposure. **163**, 1–17.

Lim, J. *et al.* (2016) The mouse fetal ovary has greater sensitivity than the fetal testis to benzo[a]pyrene-induced germ cell death. *Toxicol. Sci.*, **152**, 372–381.

Lim, J. and Luderer, U. (2018) Glutathione deficiency sensitizes cultured embryonic mouse ovaries to benzo[a]pyrene-induced germ cell apoptosis. *Toxicol. Appl. Pharmacol.*, **352**, 38–45.

Liu, L. *et al.* (2003) Oxidative stress contributes to arsenic-induced telomere attrition, chromosome instability, and apoptosis. *J. Biol. Chem.*, **278**, 31998–32004.

Luderer, U. *et al.* (2022) Exposure to environmentally relevant concentrations of ambient fine particulate matter (PM2.5) depletes the ovarian follicle reserve and causes sex-dependent cardiovascular changes in apolipoprotein E null mice. *Part. Fibre Toxicol.*, **19**, 1–21.

Luderer, U. *et al.* (2017) Ovarian effects of prenatal exposure to benzo[a]pyrene: Roles of embryonic and maternal glutathione status. *Reprod. Toxicol.*, **69**, 187–195.

Malott, K.F. *et al.* (2022) Glutathione deficiency decreases lipid droplet stores and increases reactive oxygen species in mouse oocytes. *Biol. Reprod.*, 1–14.

Matikainen, T.M. *et al.* (2002) Ligand activation of the aromatic hydrocarbon receptor transcription factor drives Bax-dependent apoptosis in developing fetal ovarian germ cells. *Endocrinology*, **143**, 615–620.

Mattison, D.R. (1980) Morphology of oocyte and follicle destruction by polycyclic aromatic hydrocarbons in mice. *Toxicol. Appl. Pharmacol.*, **53**, 249–259.

Mattison, D.R. and Thorgeirsson, S.S. (1979) Ovarian aryl hydrocarbon hydroxylase activity and primordial oocyte toxicity of polycyclic aromatic hydrocarbons in mice. *Cancer Res.*, **39**, 3471–3475.

Mishra, B. *et al.* (2016) Charged iron particles, components of space radiation, destroy ovarian follicles. *Hum. Reprod.*, **31**, 1816–1826.

Mishra, B. *et al.* (2017) Very low doses of heavy oxygen ion radiation induce premature ovarian failure. *Reproduction*, **154**, 123–133.

Motta, P.M. *et al.* (2000) Mitochondrial morphology in human fetal and adult female germ cells. *Hum. Reprod.*, **15**, 129–147.

Myers, M. *et al.* (2004) Methods for quantifying follicular numbers within the mouse ovary. *Reproduction*, **127**, 569–580.

Myers, M. *et al.* (2014) PUMA regulates germ cell loss and primordial follicle endowment in mice. *Reproduction*, **148**, 211–219.

Nakano, K. and Vousden, K.H. (2001) PUMA , a novel proapoptotic gene, is induced by p53. *Mol. Cell*, **7**, 683–694.

Neuschäfer-rube, F. *et al.* (2015) Arylhydrocarbon receptor-dependent mIndy (Slc13a5) induction as possible contributor to benzo[a]pyrene-induced lipid accumulation in hepatocytes. *Toxicology*, **337**, 1–9.

Nowinski, S.M. *et al.* (2018) Impact of mitochondrial fatty acid synthesis on mitochondrial biogenesis. *Curr. Biol.*, **28**, R1212–R1219.

National Research Council (2011) Guide for the Care and Use of Laboratory Animals 8 ed. National Research Council, National Academy of Sciences, National Academies Press.

Orrenius, S. *et al.* (2007) Mitochondrial oxidative stress: Implications for cell death. *Annu. Rev. Pharmacol. Toxicol.*, **47**, 143–183.

Paczkowski, M. *et al.* (2014) Fatty acid metabolism during maturation affects glucose uptake and is essential to oocyte competence. *Reproduction*, **148**, 429–439.

Penning, T.M. *et al.* (1996) Generation of reactive oxygen species during the enzymatic oxidation of polycyclic aromatic hydrocarbon trans-dihydrodiols catalyzed by dihydrodiol dehydrogenase. *Chem. Res. Toxicol.*, **9**, 84–92.

Pepling, M.E. (2012) Follicular assembly: Mechanisms of action. *Reproduction*, **143**, 139–149.

Pepling, M.E. *et al.* (2007) Mouse oocytes within germ cell cysts and primordial follicles contain a Balbiani body. *Proc. Natl. Acad. Sci. U. S. A.*, **104**, 187–192.

Pepling, M.E. and Spradling, A.C. (2001) Mouse ovarian germ cell cysts undergo programmed breakdown to form primordial follicles. *Dev. Biol.*, **234**, 339–351.

Prates, E.G. *et al.* (2014) A role of lipid metabolism during cumulus-oocyte complex maturation: Impact of lipid modulators to improve embryo production. *Mediators Inflamm.*, **2014**, 1–11.

Ramalho-Santos, J. *et al.* (2009) Mitochondrial functionality in reproduction: From gonads and gametes to embryos and embryonic stem cells. *Hum. Reprod. Update*, **15**, 553–572.

Ramalho-Santos, J. and Amaral, S. (2013) Mitochondria and mammalian reproduction. *Mol. Cell. Endocrinol.*, **379**, 74–84.

Safranski, T.J. *et al.* (1993) Correlations among three measures of puberty in mice and relationships with estradiol concentration and ovulation. *Biol. Reprod.*, **48**, 669–673.

Sobinoff, A.P. *et al.* (2012) Jumping the gun: Smoking constituent BaP causes premature primordial follicle activation and impairs oocyte fusibility through oxidative stress. *Toxicol. Appl. Pharmacol.*, **260**, 70–80.

Stringer, J.M. *et al.* (2020) Oocytes can efficiently repair DNA double-strand breaks to restore genetic integrity and protect offspring health. *Proc. Natl. Acad. Sci. U. S. A.*, **117**, 11513–11522.

Sui, L. *et al.* (2020) Maternal benzo[a]pyrene exposure is correlated with the meiotic arrest and quality deterioration of offspring oocytes in mice. *Reprod. Toxicol.*, **93**, 10–18.

Valsangkar, D. and Downs, S.M. (2013) A requirement for fatty acid oxidation in the hormone-induced meiotic maturation of mouse oocytes. *Biol. Reprod.*, **89**, 1–9.

Walther, T.C. and Farese, R. V. (2012) Lipid droplets and cellular lipid metabolism. *Annu. Rev. Biochem.*, **81**, 687–714.

Walther, T.C. and Farese, R. V. (2009) The life of lipid droplets. *Biochim. Biophys. Acta - Mol. Cell Biol. Lipids*, **1791**, 459–466.

Wear, H.M. *et al.* (2016) From primordial germ cells to primordial follicles: A review and visual representation of early ovarian development in mice. *J. Ovarian Res.*, **9**, 1–11.

Xue, W. and Warshawsky, D. (2005) Metabolic activation of polycyclic and heterocyclic aromatic hydrocarbons and DNA damage: A review. *Toxicol. Appl. Pharmacol.*, **206**, 73–93.

Zhang, M. *et al.* (2018) BaP exposure causes oocyte meiotic arrest and fertilization failure to weaken female fertility. *FASEB J.*, **32**, 342–352.

Zhang, X. *et al.* (2020) Study on follicular fluid metabolomics components at different ages based on lipid metabolism. *Reprod. Biol. Endocrinol.*, **18**, 1–8.

Zhong, H. and Yin, H. (2015) Role of lipid peroxidation derived 4-hydroxynonenal (4-HNE) in cancer: Focusing on mitochondria. *Redox Biol.*, **4**, 193–199.

Chapter 3

Employing the use of a representative PAHs molecule, such as BaP, can only allow for so much understanding of the mechanisms that induce ovotoxicity. As reviewed, in the introduction, PAHs exists in mixtures as the result of incomplete combustion and a poster child of real-world containing mixtures of PAHs is PM2.5. Therefore, through a multi-lab collaboration we used a Versatile Aerosol Concentration Enrichment System to expose 4-month-old Apolipoprotein E null (*Apoe -/-*) female mice to a consistent concentration of either PM2.5 or filtered air for 5 h/day, 4 days/week, for 12 weeks for a total of 240 h of exposure. The broader aim of this study was to assess the interaction between air pollution, premature ovarian aging, and development of cardiovascular disease. Wildtype mice do not develop atherosclerosis, however *Apoe-/-* mice do [112]. This experiment was performed 3 times over 3 years (2017, 2018, 2019). Females were sacrificed on the morning of proestrus. Using tissue histology, stereomicroscopy, and standard brightfield microscopy, we assessed ovarian histomorphometry of exposed and control ovaries. We observed that PM2.5-exposed females had significantly decreased primordial, primary, and secondary follicles numbers but no difference in antral follicles.

For my role in this project, I worked within a collaborative team to develop an ultra-high-performance liquid chromatography mass spectrometry (UHPLC-MS) method to measure serum and ovarian levels of 17β-estradiol (E2). Although methodology for immunoassays to measure the presence of steroids have been consistently used in the literature to assess E2 in serum and other tissues, these assays are in fact not reliable for the measurement of E2. This is in part due to the nature of immunoassays, specifically enzyme-linked immunosorbent assays (ELISAs), which rely on a discernable color change indicating

presence and concentration of the antigen in question. Therefore, this type of assay is not sensitive enough to measure the low concentrations of E2 in mouse ovaries or serum. To this end, UHPLC-MS, with an average lower detection limit of around 10 pg/mL for steroids- depending on the machine and conditions used, is a more sensitive and specific option for assessment of E2.

Over the course of 4.5 years, I worked with and learned from 4 different experts on 2 two different UHPLC-MS machines. For the better part of that time, I was spinning my wheels trying to get E2 readings on mouse serum on the less sensitive of the 2 mass specs. Eventually a new collaboration was formed with the Finlayson-Pitts laboratory group that afforded access to a more sensitive UHPLC-MS and the dedication of two very talented chemists.

From here we set out to find the lowest detectable limit of E2 for the instrument using standard curves of E2 derivatized with 1,2-dimethylimidzole-5-sulfonyl chloride to yield E2-DMIS. This process ran into a snag when it came to our attention that the concentrations of our final samples were being calculated improperly by using just strictly concentration. When derivatizing any compound, the number of molecules per sample must be accounted for, as opposed to just standard concentration. This is because when a molecule is derivatized the mass of the molecule increases therefore changing the ultimate meaning of concentration in molarity. After adjusting our sample preparation method including extraction and derivatization to account for the number of molecules as opposed to concentration, we had to – once again – assess our lower limit of detection. This confirmed that the E2 concentration in mouse serum was too low for our limit of detection; however, the ovarian E2 content was within our detectable range.

From here, I worked to adapt our extraction and derivatization method for serum to ovarian homogenates using ovaries collected from adult female wildtype mice on the morning of proestrus, the cycle stage with the highest E2 concentrations, and stored at -80° C. We were soon able to measure estradiol in experimental samples, but the signal was very low – right on the border of our detection limit for most samples in the first cohort we measured, while previous signal and measurement of E2-DMIS from wildtype ovaries was very strong and well above our detectable limit. To ensure that our methodology was not the concern, the E2 was extracted from the ovaries of adult wildtype females sacrificed on the morning of proestrus. E2 was derivatized to E2-DMIS and measured using UHPLC-MS/MS against a standard curve of stock E2-DMIS and a control of known concentration of E2 that underwent the full extraction and derivatization protocol to determine the percent recovery. This was repeated over three separate experimental replicates and demonstrated that our extraction and derivatization was very successful with a percent recovery rate of 86-88%. From here we turned our attention to the mouse model used in the project. Ovarian theca cells, interstitial cells, and corpora lutea strongly express *Apoe* [113]. Interestingly, *Apoe-/-* females have been reported to have significantly lower serum estradiol concentration compared to wildtype littermates, with knockout ovaries also having significantly decreased expression of (*Cyp19a1*), (*Hsd3b*) [114]. We surmised that *ApoE-/-* females likely had lower ovarian E2 concentrations. To ensure reproducibility of our assay we included a wildtype sample for each cohort that was measured.

Using our validated method for measuring ovarian E2 concentrations, we observed no difference between PM2.5 and filtered air exposed ovarian E2 content. This affirms our observations in this project that there were no differences in the antral follicle count

between PM2.5 and filtered air ovaries. However, the estradiol concentration was significantly decreased in *ApoE-/-* ovaries compared with wildtype.

Primary Research Article

Exposure to Environmentally Relevant Concentrations of Ambient Fine Particulate Matter ($PM_{2.5}$) Depletes the Ovarian Follicle Reserve and Causes Sex-Dependent Cardiovascular Changes in Apolipoprotein E Null Mice

Ulrike Luderer*[1,2,3], Jinhwan Lim[1], Laura Ortiz[3], Johnny D Nguyen[3], Joyce H Shin[1,3], Barrett D Allen[1], Lisa S Liao[3], Kelli Malott[1,3], Veronique Perraud[4], Lisa M. Wingen[4], Rebecca J Arechavala[1,3], Bishop Bliss[1,3], David A Herman[3], Michael T Kleinman[1,3]

[1]Department of Environmental and Occupational Health,

[2]Department of Developmental and Cell Biology,

[3]Department of Medicine,

[4]Department of Chemistry, University of California Irvine, Irvine, CA 92617 USA

*Corresponding author: Dr. Ulrike Luderer

Center for Occupational and Environmental Health

100 Theory Drive, Suite 100

Irvine, CA 92617

uluderer@uci.edu

Abstract

Background: Fine particulate matter ($PM_{2.5}$) exposure accelerates atherosclerosis and contains known ovotoxic chemicals. However, effects of exposure to $PM_{2.5}$ on the finite ovarian follicle pool have hardly been investigated, nor have interactions between ovarian and cardiovascular effects. We hypothesized that subchronic inhalation exposure to human-relevant concentrations of $PM_{2.5}$ results in destruction of ovarian follicles via apoptosis induction, as well as accelerated recruitment of primordial follicles into the growing pool. Further, we hypothesized that destruction of ovarian follicles enhances the adverse cardiovascular effects of $PM_{2.5}$ in females.

Results: Hyperlipidemic Apolipoprotein E (*Apoe*) null ovary-intact or ovariectomized female mice and testis-intact male mice were exposed to concentrated ambient $PM_{2.5}$ or filtered air for 12 weeks, 5 days/week for 4h/day using a Versatile Aerosol Concentration Enrichment System. Primordial, primary, and secondary ovarian follicle numbers were decreased by 45%, 40%, and 17%, respectively, in $PM_{2.5}$-exposed ovary-intact mice compared to controls ($P<0.05$). The percentage of primary follicles with granulosa cells positive for the mitosis marker Ki67 was increased in the ovaries from $PM_{2.5}$-exposed females versus controls ($P<0.05$), consistent with increased recruitment of primordial follicles into the growing pool. Exposure to $PM_{2.5}$ increased the percentages of primary and secondary follicles with DNA damage, assessed by γH2AX immunostaining ($P<0.05$). Exposure to $PM_{2.5}$ increased the percentages of apoptotic antral follicles, determined by TUNEL and activated caspase 3 immunostaining ($P<0.05$). Removal of the ovaries and $PM_{2.5}$-exposure exacerbated the atherosclerotic effects of hyperlipidemia in females ($P<0.05$). While there were statistically significant changes in blood pressure and heart rate variability in $PM_{2.5}$-compared to Air-

exposed gonad-intact males and females and ovariectomized females, the changes were not consistent between exposure years and assessment methods.

Conclusions: These results demonstrate that subchronic $PM_{2.5}$ exposure depletes the ovarian reserve by increasing recruitment of primordial follicles into the growing pool and increasing apoptosis of growing follicles. Further, $PM_{2.5}$ exposure and removal of the ovaries each increase atherosclerosis progression in *Apoe-/-* females. Premature loss of ovarian function is associated with increased risk of osteoporosis, cardiovascular disease and Alzheimer's disease in women. Our results thus support possible links between $PM_{2.5}$ exposure and other adverse health outcomes in women.

Keywords: $PM_{2.5}$, ovary, ovarian follicle, atherosclerosis, blood pressure, heart rate variability, ovariectomy, sex difference

Background

Particulate matter (PM) air pollution classifications are based on the aerodynamic diameter of the particles, which can be liquid or solid. Fine PM, less than 2.5 μm in diameter ($PM_{2.5}$), are mainly deposited in the lungs. $PM_{2.5}$ varies in composition depending on the sources, geographic location, season, and climate. Similar to many other urban areas worldwide, $PM_{2.5}$ from human activities in southern California's South Coast Air Basin is mainly composed of ammonium nitrate from atmospheric chemical reactions of oxides of nitrogen from mobile (vehicle exhaust) and stationary combustion sources, elemental and organic carbon compounds from combustion sources, and ammonium sulfate from atmospheric chemical reactions of sulfur oxides from combustion sources (1). $PM_{2.5}$ are regulated in the United States under the Clean Air Act National Ambient Air Quality Standards (NAAQS). However, despite dramatic improvements over the past half century in air quality, the South Coast Air Basin remains in non-attainment of the current $PM_{2.5}$ standard.

The ovarian follicle, which consists of the oocyte surrounded by specialized somatic cells, is the functional unit of the ovary. Ovarian follicles progress from the immature, quiescent primordial follicle stage, through primary, secondary, antral, and preovulatory stages (2). The somatic granulosa cells form first and are in direct communication with the oocyte. The theca cells differentiate from ovarian stromal cells, forming the outer somatic cell layers of secondary and antral follicles. Unlike the testes, the ovaries do not possess germline stem cells in postnatal life, and thus females are born with a finite complement of oocytes, which are packaged in primordial follicles (3, 4). Destruction of primordial follicles can therefore cause early onset of ovarian failure. When ovarian failure occurs prior to the

age of 40 in women, it is called premature ovarian failure or primary ovarian insufficiency (POF/POI). POF/POI is associated with increased risk of cardiovascular disease, Alzheimer's disease, and osteoporosis (5-8).

Estradiol synthesis occurs primarily in antral follicles and requires enzymes expressed in the theca cells, which synthesize androstenedione and testosterone, and granulosa cells, which aromatize testosterone to estradiol (9). Destruction of antral follicles results in decreased estradiol synthesis and disrupted estrous cycles. Apolipoprotein E (*Apoe*) is strongly expressed in ovarian theca cells, interstitial cells, and corpora lutea of rats, mice, and primates (10-14). APOE regulates androgen synthesis in cultured rat theca cells via regulation of expression of P450 17α-hydroxylase, C17-20 lyase (*Cyp17a1*), the rate-limiting enzyme for androgen synthesis, which converts progesterone to androstenedione (15). Female *Apoe-/-* mice have been reported to have decreased serum estradiol concentrations compared to non-littermate wild type control females (10).

Epidemiological studies have associated exposure to $PM_{2.5}$ with multiple adverse health effects, including asthma, chronic obstructive pulmonary disease, cardiovascular disease, and adverse pregnancy outcomes (16-18). Post-menopausal women are at increased risk of cardiovascular disease, and this may be attributed to ovarian dysfunction and reduced ovarian reserve (19-21). Many experimental studies of atherosclerosis in mice have used the *Apoe-/-* null mouse model, which lacks the APOE cholesterol transport protein that mediates binding of low-density lipoproteins (LDL) and very low-density lipoproteins (VLDL) to LDL receptors in liver and other tissues. Unlike wild type mice, *Apoe-/-* mice develop atherosclerosis (22, 23). Prior studies showed that exposure to $PM_{2.5}$ accelerates

atherosclerosis progression in male *Apoe-/-* mice (24, 25), but this has not been studied in female *Apoe-/-* mice.

The first studies of which we are aware that relate to effects of $PM_{2.5}$ on ovarian function were conducted by one group, who exposed female mice to highly polluted urban air or filtered air for two generations. They found evidence for decreased fertility, increased incidence of irregular estrous cycles, and decreased numbers of antral follicles with exposure to polluted air (26, 27). Subsequent work by the same group exposed mice during prenatal development and/or postnatally for 1 hour daily to diesel exhaust, a major source of $PM_{2.5}$ (28). They reported that the area of the ovary containing primordial follicles was significantly decreased in mice exposed to diesel exhaust prenatally, postnatally or during both developmental periods compared to filtered air controls. Two recent publications have reported on effects of tracheal instillation of $PM_{2.5}$ (29) or inhalational exposure (30) to $PM_{2.5}$ on ovarian function. Zhou et al (30) reported an increased percentage of irregular estrous cycles and decreased primordial follicle numbers in mice after 4 months of exposure to ambient $PM_{2.5}$ compared to controls exposed to filtered air. Liao et al (29) reported increased oxidative DNA damage and apoptosis in the ovaries of mice after tracheal instillation of $PM_{2.5}$. However, no studies have investigated the ovarian effects of exposure to $PM_{2.5}$ in *Apoe-/-* mice despite the importance of APOE in ovarian function.

It is recognized that ambient $PM_{2.5}$ contains polycyclic aromatic hydrocarbons (PAHs) and nitro-PAHs (31). PAHs are produced during incomplete combustion of organic materials such as fossil fuels, tobacco, wood, and foods. Like $PM_{2.5}$, cigarette smoke also contains dozens of PAHs, and smoking is associated with decreased fertility in women (32, 33).

Consistent with the epidemiological data, exposure of female mice to tobacco smoke caused ovarian follicle loss (34). Exposure of female mice to PAHs such as benzo[a]pyrene (BaP) or 9,10-dimethyl-1,2-benzanthracene by oral or intraperitoneal routes causes dose-dependent destruction of ovarian primordial, primary, and secondary follicles (35-38). Inhalation exposure of adult female rats to BaP dose-dependently decreased fertility (39).

Here, we describe rodent inhalation exposure experiments designed to assess the interaction of $PM_{2.5}$ exposure effects on ovarian function and the cardiovascular system. We hypothesized that 1) Subchronic inhalation exposure to human-relevant concentrations of $PM_{2.5}$ results in destruction of ovarian follicles and that this accelerates atherosclerosis in *Apoe-/-* mice. 2) If ovarian follicle destruction enhances atherosclerosis, then removal of the ovaries should enhance atherosclerotic effects of $PM_{2.5}$ to an even greater extent. 3) The mechanism of follicle destruction by $PM_{2.5}$ involves apoptosis of follicles at all stages of development and accelerated recruitment of primordial follicles into the growing pool.

Results

Characterization of ambient $PM_{2.5}$

Mice were exposed via whole body exposure to concentrated ambient $PM_{2.5}$ or filtered air (Air) for 5 hours per day, 4 days per week for 12 weeks in three cohorts, which were performed in 2017, 2018, and 2019. Particle mass and number concentrations averaged over the 12-week exposures are shown in Table 3.1 for each year. The average mass concentrations were very similar between the exposure years, 130 ± 5 $\mu g/m^3$ in 2017, 123 ± 11 $\mu g/m^3$ in 2018, and 110 ± 2 $\mu g/m^3$ in 2019. In 2017 gonad-intact male and female mice were studied; in 2018 gonad-intact and ovariectomized (OVAX) female mice were

studied; and in 2019 the effect of $PM_{2.5}$ exposure on ovarian estradiol levels in gonad-intact females was studied.

Table 3.1: Particle concentrations averaged over the exposure periods for each year of the study (Means ± standard deviations)

	2017		2018		2019	
	Particle Number (cm^{-3})	Particle Mass ($\mu g\ m^{-3}$)	Particle Number (cm^{-3})	Particle Mass ($\mu g\ m^{-3}$)	Particle Number (cm^{-3})	Particle Mass ($\mu g\ m^{-3}$)
Purified Air	10 ± 20	≤ 5	12 ± 5	≤ 5	83 ± 3	3.5 ± 0.3
Ambient Air	(1.1± 0.1) x 10^4	18 ± 1	(1.5± 0.1) x 10^4	30 ± 8	(1.3 ± 0.1) x 10^4	27 ± 0.2
$PM_{2.5}$	(8.6 ± 2.0) x 10^4	130 ± 5	(9.5 ± 2.0) x 10^4	123 ± 11	(8.3 ± 0.5) x 10^4	110 ± 2

We estimated the total exposure to PAHs in $PM_{2.5}$ during the course of the 12 week exposure by first calculating the total amount of air inhaled and exhaled: minute ventilation of 1.46 ml per gram body weight (40) x 20 g body weight x 300 min per 5 hour exposure session x 48 sessions x 10^{-6} m^3/ml = 0.42 m^3. A representative estimation of PAHs in particles to which mice in this study were exposed was based on previous studies performed close to heavily trafficked roadways in Los Angeles, in which about 2 ng/m^3 of low molecular weight PAHs and 2ng/m^3 of high molecular weight PAHs were measured in concentrated ambient $PM_{2.5}$ (41, 42). Therefore, we estimated that the mice could have been exposed to about 1.7 ng of total PAHs over the course of the entire 12-week exposure. This translates to 85 ng/kg for a 20 g mouse.

Exposure to $PM_{2.5}$ disrupted estrous cycling

There were no statistically significant differences in estrous cycling or in ovarian follicle counts in the Air exposed control mice during the 2017 and 2018 exposure years, so the estrous cycle and follicle count endpoints from both years were combined for analyses.

Effects of 12-week exposure to concentrated ambient $PM_{2.5}$ on estrous cycling are summarized in Table 3.2. Mice exposed to $PM_{2.5}$ were statistically significantly more likely to have irregular estrous cycles, defined as any cycles shorter than 4 days or longer than 5 days, than control mice (P=0.008, Fisher's exact test). 35% of $PM_{2.5}$-exposed mice had irregular cycles, while all the control mice had regular 4- to 5-day cycles. Estrous cycles were slightly, but non-statistically significantly longer in mice exposed to $PM_{2.5}$. The percentage of days with leukocytic vaginal cytology, characteristic of metestrus and diestrus, was statistically significantly decreased in mice exposed to $PM_{2.5}$ (P=0.027, 2-way ANOVA), while the percentage of days with predominantly cornified cytology, characteristic of estrus, was non-significantly increased.

Table 3.2: Effects of exposure to $PM_{2.5}$ on estrous cycles

	Filtered air [a]	**$PM_{2.5}$** [a]
Cycle length (days)	4.3 ± 0.1	4.6 ± 0.1
% with abnormal cycles[b]	0	35
% days with leukocytic cytology[c]	39.2 ± 1.4	33.0 ± 2.3
% days with cornified cytology	28.1 ± 1.3	32.8 ± 3.4

[a] N=20/group

[b] Not having 4 or 5 day cycles, P=0.008, Fisher's exact test

[c] P=0.027, 2-way ANOVA

Exposure to $PM_{2.5}$ decreased ovarian follicle numbers

Exposure to ambient $PM_{2.5}$ decreased the numbers of ovarian primordial follicles by 45% (P=0.031, 2-way ANOVA; Figure 3.1A) and primary follicles by 40% (P=0.006, 2-way ANOVA; Figure 3.1A). Healthy secondary follicle numbers were significantly decreased by 17% (P=0.048, 2-way ANOVA; Figure 3.1B), while healthy antral follicles and atretic

secondary and antral follicle numbers were not affected (Figure 3.1B). Corpora lutea numbers also were not affected (data not shown).

Exposure to $PM_{2.5}$ increased DNA damage in ovarian follicles

We performed immunostaining for γH2AX, which mediates recruitment of DNA repair proteins to sites of DNA damage and is a marker for DNA damage (43-45), on ovaries from the 2017 cohort. There was a statistically significant increase in the fraction of primary follicles with γH2AX-positive granulosa cells (P=0.004, Mann Whitney test; P=0.001, t-test) and in the fraction of secondary follicles with γH2AX-positive granulosa cells (P=0.022, Mann Whitney test; P=0.017, t-test), while the fractions of primordial and antral follicles with γH2AX-positive granulosa cells were unchanged by $PM_{2.5}$ exposure (Figure 3.2A). There was a statistically significant increase in the fraction of secondary follicles with γH2AX-positive oocytes in $PM_{2.5}$ exposed mice (P=0.040, t-test; P=0.086, Mann Whitney test), and no effect of $PM_{2.5}$ exposure on percentages of primordial, primary, or antral follicles with γH2AX-positive oocytes (Figure 3.2B).

Exposure to $PM_{2.5}$ increased the percentage of apoptotic antral follicles

TUNEL was used to identify follicles in late stages of atresia (apoptotic degeneration) in ovaries from the 2017 cohort. Ovaries from $PM_{2.5}$ exposed mice had statistically significantly increased percentages of antral follicles with TUNEL-positive granulosa cells (P=0.036 Mann Whitney test; P=0.058, t-test; Figure 3.3A) and percentages of antral follicles with activated caspase 3- positive granulosa cells (P=0.032 Mann Whitney test; P=0.065, t-test; Figure 3.3B). There were no statistically significant exposure-related differences in the percentages of TUNEL-positive secondary follicles or of activated caspase 3-positive

secondary follicles (Figure 3.3A and 3.3B). TUNEL- or activated caspase 3- positive primordial and primary follicles were very rarely observed in either experimental group (data not shown).

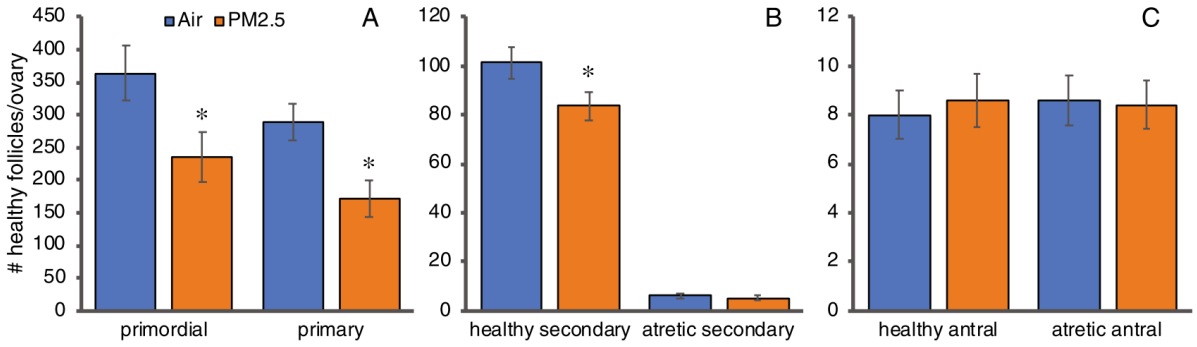

Figure 3.1 Effects of $PM_{2.5}$ exposure on ovarian follicle numbers: 3-month-old female mice were exposed to concentrated ambient $PM_{2.5}$ or filtered air 4 h per day, 5 days per week for 12 weeks and were euthanized 24 h after the last exposure day for enumeration of ovarian follicles as described in Methods. Graphs show the means ± SEM number of follicles per ovary. **A** Healthy primordial and primary follicle numbers were significantly decreased in $PM_{2.5}$ exposed mice compared to air controls. **B** Healthy, but not atretic secondary follicle numbers were significantly decreased in $PM_{2.5}$ exposed mice compared to air controls. **C** Neither health, nor atretic antral follicle numbers were significantly changed in $PM_{2.5}$ exposed mice compared to air controls. *P<0.05 compared to air controls. N=20/group

Exposure to $PM_{2.5}$ increased primordial follicle recruitment

We utilized immunostaining for Ki67 to identify actively dividing granulosa cells in follicles in ovaries from the 2017 cohort. Ki67 protein is expressed throughout the cell cycle, but not during G_0 (46). Compared to filtered air exposed mice, ovaries from $PM_{2.5}$-exposed mice had statistically significantly increased percentage of primary follicles with Ki67-positive, mitotic granulosa cells, consistent with increased recruitment of primordial follicles into the growing pool (P=0.040, t-test; P=0.055, Mann Whitney test; Figure 3.4). Essentially all secondary and antral follicles had numerous Ki67-positive granulosa cells regardless of

$PM_{2.5}$ exposure, as expected in these rapidly growing follicles (Figure 3.4 representative images).

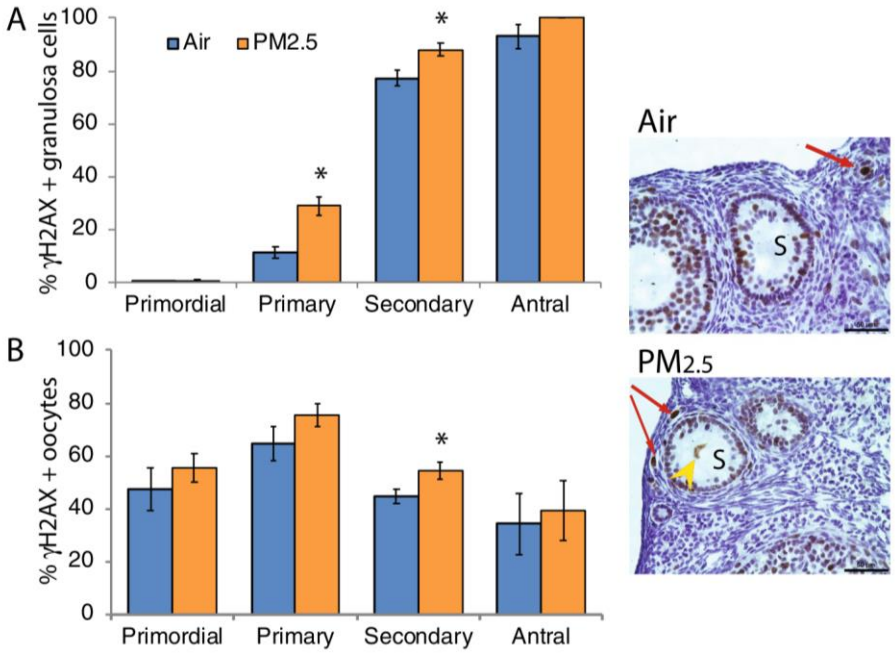

Figure 3.2 Effects of $PM_{2.5}$ exposure on DNA damage in ovarian follicles: Female mice were exposed to concentrated ambient $PM_{2.5}$ or filtered air as described for Fig. 1 and ovaries were processed for immunostaining for ɣH2AX as described in Methods. The graphs show the means ± SEM percentages of follicles with ɣH2AX-positive granulosa cells (**A**) or oocytes (**B**). Representative photomicrographs taken with 40X objective show secondary follicles (S) with ɣH2AX-positive, brown-stained nuclei of granulosa cells and oocytes (yellow arrow; the nucleus does not appear round because of fixation artifact) and primordial and primary follicles with ɣH2AX-positive granulosa cells (**A**) and of secondary follicles with ɣH2AX-positive oocytes (**B**). *P<0.05 compared to air controls. N=6-7/group. Scale bars, 50 µm

Exposure to $PM_{2.5}$ did not affect ovarian content of estradiol

Estradiol concentrations were measured in extracts of whole, proestrous ovaries from the 2018 and 2019 cohorts, which were derivatized with 1,2-dimethylimidazole-5-sulfonyl chloride (DMIS) and quantified using LC-MS/MS. The difference in ovarian estradiol content between ovaries of mice exposed to Air and $PM_{2.5}$ was not statistically significant

(Table 3.3). Ovarian estradiol content also did not differ by exposure year (2018 or 2019) or whether the animal had an implant. Some mice had cycles of variable lengths; in those cases, one could not be sure that the mouse was euthanized on proestrus, despite vaginal cytology consistent with proestrus. There was a statistically significant difference in ovarian estradiol content between mice with all cycles of the same length compared to mice with variable length cycles by t-test and in a 2-way ANOVA with exposure, with higher estradiol content in mice with variable length cycles. The effect of exposure was not statistically significant in either analysis. Interestingly, the estradiol contents of ovarian extracts from unexposed wild type mice euthanized on proestrus (the cycle stage with highest estradiol concentrations), were significantly higher than the estradiol content of ovaries from either control or $PM_{2.5}$ exposed *Apoe-/-* mice (P=0.038, Mann Whitney test; P=0.049, t-test, wild type compared to Air exposed *Apoe-/-* mice; P=0.021, Mann Whitney; P=0.010 t-test, wild type compared to $PM_{2.5}$ exposed *Apoe-/-* mice). The latter results suggest an effect of *Apoe* deletion on ovarian estradiol synthesis.

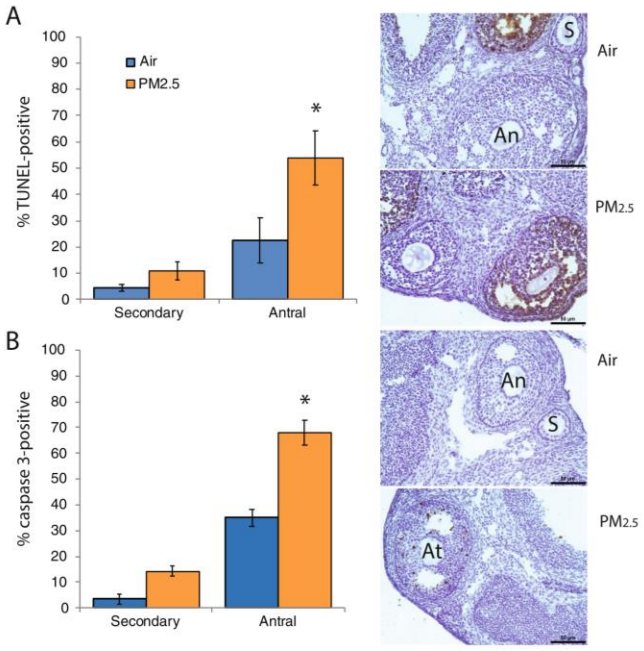

Figure 3.3 Effects of $PM_{2.5}$ exposure on apoptosis in ovarian follicles. Female mice were exposed to concentrated ambient $PM_{2.5}$ or filtered air as described for Fig. 1 and ovaries were processed for TUNEL or immunostaining for activated caspase 3 as detailed in Methods. The graphs show the means ± SEM percentage of TUNEL- (**A**) or activated caspase 3- (**B**) positive secondary or antral follicles. A Representative photomicrographs taken with 20 X objective show TUNEL-positive antral follicles with brown stained nuclei in granulosa cells, as well as TUNEL-negative secondary (S) and antral (An) follicles in air control and $PM_{2.5}$ ovaries. $PM_{2.5}$ exposure significantly increased the percentage of antral follicles with TUNEL-positive granulosa cells. B Representative photomicrographs taken with 20 X objective show activate caspase 3-positive antral follicles with brown stained nuclei in granulosa cells (At), as well as caspase 3-negative secondary (S) and antral (An) follicles in air control ovaries. $PM_{2.5}$ exposure significantly increased the percentage of antral follicles with activated caspase 3-positive granulosa cells. *P<0.05 compared to air controls. N=6-7/group. Scale bars, 50 μm.

Plaque Formation in Arteries of SHAM and OVAX Mice

Aortic arch cross-sections from ovariectomized (OVAX) mice or mice that underwent a sham surgery prior to being exposed to Air or $PM_{2.5}$ for 12 weeks were stained with Oil Red O and counterstained with hematoxylin. Typical sections are shown in Figure 3.5A. Air and $PM_{2.5}$-exposed OVAX mice and $PM_{2.5}$-exposed SHAM mice had greater atherosclerosis progression than ovary-intact SHAM controls, as indicated by the percentage of endothelial

cell area staining positive with Oil Red 'O' dye (Figure 3.5B). We note that the effects of both interventions were not additive; plaque area increases in $PM_{2.5}$-exposed OVAX mice were slightly higher than in $PM_{2.5}$ SHAM mice, but the difference was not statistically significant. $PM_{2.5}$ exposure reduced the percent area taken up by the lumen in SHAM mice compared to Air exposed SHAM; this difference approached statistical significance (P=0.051).

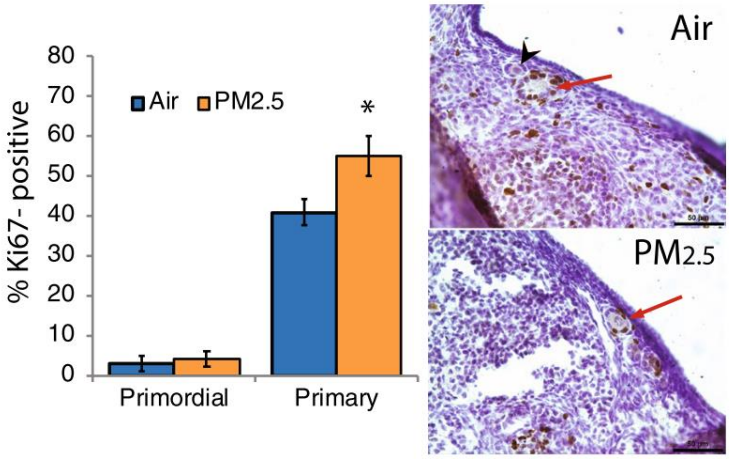

Figure 3.4 Effects of $PM_{2.5}$ exposure on activation of primordial ovarian follicles. Female mice were exposed to concentrated ambient $PM_{2.5}$ or filtered air as described for Fig. 1 and ovaries were processed for immunostaining for the proliferation protein Ki67 as detailed in Methods. Representative photomicrographs taken with 40 X objective show Ki67-positive follicles with brown stained granulosa cell nuclei in air control and $PM_{2.5}$ ovaries. Red arrows point to primary follicles with Ki67-positive granulosa cells. Black arrowhead points to primordial follicles with Ki67-negative granulosa cells. Scale bars, 50 µm. The graph shows the means ± SEM percentages of Ki67-positive primordial and primary follicles with Ki67-positive granulosa cells. *P<0.05 compared to air controls. N= 6/group.

Table 3.3: Effects of exposure to $PM_{2.5}$ on ovarian estradiol content

	Apoe-/- Air	*Apoe-/-* $PM_{2.5}$	Wild type unexposed
N	26	24	3
Estradiol (pg/mg ovary)	20.7±12.0	8.8±3.9	38.7±21.9

Blood pressure

Baseline blood pressures were measured for one week, the week prior to actual PM exposures while the mice were breathing purified air. Baseline measurements might be expected to be somewhat elevated since the mice, although acclimated to the system for one week prior to the baseline, might still have been not completely used to the level of handling and confinement. Blood pressure data were acquired during the final 6 weeks of the exposure (weeks 6-11), daily averaged over 4 h via telemetry in mice implanted with transmitters, and via tail cuff once per week in mice with and without implanted transmitters in 2017 and in mice without transmitters only in 2018. Blood pressure data are presented in Table 3.4 and the changes in blood pressure during the final weeks of exposure compared to baseline are presented in Supplemental Table 3.1.

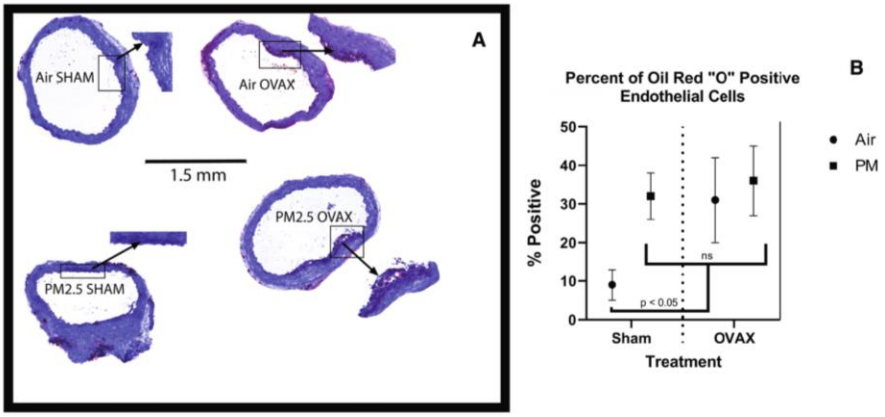

Figure 3.5 Effects of ovariectomy and $PM_{2.5}$- exposure on atherosclerosis. **A** Representative images of atherosclerotic plaques in Air- and $PM_{2.5}$ – exposed and ovariectomized (OVAX) and ovary intact (Sham) mice. Cross-sections of aortic root were stained with the lipid stain Oil Red O and counterstained with hematoxylin. Scale bar 1.5 mm for all four aortic root cross-sections. Areas within rectangles are magnified in insets. **B** Means ± SEM percentages of Oil Red O-positive endothelial cell area, no significant difference among Sham $PM_{2.5}$, OVAX Air, and OVAX $PM_{2.5}$; all three groups differed significantly ($P<0.05$) from Sham Air. N=3-4/group

Table 3.4: Effects of exposure to $PM_{2.5}$ and ovariectomy on aortic arch lumen area

Area	Air OVAX	$PM_{2.5}$ OVAX	Air SHAM	$PM_{2.5}$ SHAM
Lumen	3.84±0.47	3.00±0.31	3.21±0.29	2.96±0.28
Wall+ Plaque + Lumen	6.54±0.50	5.68±0.43	5.30±0.38	5.96±0.11
% lumen area	0.58±0.03	0.59±0.02	0.60±0.02	0.50±0.04*

N = 3-4/group; * P=0.051, compared to Air SHAM

At baseline prior to $PM_{2.5}$ exposure, the 2017 cohort transmitter males to be exposed to $PM_{2.5}$ had a higher diastolic blood pressure (DBP) than males allocated to the Air group, while there was no significant difference at baseline in diastolic blood pressure for transmitter females or in systolic blood pressure for either sex (Table 3.5). Despite systolic blood pressure (SBP) dropping in all transmitter males from baseline measures, $PM_{2.5}$ males had significantly higher SBP, and a trend of higher DBP compared to Air males as well (Table 3.5). The decrease in DBP from baseline, but not the decrease in SBP, differed significantly between Air and $PM_{2.5}$-exposed males (Supplemental Table 1). Air-exposed females exhibited a drop in SBP and DBP during weeks 6-11 compared to baseline, while SBP and DBP increased from baseline in $PM_{2.5}$-exposed females (Table 3.5 and Supplemental Table 1). Both SBP and DBP during the final 6 weeks of exposure were significantly increased in $PM_{2.5}$ exposed females compared to air controls (Table3. 5), and the changes in SBP and DBP from baseline also differed significantly between Air and $PM_{2.5}$-exposed females (Supplemental Table 1). The effects of $PM_{2.5}$ exposure were broadly consistent in both males and females when comparing intra-arterial and tail cuff blood pressures from transmitter-implanted mice (top two sections of Table 3.5). Table 3.5 also shows that effects of $PM_{2.5}$ exposure differed based on blood pressures obtained via tail cuff from the transmitter mice

compared to the non-implanted mice. In contrast to the increased blood pressure observed in transmitter females, there were no statistically significant differences in SBP or DBP between $PM_{2.5}$ and Air-exposed non-implanted females during the final 6 weeks of exposure.

Table 3.5. Intra-arterial and tail cuff systolic blood pressure (SBP) and diastolic blood pressure (DBP) in male and female *Apoe-/-* mice, 2017 cohort[#]

		Male			Female		
		Air	$PM_{2.5}$	*p-value	Air	$PM_{2.5}$	*p-value
		Transmitter - Intra-arterial					
Baseline	SBP	116.4 ± 1.0	119.1 ± 0.8	0.340	114.4 ± 2.8	117.3 ± 0.5	0.101
	DBP	96.7 ± 1.2	101.6 ± 1.0	0.003	97.6 ± 2.5	98.8 ± 0.7	0.271
Weeks 6-11	SBP	114.0 ± 1.4	117.2 ± 0.7	0.033	101.2 ± 1.7	122.7 ± 0.7	<0.001
	DBP	95.9 ± 0.9	97.6 ± 0.5	0.089	84.3 ± 1.6	102.6 ± 0.9	<0.001
		Transmitter – Tail Cuff					
Baseline	SBP	123.8 ± 5.7	139.4 ± 9.8	0.203	143.7 ± 4.6	123.4 ± 8.5	0.070
	DBP	96.5 ± 2.7	111.2 ± 7.8	0.115	112.7 ± 3.0	96.6 ± 8.3	0.105
Weeks 6-11	SBP	129.0 ± 4.1	135.7 ± 4.3	0.264	145.0 ± 5.7	132.3 ± 8.5	0.099
	DBP	98.8 ± 4.1	105.7 ± 4.3	0.248	114.3 ± 5.0	103.8 ± 8.3	0.133
		Non-transmitter - Tail Cuff					
Baseline	SBP	145.4 ± 4.9	139.3 ± 6.0	0.445	127.9 ± 4.2	135.5 ± 4.4	0.226
	DBP	116.6 ± 4.3	103.2 ± 4.2	0.038	100.5 ± 4.4	105.5 ± 4.0	0.404
Weeks 6-11	SBP	140.1 ± 6.5	139.8 ± 6.2	0.942	139.2 ± 9.3	140.1 ± 4.4	0.817
	DBP	109.3 ± 5.4	109.1 ± 5.2	0.950	112.2 ± 7.5	111.2 ± 4.0	0.769

N=10/experimental group, Non-transmitter; N=4-5/experimental group, Transmitter. # Blood pressures are in mmHg. *P-values are for $PM_{2.5}$ versus Air of same sex and BP measurement method, t-test.

For the 2018 cohort, there were again differences in the effects of $PM_{2.5}$ depending on whether the mice had telemetry implants or not. In mice with implants, there was no effect of chronic $PM_{2.5}$ exposure on SBP or DBP (Table 3.6) or on the change in SBP or DBP from baseline (Supplemental Table 2) in ovariectomized female ApoE-/- mice. In the SHAM group at baseline the mice to be exposed to $PM_{2.5}$ had significantly higher SBP. However, over the course of the exposure SBP and DBP dropped in $PM_{2.5}$ animals and rose in the Air group. This led to a significant difference in both systolic and diastolic blood pressure between $PM_{2.5}$- and air-exposed SHAM animals, with $PM_{2.5}$-exposure leading to a decrease in SBP and DBP compared to Air-exposure and a decrease in SBP and DBP from baseline (Supplemental Table 2) in the ovary-intact SHAM animals. In contrast, in the non-implanted mice in which blood pressure was measured by tail cuff, there were no statistically significant differences in SBP or DBP between $PM_{2.5}$- and Air-exposed SHAM mice, while SBP and DBP both increased in ovariectomized mice exposed to $PM_{2.5}$ compared to Air. The lack of a statistically significant effect of $PM_{2.5}$ exposure on either SBP or DBP measured by tail cuff was consistent for ovary-intact, non-implanted females in both the 2017 and 2018 cohorts (Tables 3.4 and 3.5). Ovariectomy significantly decreased the change in SBP and increased the change in DBP from baseline in Air-exposed mice, while it significantly increased the changes in SBP and DBP from baseline in $PM_{2.5}$-exposed mice ($P<0.001$; Supplemental Table 3).

Table 3.6: Intra-arterial and tail cuff systolic blood pressure (SBP) and diastolic blood pressure (DBP) in OVAX and SHAM female ApoE-/- mice, 2018 cohort

			OVAX			SHAM		
			Air	$PM_{2.5}$	p-value	Air	$PM_{2.5}$	p-value
			Transmitter - Intra-arterial					
Baseline	SBP	mmHg	122.8 ± 1.3	121.3 ± 1.5	0.454	123.5 ± 0.9	127.4 ± 1.3	0.020
	DBP	mmHg	99.3 ± 2.2	95.6 ± 1.4	0.139	99.2 ± 1.2	99.6 ± 1.0	0.778
Weeks 6-11	SBP	mmHg	123.6 ± 0.6	123.7 ± 0.6	0.931	129.8 ± 0.5	122.4 ± 1.1	<0.001
	DBP	mmHg	102.0 ± 1.0	100.7 ± 0.6	0.242	101.3 ± 0.5	96.6 ± 0.9	<0.001
			Non-transmitter - Tail Cuff					
Baseline	SBP	mmHg	125.2 ± 3.8	131.7 ± 4.8	0.302	136.9 ± 5.4	133.6 ± 3.2	0.609
	DBP	mmHg	103.1 ± 3.1	107.9 ± 2.9	0.274	109.3 ± 4.5	108.9 ± 3.0	0.946
Weeks 6-11	SBP	mmHg	134.8 ± 2.8	145.3 ± 3.4	0.018	140.4 ± 2.4	138.5 ± 2.8	0.602
	DBP	mmHg	111.1 ± 2.5	119.1 ± 3.2	0.054	113.2 ± 2.4	112.5 ± 2.4	0.851

N=10, Non-transmitter; N=4-5, Transmitter; P-values are for $PM_{2.5}$ versus Air of same group and BP measurement method, t-test

Blood pressure measurements obtained via tail cuff were consistently higher than intra-arterial blood pressures obtained via telemetry, whether obtained from mice with or without implants (Tables 3.5 and 3.6). The differences in SBP obtained via telemetry versus tail cuff from the same mice were statistically significant for Air-exposed males and females (P=0.015, P<0.001, respectively) at baseline and weeks 6-11 (P=0.002, P<0.001, respectively), as well as for $PM_{2.5}$-exposed males during weeks 6-11 (P<0.001; Table 3.5). The differences in DBP obtained via telemetry versus tail cuff from the same mice were

statistically significant for Air-exposed females at both baseline and weeks 6-11 (P=0.017, P<0.001, respectively; Table 3.5). There were also statistically significant differences in tail cuff blood pressures between mice within the same exposure group depending on whether they had telemetry implants or not. Both Air-exposed males and females had significantly different SBP at baseline by transmitter status, and Air exposed males also had significantly different DBP at baseline by transmitter status (Table 3.5). Interestingly, the tail cuff SBP and DBP at baseline were lower in the males with transmitters, while in the females they were higher in those with transmitters. By the second half of the exposure period, there were no longer any tail cuff blood pressure differences in females by transmitter status. In males, the lower SBP and DBP in mice with transmitters compared to those without approached significance in the second half of the exposure period (P=0.057 and P=0.065, respectively).

Heart rate variability

During the 2017 exposures, heart rate (HR) did not change significantly in response to $PM_{2.5}$ in either male or female mice (Table 3.7). Over the course of the exposure, there was a general tendency towards decreased HR variability (HRV) in all $PM_{2.5}$ exposed mice relative to their Air controls, but there were differences between males and females. SDNN did not show a significant difference in males during the last 6 weeks of the exposure, but the decrease in SDNN was clear in $PM_{2.5}$-exposed females. Significant decreases in RMSSD in both males and females reflect changes to parasympathetic nervous system inputs to the heart after sub-chronic $PM_{2.5}$ exposure. Sex-differences are evident in the $PM_{2.5}$-induced HRV changes, with females showing a greater negative HRV response than males.

Table 3.7. Percent change from baseline ± SEM in heart rate variability measures during weeks 6-11 in male and female ApoE-/- mice, 2017 cohort

		Male			Female		
		Air	$PM_{2.5}$	p-value	Air	$PM_{2.5}$	p-value
HR	*% change*	2.3 ± 0.7	1.6 ± 0.5	0.396	7.1 ± 0.7	7.5 ± 1.3	0.786
SDNN	*% change*	3.2 ± 2.4	1.5 ± 1.4	0.527	-2.8 ± 2.2	-12.5 ± 2.3	0.002
RMSSD	*% change*	12.7 ± 3.8	-3.6 ± 2.5	<0.001	17.4 ± 8.1	-12.5 ± 2.1	0.001

HR – heart rate, SDNN – standard deviation of normal RR intervals, RMSSD – root mean squared of successive differences of normal RR intervals. P-values are for $PM_{2.5}$ versus Air of same sex and BP measurement method, t-test

$PM_{2.5}$ exposure in the 2018 cohort led to significantly higher HR in both OVAX and SHAM groups (Table 3.8). During the final six weeks of the study, SDNN was more negative in the ovariectomized animals, but was not significantly affected by exposure in either group. RMSSD was significantly higher in $PM_{2.5}$-exposed OVAX animals and trended similarly in the SHAM $PM_{2.5}$ group, although not reaching significance. The increase in RMSSD in $PM_{2.5}$-exposed mice indicates an increase in parasympathetic response.

Table 3.8. Percent change from baseline ± SEM in heart rate variability measures during weeks 6-11 in OVAX and SHAM female ApoE-/- mice, 2018 cohort

		OVAX			SHAM		
		Air	$PM_{2.5}$	p-value	Air	$PM_{2.5}$	p-value
HR	*% change*	2.6 ± 0.5	3.6 ± 0.5	0.046	2.8 ± 0.5	4.9 ± 0.5	<0.001
SDNN	*% change*	-4.6 ± 1.3	-5.0 ± 1.2	0.142	2.8 ± 1.4	-1.1 ± 1.4	0.134
RMSSD	*% change*	-2.9 ± 1.5	2.0 ± 1.6	0.027	-8.3 ± 2.7	-0.9 ± 1.7	0.285

HR – heart rate, SDNN – standard deviation of normal RR intervals, RMSSD – root mean squared of successive differences of normal RR intervals. P-values are for $PM_{2.5}$ versus Air of same group, t-test

Discussion

Our data show for the first time that inhalational exposure to concentrated ambient $PM_{2.5}$ at concentrations to which humans are exposed depletes the ovarian follicle reserve in female *Apoe-/-* mice. Our data show that exposure for 5 hours per day, 4 days per week for 12 weeks to average concentrations of 120-130 $\mu g/m^3$ decreased the irreplaceable reserve of ovarian primordial and primary follicles by 45% and 40%, respectively. More mature secondary follicles were decreased by 17%. Our data further support that these decreases in follicle numbers are caused by accelerated recruitment of primordial follicles into the growing pool and DNA damage-induced apoptosis of growing follicles. $PM_{2.5}$-exposed female mice were also significantly less likely to have normal estrous cycles, defined as 4 to 5 days in length. Atherosclerotic plaques developed in all mice as expected, and $PM_{2.5}$-exposed ovary-intact and ovariectomized mice and filtered air-exposed ovariectomized mice had larger plaque area than filtered air-exposed controls. Blood pressure and heart rate variability were significantly affected by $PM_{2.5}$ exposure in gonad-intact males and females, as well as in ovariectomized female mice.

The 24-hour time-weighted average $PM_{2.5}$ concentrations to which the mice in this study were exposed averaged 27 to 29 $\mu g/m^3$, below the US NAAQS 24-hour average value for $PM_{2.5}$ of 35 $\mu g/m^3$ (98^{th} percentile averaged over three years; (47)). Peak $PM_{2.5}$ concentrations, above 130 $\mu g/m^3$ for 2 to 4 hr are often observed over wide areas during wildfire episodes, such as the large fires in California and Oregon during September 2020 (https://gispub.epa.gov/airnow; (48)). Moreover, 24-hour time-weighted average concentrations of 130 $\mu g/m^3$ or higher are common in cities in India, China, Pakistan,

Bangladesh, and other nations (49, 50). Importantly, size analyses of the exposure atmospheres in our study made using an SMPS (TSI, Inc.) demonstrated that the mobility diameters of the vast majority of particles in the concentrated ambient $PM_{2.5}$ were less than 160 nm, and most of the particles were in the ultrafine range (<100 nm; data not shown). Ultrafine particles are mainly deposited in the alveoli (51). However, because of their small size, they are not efficiently cleared from the alveoli by macrophages and are able to penetrate across the lung interstitium and translocate into the circulation to reach other target organs (51, 52). In addition, the ultrafine fraction of PM is enriched in organic substances, such as PAHs (24).

Most physiological ovarian follicle exhaustion in the adult ovary occurs after recruitment of primordial follicles into the growing pool. Once recruited, a follicle can develop to the preovulatory stage or die along the way. Only follicles that have reached the preovulatory stage at the time of the preovulatory surge of gonadotropins are capable of ovulating in response to the surge. More than 95% of follicles do not reach the preovulatory stage and undergo a process of degeneration called atresia. This occurs predominantly at the antral stage, when follicles are dependent on gonadotropin support for survival (53-56). Atresia of antral follicles is characterized by apoptotic death of the granulosa cells, which ultimately also results in death of the oocyte. Apoptotic death of antral follicles can be induced via activation of the intrinsic (mitochondrial) or extrinsic (receptor-mediated) pathways, both of which converge on activation of caspase 3 (56). Exposure to toxicants that induce apoptosis at any stage of follicle development and/or that accelerate recruitment of primordial follicles into the growing pool can accelerate the exhaustion of the ovarian follicle pool, resulting in premature ovarian failure (57). Ionizing radiation and anticancer drugs are

among the most investigated ovarian toxicants. Many of these agents initiate apoptosis in ovarian follicles by directly or indirectly (via generation of reactive oxygen species, ROS) damaging DNA (57). Our prior work showed that the mutagenic PAH 9,10-dimethyl-1,2-benzanthracene increases ROS generation and protein levels of the proapoptotic BCL-2 family member BAX and activated caspase 3 in granulosa cells of cultured rat antral follicles (58). These prior findings suggested to us that exposure to $PM_{2.5}$, as a source of PAHs, may cause follicle depletion via similar mechanisms. The present results show that exposure to $PM_{2.5}$ increased the percentage of primary follicles that are positive for the mitosis marker Ki67. Because we grouped transitional follicles (those that display characteristics of both primary and primordial follicles) with primary follicles when enumerating follicles, these data provide evidence for increased recruitment of primordial follicles into the growing pool. Accelerated recruitment of primordial follicles could be related to the decreased number of secondary follicles. Prior work has shown that depletion of secondary follicles by treatment with the anticancer drug cyclophosphamide results in decreased ovarian mRNA expression of Anti-Müllerian Hormone (AMH) (59, 60). AMH produced by growing follicles normally inhibits primordial follicle recruitment, and lower AMH levels result in accelerated recruitment of primordial follicles (61, 62). The present results also demonstrate that exposure to $PM_{2.5}$ increased DNA damage, measured by γH2AX immunostaining in primary and secondary follicles, and increased apoptosis, measured by activated caspase 3 immunostaining and TUNEL, in antral follicles. $PM_{2.5}$ contains numerous PAHs, metabolic activation of which leads to formation of bulky DNA adducts that result in phosphorylation of H2AX (63). For example, benzo[a]pyrene diol epoxide, *o*-quinone, and radical cation metabolites react with DNA to form bulky adducts, and the *o*-semiquinone and *o*-quinone

metabolites can undergo redox cycling, leading to formation of reactive oxygen species and oxidative DNA damage (64). Chromium and arsenic are carcinogenic metals found in $PM_{2.5}$, both of which cause oxidative stress and induce oxidative DNA damage (65, 66). Arsenic has also been shown to disrupt multiple DNA repair pathways (66). We did not observe evidence of apoptosis in primordial or primary follicles; however, it is possible that other cell death mechanisms may be at play in these follicles. For example, a recent study showed that exposure to diesel exhaust particle extract decreased autophagic turnover and decreased neuron numbers in the brains of zebrafish and that stimulation of autophagic turnover rescued the decrease in neurons (67).

We estimated that the mice in our study were exposed to 85 ng/kg body weight of total PAHs during the exposure period, based on representative PAH content for ambient particles in the southern California air basin. Compared to prior experimental work with individual PAHs in this and other laboratories, this is orders of magnitude lower than the ED_{50} for primordial follicle depletion (dose at which 50% of primordial follicles are depleted) by individual PAHs administered via intraperitoneal injection (37, 38, 68). For example, the ED_{50} values for primordial follicle depletion for three different PAHs (benzo[a]pyrene, 7,12-dimethylbenz[a]anthracene, and 3-methylcholanthrene) in C57BL/6J mice dosed daily for 15 days by intraperitoneal injection were two to four orders of magnitude higher than the estimated dose of total PAHs in the current study (37). For a single intraperitoneal injection of the same PAHs, the ED_{50} for primordial depletion was four to five orders of magnitude higher than the estimated dose of total PAHs in the current study (68). Acknowledging the different route of administration in these prior studies, these comparisons nonetheless lead to the conclusion that the ovotoxicity of $PM_{2.5}$ observed in our study is likely not due solely

to its PAH content. $PM_{2.5}$ is a complex mixture, which contains other known ovotoxicants, such as the metals arsenic and chromium (42, 69-71), as well as many compounds that have not been investigated for ovarian toxicity. Additive or synergistic effects of multiple ovotoxicants present in $PM_{2.5}$ in defined mixtures have been investigated to a very limited extent to our knowledge. Two studies by one group have investigated the effects of two PAH mixtures in cultured granulosa cell lines. One mixture (M1) contained all 16 USEPA priority PAH pollutants and the other (M2) contained the 5 most abundant of the 16 at concentrations found in human maternal and cord blood; the PAHs in M2 are lower molecular weight and are not classified as human carcinogens (43, 72). The authors reported that the effects of the two mixtures on gene expression, cell proliferation, and apoptosis activation differed from one another and differed between a "normal" granulosa cell line and a granulosa cell tumor line; however, the experiments were not designed to differentiate between additive or synergistic effects of the compounds in the mixtures (19, 43).

We observed that the percentage of mice with irregular estrous cycles increased in the $PM_{2.5}$ exposed group. The estrous cycle is regulated by the hypothalamic-pituitary-ovarian axis (73). After ovulation, if fertilization does not occur, a new cohort of antral follicles begins to grow. These follicles produce estradiol, which exerts negative feedback on the hypothalamus and the pituitary gland to inhibit synthesis and secretion of gonadotropin releasing hormone and the gonadotropins (luteinizing hormone, LH and follicle stimulating hormone, FSH), respectively (73). As the antral follicles grow, they produce more estradiol. Once estradiol surpasses a threshold, it exerts a positive feedback on the hypothalamus and pituitary gland, triggering the preovulatory surges of LH and FSH on the evening of proestrus of the estrous cycle. We observed increased apoptosis of antral follicles in $PM_{2.5}$ compared

to Air-exposed mice in the present study, but this was not associated with significantly decreased ovarian estradiol content in the $PM_{2.5}$-exposed mice.

Only a few epidemiological studies have examined the effects of air quality on female reproduction other than pregnancy outcomes. One study found that conception rates from assisted reproduction decreased with higher modeled exposure to $PM_{2.5}$ during embryo culture in the IVF laboratory (74). Risk of menstrual irregularity during high school increased with increasing exposure to total suspended particulate matter during high school in women in the Nurses Health Study II (75). Prior to our study, very little experimental research had been conducted on the effects of exposure to particulate matter air pollution on ovarian follicles (76). In a recent study, Zhou et al exposed female C57BL/6J mice via inhalation to ambient $PM_{2.5}$ (median concentration of 36.3 $\mu g/m^3$) or filtered air for 4 months, 12 h/day (30). Consistent with our results in *Apoe-/-* mice, they reported statistically significant increases in the percentage of mice with irregular estrous cycles and decreases in primordial follicle numbers. In contrast to our results, they also reported statistically significantly decreased antral follicle numbers, and they did not report statistically significant decreases in primary or secondary follicle numbers. These differing results may be due to different follicle counting methodology used and that they did not euthanize the mice on the same estrous cycle stage. It is well-established that antral follicle and corpora lutea numbers vary with estrous cycle stage (53, 77). Two experimental studies by one group exposed wild type Kunming (29) or ICR (78) mice to $PM_{2.5}$ suspended in saline solution by tracheal instillation and reported increased oxidative DNA damage, increased levels of the proapoptotic BAX protein, and caspase 3 activation in the ovaries. However, these studies had several limitations - the tracheal instillation route is not relevant to

humans, the total and daily doses were very high, the follicle and cell types positive for the DNA damage and apoptosis markers were not identified, and no follicle staging or enumeration was performed. Several studies have examined the effects of prenatal exposure to diesel exhaust on ovarian follicles. Exposure to diesel exhaust for one hour daily at target concentration of 600$\mu g/m^3$ during pregnancy and/or postnatally for the first two months of life was reported to decrease the fractional area of the ovary taken up by primordial follicles in mice (28). The fractional area taken up by primary follicles was reportedly decreased in the prenatal only exposure group compared to the other three groups, while secondary and antral follicle area did not differ among groups (28). We note that this study was limited in that follicle area was only assessed in 10 nonoverlapping fields at 100x magnification per ovary, and how these fields were chosen was not described (28). Another study examined the effects of prenatal exposure of rabbits to diesel exhaust containing 1 mg/m^3 of $PM_{2.5}$ for 2 h/day, 5 days/week from days 3 to 28 of gestation on ovarian follicles in the offspring at 7.5 months of age (79). Follicles were counted in five sections per ovary, and results were expressed per unit area. No statistically significant effects on follicle density were observed (79). These studies were limited in that neither utilized nonbiased stereological methods to assess ovarian follicle numbers (80, 81).

Apoe-/- null mice used in this study lack the APOE cholesterol transport protein, which mediates binding of low-density lipoproteins (LDL) and very low-density lipoproteins (VLDL) to LDL receptors in liver and other tissues, including the ovaries. *Apoe* is strongly expressed in ovarian theca cells, interstitial cells, and corpora lutea of rats, mice, and primates (10-14). APOE regulates androgen synthesis in cultured rat theca cells via regulation of expression of P450 17α-hydroxylase, C17-20 lyase (*Cyp17a1*), the rate-limiting

enzyme for androgen synthesis, which converts progesterone to androstenedione (15). We included control ovaries from wild type mice known to be in proestrus (cycle stage with highest estradiol levels) with the experimental ovaries in our estradiol assays. Interestingly, we noted that these wild type mice all had high ovarian estradiol content, while only some of the *Apoe-/-* Air or $PM_{2.5}$-exposed mice had comparable estradiol content, despite also being euthanized on proestrus. This suggests that *Apoe-/-* mice have a deficit in estradiol synthesis, which is consistent with one other publication that reported lower serum estradiol concentrations in *Apoe-/-* mice on the day of diestrus (cycle stage with low estradiol levels) at 100 days of age compared to non-littermate C57BL/6J mice (10).

Very little is known about the roles of APOE in primordial and primary follicles. One study reported that primordial follicle numbers were increased in *Apoe-/-* mice compared to wild type mice prior to puberty, while there were significantly fewer primordial follicles at 100 days of age (10). However, non-littermate wild type C57BL/6J controls from a different supplier than the *Apoe-/-* mice were used in that study. The same study reported that fertility of *ApoE-/-* females is not significantly different from the wild type C57BL/6J controls with respect to total numbers of pups, number of litters or average number of pups per litter, over a reported 6-month breeding study (10). We cannot exclude that *Apoe* deletion may have increased ovarian sensitivity to $PM_{2.5}$ exposure in the present study. Therefore, in future studies, we plan to compare the ovarian effects of *Apoe* deletion and exposure to $PM_{2.5}$ alone and in combination.

Apoe-/- null mice develop hyperlipidemia and atherosclerosis, with fatty streaks developing at 3 months of age, atherosclerotic plaques evident by 20 weeks of age, and

progression of lesions over time (22, 23). Prior studies have reported that exposure to $PM_{2.5}$ exacerbates atherosclerotic plaque development in male *Apoe-/-* mice (24, 25, 82), but to our knowledge no published studies have investigated the effects of $PM_{2.5}$ on this endpoint in female *Apoe-/-* mice. We hypothesized that $PM_{2.5}$-induced decline in ovarian function would exacerbate atherosclerotic effects of $PM_{2.5}$ in females and therefore that ovariectomized females, which lack all ovarian function, would experience more pronounced cardiovascular effects of $PM_{2.5}$ than ovary-intact females. Consistent with our hypothesis, there were statistically significant effects of ovariectomy and $PM_{2.5}$ exposure on two measures of atherosclerosis progression, lumen area and percentage of endothelial cell area positive for the lipid marker Oil Red O. The percent lumen area was smaller in the $PM_{2.5}$ exposed SHAM mice than all the other groups, and the percentage of positive endothelial cells was increased by OVAX and $PM_{2.5}$ alone. However, the combined effect of OVAX plus $PM_{2.5}$ exposure on Oil Red O positive endothelial cell area was less than additive. The effect of ovariectomy alone is consistent with a prior study, which reported larger and more extensive atherosclerotic plaques in ovariectomized female *Apoe-/-* mice compared to ovary-intact controls (22). A possible mechanism is suggested by a report that estradiol increases nitric oxide and protein *S*-nitrosylation in cultured primary vascular smooth muscle cells; the authors postulated this may play a role in the higher levels of plasma nitric oxide and protein *S*-nitrosylation and lower susceptibility to atherosclerosis in female compared to male *Apoe-/-* mice (83). With regard to heart rate and heart rate variability, both heart rate and RMSSD increased with $PM_{2.5}$ exposure in both OVAX and SHAM females in the 2018 cohort, but the change in RMSSD compared to baseline was statistically significant only in the OVAX mice.

Effects of $PM_{2.5}$ exposure on blood pressure differed depending on whether mice had implanted transmitters and if they had transmitters whether blood pressure was measured via the transmitter or via tail cuff. Transmitter blood pressure measurements were not affected by $PM_{2.5}$ exposure in OVAX mice, but transmitter blood pressure was decreased in SHAM mice. In contrast, tail cuff SBP was increased with $PM_{2.5}$ exposure in OVAX mice without transmitters, while blood pressure was not affected in SHAM mice without transmitters. An effect of transmitter implants on blood pressure was further supported by males with transmitters having lower tail cuff blood pressures and females with transmitters having lower tail cuff blood pressures than mice of the same sex without transmitters during the baseline measurement periods. These differences were no longer statistically significant during the last 6 weeks of exposure, which could suggest that they may have been prolonged effects of the stress of the implantation surgery.

In agreement with a previous study (42), we observed no effect of $PM_{2.5}$ exposure on heart rate in male *Apoe-/-* mice. Female mice were not included in that prior study. Keebaugh et al (42) also observed decreases in both low frequency heart rate variability and high frequency heart rate variability, indicating decreased parasympathetic influence on the heart. Consistent with those prior findings, $PM_{2.5}$ exposure was associated with a significant decrease in RMSSD, a measure of parasympathetic inputs to the heart, for gonad-intact males and females in the 2017 cohort of the present study. In contrast, we observed statistically non-significant decreases in SDNN and significant increases in heart rate in ovary-intact and ovariectomized females and significant increase in RMSSD in ovariectomized females in the 2018 cohort. Stresses related to the ovariectomy and sham surgeries in the 2018 cohort may have influenced blood pressures and HRV outcomes, making it difficult to compare results

from ovary-intact mice between the 2017 and 2018 cohorts. However, we observed no cohort effect on ovarian follicle counts.

We observed that blood pressures measured via tail cuff were generally higher than those measured via telemetry. It has previously been reported that both SBP and DBP increase in male and female mice immediately upon handling or movement of their cage by about 50 and 30 mmHg, respectively, and slowly return to baseline over a period of about one hour (72). In our study, mice were acclimated for approximately 10 minutes to the restraining tube used for tail cuff blood pressure measurement prior to measurement onset. Therefore, our results are consistent with those of Wilde et al (72) in showing increased blood pressure in mice after 10 minutes of restraint.

Conclusions

In conclusion, inhalational exposure of adult female *Apoe-/-* mice to concentrated ambient $PM_{2.5}$ at environmentally relevant concentrations depleted ovarian primordial, primary, and secondary follicles by 45%, 40%, and 17%, respectively. The effects of $PM_{2.5}$ exposure on ovarian follicle numbers were consistent between two consecutive exposure years. Our data support that the mechanism of follicle depletion involves increased recruitment of primordial follicles into the growing pool and induction of DNA damage and apoptotic death in growing follicles. Both exposure to $PM_{2.5}$ and ovariectomy increased atherosclerotic plaque progression compared to intact, non-ovariectomized females. However, the effects of both interventions were not additive; plaque increases in $PM_{2.5}$-exposed OVAX mice were slightly higher than in $PM_{2.5}$-exposed SHAM mice but the difference was not statistically significant. Because primordial follicles are non-renewable, their

depletion causes premature ovarian failure. In addition to causing infertility, premature ovarian failure, often called premature menopause, in women is associated with increased risk of developing cardiovascular disease, osteoporosis, and Alzheimer's disease (5-8). Therefore, our results suggest that exposure to $PM_{2.5}$ could increase women's risk for these chronic diseases by hastening the onset of menopause.

Materials & Methods

Chemicals and reagents

All chemicals and reagents were obtained from Sigma Aldrich (St. Louis, MO) or Fisher Scientific unless otherwise noted.

Animals

The experiments were conducted using genetically modified mice in which part of exon 3 and part of intron 3 of the *Apoe* gene were deleted, resulting in no expression of APOE protein (B6;129P2-*Apoe*^{tm1Unc}/J; hereafter referred to as *ApoE-/-*)(84). The mice were bred in house by mating *ApoE-/-* females and males from stock originally purchased from Jackson Labs, where they were backcrossed at least 10 generations onto a C57BL/6J genetic background (Strain # 002052; https://www.jax.org/strain/002052). This mouse strain was chosen because it is a model of choice for the investigation of atherosclerosis (23) because wild type mice do not develop atherosclerosis. Mice were housed in an Association for Assessment and Accreditation of Laboratory Animal Care International (AAALACI)-accredited vivarium on a 12-hour light/12-hour dark cycle with food and water available ad libitum. Temperature was maintained at 70°C and relative humidity averaged 48%. The experiments described herein were performed in three cohorts, one in 2017, one in 2018, and one in 2019. In 2017 gonad-

intact male and female mice were studied; in 2018 ovary-intact SHAM and ovariectomized (OVAX) female mice were studied to investigate the effects of ovariectomy on the cardiovascular parameters; in 2019 ovary-intact females were studied to examine the effects of $PM_{2.5}$ exposure on ovarian estradiol concentrations. $PM_{2.5}$ concentrations were slightly different from year to year, but the mean concentrations were not significantly different (Table 3.1). The experimental groups, ages at surgeries and exposure onset, and endpoints analyzed for each year are shown in Table 3.9.

Surgery and biopotential data collection: Ovariectomies were performed when the mice were 12 weeks of age via small bilateral incisions about 5mm below the rib cage under isoflurane anesthesia (85). Sham ovariectomized mice underwent an identical procedure, except ovaries were not excised. Mice were provided subcutaneous ketoprofen for 2 days after surgery for analgesia and subcutaneous enrofloxacin for 4 days.

At 3 months of age in the 2017 cohort, and 2 weeks after ovariectomy or sham surgery in the 2018 cohort, 4 or 5 mice from each experimental group were implanted with telemetry devices (HD-X11, Data Sciences International) which allow collection of electrocardiograms (ECG), blood pressure (BP), body temperature and activity. ECG leads were placed in a lead II configuration. Blood pressure was measured through a pressure transduction catheter inserted into the right carotid artery. Mice were provided subcutaneous analgesia after surgery, buprenorphine for 2 days in the 2017 study or ketoprofen for 3 days in the 2018 study, and subcutaneous enrofloxacin for 7 days. After surgery, we allowed for two weeks of recovery followed by one week of acclimation to the exposure chambers and one week of

baseline exposure to filtered air. Data from the telemetry devices were recorded, using the iox2® (EMKA Technologies, Falls Church, VA, USA) acquisition system, starting 6 hours after the exposure period, overnight when undisturbed in housing.

Heart rate variability and blood pressure: Inter-beat intervals (RR) were extracted from ECG recordings and analyzed for heart rate variability (HRV) measures using ecgAUTO® (EMKA Technologies, Falls Church, VA, USA). HRV measures in the time-domain, standard deviation of normal RR intervals (SDNN) and root mean square of successive differences of normal RR intervals (RMSSD), indicate the magnitude of variance in the heart's rhythm. SDNN represents total HRV, while RMSSD is conventionally interpreted as an indicator of the heart's response to parasympathetic, or vagal, inputs (86). HRV was assessed in 3-minute epochs at 30-minute intervals (87) from 19:00-24:00 each night. Intra-arterial blood pressure was recorded simultaneously. To normalize for inter-individual variability, HRV and blood pressure data were analyzed in terms of percent changes from baseline for each respective animal and averaged by exposure group and sex or treatment group. Blood pressure data were also analyzed without this transformation. To assess chronic exposure-related changes of HRV and BP from the long-term studies, the final 6 weeks were grouped.

Table 4.9: Experimental Design

	2017 cohort	2018 cohort	2019 cohort
Exposure months	March-June	August-November	August-November
Age at first surgery	3 months	3 months	3 months
Age at start of exposure	4 months	4 months	4 months
Exposure duration	12 weeks	12 weeks	12 weeks
Experimental groups	Gonad intact male Air Gonad intact male $PM_{2.5}$ Gonad intact female Air Gonad intact female $PM_{2.5}$	Sham female Air Sham female $PM_{2.5}$ OVAX female Air OVAX female $PM_{2.5}$	Sham female Air Sham female $PM_{2.5}$
Endpoints	Male and female -BP (tail cuff and transmitter) -ECG (transmitter) Female only - estrous cycling - follicle counts - ovarian IHC (PUMA, activated caspase 3, γH2AX, Ki67) - ovarian TUNEL	Sham and OVAX -BP (tail cuff and transmitter) -ECG (transmitter) -Oil red O aorta Sham only - ovarian estradiol - estrous cycling	Sham - ovarian estradiol - estrous cycling

Blood pressure was also measured using the CODA HT-8 tail cuff blood pressure system system (Kent Scientific) once per week, except during the final week of exposure, in mice with and without implanted transmitters in 2017 and in mice without transmitters only in 2018. Mice were acclimated in the restraint tube for 10 minutes prior to blood pressure measurement.

Exposure to $PM_{2.5}$

Starting at 4 months of age, mice were exposed to concentrated ambient $PM_{2.5}$ for a cumulative total of 240 hours, nominally 5 hours per day, 4 days per week for 12 weeks

adjusted as needed for technical issues and holidays. Exposures were performed using a Versatile Aerosol Concentration Enrichment System (VACES) (88-90) coupled with custom-designed individual exposure 12.4 cm high x 77.2 cm^2 compartments within a larger chamber (91) on the University of California Irvine campus near the intersection of two heavily trafficked roadways. Control mice were exposed to filtered air (Air) under conditions identical to the animals that were exposed to $PM_{2.5}$. The exposures reported herein were conducted March through June 2017, August through November 2018, and August through November 2019.

All mice were euthanized at 7 months of age, 24 h after the last exposure. Ovary-intact female mice were euthanized on the day of proestrus of the estrous cycle, based on vaginal cytology containing a mixture of nucleated and cornified epithelial cells, 24 h after the last exposure. Mice were first anesthetized with isoflurane, then underwent exsanguination by cardiac puncture. For both the 2017 and 2018 cohorts, one ovary with attached oviduct was fixed in Bouin's fixative overnight at 4°C for stereology. For the 2017 cohort the other ovary with attached oviduct was fixed in 4% paraformaldehyde in phosphate buffered saline (PBS) overnight at 4°C followed by cryoprotection in 30% sucrose in PBS until the tissue sank; these ovaries were used for immunostaining. For the 2018 cohort the second ovary and for the 2019 cohort both ovaries were snap frozen and stored at -80°C for subsequent estradiol measurements. For the 2018 and 2019 cohorts, aortas were dissected and fixed in 4% paraformaldehyde for analysis of atherosclerosis.

Male mice and ovariectomized females were euthanized in the same manner 24 h after the last exposure.

Size-resolved Particle Number and Mass Concentrations

A TSI Scanning Mobility Particle Sizer (SMPS, Shoreview, MN, USA) was used to measure the ultrafine particle fraction of $PM_{2.5}$ and particles up to about 1 μm. An optical particle counter was used to measure particle concentrations in the size range of 0.5 μm to 2.5 μm. In addition to monitoring particle mass, a TSI condensation particle counter (Model 3022) was run in parallel to measure total particle number concentrations. A TSI DustTrak optical mass monitor (Model 8520) was used to provide integrated $PM_{2.5}$ mass concentrations.

Estrous cycle monitoring

For evaluation of estrous cycling, female mice were individually housed, and vaginal lavage using 0.9% NaCl (92) was performed every morning for at least 14 days. Cells in the lavage fluid were examined by light microscopy immediately after collection, and the predominant cell types present in the fluid were recorded. Mice with telemetry implants were excluded from analyses of the effect of $PM_{2.5}$ exposure on estrous cycling and ovarian endpoints to exclude any effects of the implants on these endpoints.

Ovarian Follicle Counts

Bouin's fixed ovaries from mice without telemetry implants were embedded in glycolmethacrylate resin (Technovit 8100; Heraeus Kulzer GmBH, Wehrheim, Germany), sectioned at 20 μM, and stained with hematoxylin and eosin.

Stereological methods were used to obtain unbiased estimates of ovarian follicle numbers (81, 93). Ovarian follicles were counted blind to the treatment group using Stereo Investigator software (MBF Bioscience) with an Olympus BX40 light microscope equipped with 4× UPlanFl, 10× Plan, 40x PlanApo N340 and 60× PlanApo objectives, a joystick controller for a motorized XY stage (Ludl Electronic Products), and an Optronics MicroFire digital camera. We used the fractionator/optical dissector method to obtain unbiased and efficient estimates of primordial and primary follicle numbers by counting follicles in a defined fraction of the whole ovary (81). Three levels of sampling were used to determine the estimated number of primordial and primary follicles in the ovary. For both the 2017 and 2018 ovary cohorts, follicles were counted in 6% of the ovarian volume. The first level of sampling was at the level of the sections – in 2017 every 3rd section was counted and in 2018 every 5th section of the ovary was counted. The second level of sampling was a fraction of the area of each section. In 2017, 45 µm x 45 µm counting frames were superimposed onto the sections in sampling grids that were subdivided into 90 µm x 90 µm squares, while in 2018 the counting frames were 175 µm x 175 µm within 250 µm x 250 µm squares. Follicles were counted if the oocyte fell within the counting frame and/or touched the inclusion boundaries and did not touch the exclusion boundaries. Lastly, the optical dissector height was set to 8 out of 13 µm (2017) or 10 out of 17 µm (2018) with guard zones on the top and the bottom of the section to account for irregularities of the sections. By multiplying the raw counts by the reciprocal of the counting fraction, the number of follicles in the entire ovary was estimated. Secondary, antral, and preovulatory follicles, and corpora lutea were followed through every section to avoid counting any of these large structures more than once. The total number of healthy or atretic secondary and antral follicles or corpora lutea

was calculated as the sum of the counts. Healthy follicles were classified as primordial (single layer of fusiform granulosa cells), primary (single layer with two or more cuboidal granulosa cells), secondary (greater than one layer of granulosa cells with no antrum), or antral (94, 95). Atretic follicles were identified as previously described (53, 96, 97).

Estradiol measurement using LC-MS/MS

We adapted the LC-MS/MS estradiol assay method published by Keksi-Rahkonen et al (98), which incorporates derivatization of estradiol with 1,2-dimethylimidazole-5-sulfonyl chloride (DMIS).

Sample preparation: One ovary per animal from the 2018 cohort and both ovaries from each animal from the 2019 cohort were suspended in ice cold 325 µL of 0.5% bovine serum albumin (BSA) + 5 mM EDTA pH7.4. Bilateral ovaries from proestrous, wild type C57BL/6J mice were included as assay positive controls, as this is the cycle stage when ovarian estradiol concentrations are highest (99). Ovaries were homogenized on ice using a Kontes mortar and pestle apparatus for 30 seconds per ovary, or until ovarian tissue was fully dissociated. Samples were then centrifuged at 15,800 x g for 10 minutes and 300 µL of supernatant was aliquoted into separate microfuge tubes. Blanks were prepared using 300 µL of 0.5% BSA + 5 mM EDTA. An aliquot of the internal standard, d4-17β-estradiol (5 ng/mL), was spiked into each ovary sample (2.5 µL) and BSA blanks (5 µL). Calibration curve standards were made using 100 µL of a stock solution of 17β-estradiol diluted to 100 ng/mL in 0.5% BSA + 5 mM EDTA. The blanks, ovary samples, and calibration standard were all

suspended in 1 mL of 3:2 hexanes: ethyl acetate then vortexed vigorously for 30 seconds per sample, inverting periodically. All samples were then centrifuged at 15,800 x g for 5 minutes and 950 µL of the organic phase was aliquoted into new microfuge tubes. A fresh aliquot of 500 µL of deuterated 17β-estradiol (d4-17β-estradiol, 5 ng/mL) was made to assess percent recovery. All samples, including the internal standard aliquot were evaporated to dryness under N_2 gas. Then all samples, blanks, and standards were suspended in 50 µL of derivatizing agent, DMIS (1,2-dimethyl-1H-imidazole-4-sulfonyl chloride), at 1 mg/mL in acetone then 100 µL of 50 mM of sodium bicarbonate pH 10.5 was added and incubated at 60°C for 15 minutes. Following incubation, samples were resuspended in 343 µL of ethyl acetate and vortexed vigorously, then centrifuged at 15,800 x g for 5 minutes and 330 µL of the organic phase was aliquoted into fresh tubes. All samples, blanks, and standards were then evaporated to dryness under N_2 gas and resuspended in 500 µL of methanol for the standards, 150 µL for the blanks, and 75 µL for ovary samples. Finally, the calibration curve standards were prepared by successive dilutions of the stock solution of the derivatized 17β-estradiol and each final standard solution (291 µL) was spiked with 9 µL of the d_4-DMIS internal standard stock solution in methanol.

LC-MS/MS: The extracts (50-µL injection volume) were analyzed using a UPLC-PDA-MS platform (Waters) equipped with an Acquity H Class PLUS system (including a quaternary solvent manager, a sampler manager using a flow-through needle mechanism, a column heater and a photodiode array detector) coupled to a Xevo TQD triple quadrupole mass spectrometer. The separation was achieved using an Acquity UPLC BEH C18 1.7 µm, 50 ×

2.1 mm (Waters) column fitted with a VanGuard pre-column (UPLC BEH C18, 1.7 μm 5 x 2.1 mm; Waters) and maintained at 40°C. The mobile phase combination was (A) 0.2% acetic acid (99.7 %, Optima LC-MS; Fisher) in 18.2 MΩ cm milliQ water (Millipore; model ZD5211584) and (B) LC-MS grade methanol (Optima LC-MS; Fisher). The eluent gradient was as follows: 0-6 min linear gradient from 30% B to 95% B, 6-8 min hold at 95% B, 8-12 min linear gradient back to 30% B and finally 12-14 min hold at 30% B with a flow rate of 0.3 mL min^{-1}. UV-vis absorption spectra were acquired using a photodiode array detector (PDA eLambda; Waters) over the full 190-500 nm wavelength range. Exiting the PDA, the samples were introduced into the mass spectrometer using an atmospheric pressure photoionization source (APPI; Waters). Toluene (OmniSolv; EMD) was combined with the eluent post-column at a flow rate of 40 μL min^{-1} and used as an ionization dopant from 5-8 min. APPI source conditions were as follows: repeller voltage, 3.00 kV; cone voltage, 50 V; APPI probe temperature, 500°C; desolvation gas flow rate, 250 L hr^{-1}; source temperature, 150°C. The analysis was performed in positive ion mode using a multiple reaction monitoring (MRM) approach. The m/z 431 => m/z 96 transition was used for the derivatized estradiol product (E2-DMIS) while the m/z 435 => m/z 96 transition was used for deuterated derivatized estradiol internal standard (d_4-DMIS)(98). The data were acquired using MassLynx software (Waters) and then batch-processed using TargetLynx for quantitative analysis (Waters) using an internal calibration method.

Extraction recoveries were evaluated weekly using the average d_4-DMIS internal standard concentrations from the spiked ovary samples and comparing them to the d_4-DMIS

concentrations in the spiked calibration standard solutions. From those, recoveries ranging from 80 to 89% were determined and applied to the ovary samples.

Immunohistochemistry

Ovaries fixed in 4% paraformaldehyde were cryoprotected in 30% sucrose in PBS at 4°C, embedded in Optimal Cutting Temperature (OCT) compound, and stored at -80°C before being serially sectioned using a cryostat at a thickness of 10μm. Sections were mounted 4 per slide in 4 sets so that sections on a slide were separated by 40 μm from one another in the ovary. Immunohistochemistry was performed using the Vectastain ABC kit (PK-4001; Vector Laboratories, Burlingame, CA, USA). Briefly, sections were thawed and heated for 15 min at 95°C in a 10mM citrate buffer (pH 6.0). The primary antibodies—rabbit anti-cleaved caspase-3 Asp 175 (1:100; Cell Signaling #9661, Beverly, MA, USA), rabbit anti-Ki67 (1:500; Abcam #15580, Cambridge, MA, USA) and rabbit anti- phosphorylated histone 2AX (γH2AX) (1:200; Cell Signaling #9718)—were detected using biotinylated goat anti-rabbit secondary antibody in 5% normal goat serum. All immunostaining procedures included avidin/biotin and 3% hydrogen peroxide blocking steps. Peroxidase activity was visualized using 3,3´-diaminobenzidine (DAB) as substrate (Roche). Sections were counterstained with hematoxylin. The following negative controls were included in every experiment: secondary antibody without primary antibody; primary antibody without secondary antibody; and primary antibody replaced by rabbit IgG with secondary antibody.

The numbers of follicles with oocytes or granulosa cells positive or negative for Ki67, cleaved caspase-3, and γH2AX immunostaining were counted in 3 or 4 slides (12-16 sections, 4

sections/slide) per endpoint distributed throughout the ovary by an investigator blind to exposure group using an Olympus BX-60 microscope with 10, 20, and 40x U PLAN FLUO objectives equipped with a Retiga 2000R cooled CCD digital camera system with Q-Capture Pro software. The fractions of positive primordial and primary follicles (containing one or more positive granulosa cells per largest cross-section or containing positive oocytes) and secondary and antral follicles (containing three or more positive granulosa cells per largest cross-section or containing positive oocytes) were calculated and used for data presentation and analysis.

Terminal deoxynucleotidyl transferase dUTP nick end-labeling (TUNEL)

TUNEL was carried out using the In Situ Cell Death Detection Kit POD (Roche) as previously described (94). Negative controls without terminal transferase and positive controls treated with DNAse I were included in every experiment. The numbers of TUNEL positive and negative secondary and antral follicles (containing 3 or more TUNEL positive granulosa cells per largest cross-section) were counted in 12 sections (3 individual runs, 4 sections/run) distributed throughout the ovary blind to experimental group. Primordial follicles never and primary follicles almost never had TUNEL positive cells. The percentages of TUNEL positive secondary and antral follicles were calculated and used for data presentation and analyses.

Arterial Histology

The aortic root was embedded in OCT, stored frozen (-80 ◦ C), cryosectioned at 10 μm, stained with Oil Red-O and counterstained with hematoxylin to measure the degree of

plaque formation. Images of the aortic root were acquired at 10x magnification, recorded and digitized. ImageJ software (NIH) was used to outline both the total endothelial layer area and the Oil Red O-positive endothelial cell area for each section and expressed as percent Oil Red-O area. For each slide, the total cross-sectional area and the unobstructed lumen area were measured using ImageJ; the percent lumen area was determined. Slides from 3 to 4 individual mice in each exposure group were averaged across all the sections for each animal for data analysis and presentation.

Statistical analyses

Data are presented as means ± SEM unless otherwise noted. Follicle count and estrous cycle data were analyzed by 2-way ANOVA with exposure and year of experiment as independent variables. Immunostaining data expressed as fractions were analyzed by non-parametric Mann Whitney U test or fractions were arcsine square root transformed and analyzed by t-test (100). The results of the two different analyses were very similar and are presented for all endpoints. Heart rate variability and blood pressure variables were analyzed using independent samples t-test following assessment of equality of variances using Levene's test with significance assessed at $P \leq 0.05$. Statistical analyses were performed using SPSS 25 for MacIntosh or SPSS for Windows (IBM Corporation, Armonk, NY, USA).

Declarations

Ethics approval: All experiments involving animals were approved by the University of California Irvine Institutional Animal Care and Use Committee and were performed in accordance with the *Guide for the Care and Use of Laboratory Animals* (101).

Consent for publication: Not applicable.

Availability of data and materials: The datasets used during the current study are available from the corresponding author on reasonable request.

Competing Interests: The authors declare that they have no competing interests.

Funding was provided by California Air Resources Board Contract Number 16RD005 to M.T.K. and U.L.; NIH R01ES020454 to U.L.; and UC Irvine Summer Undergraduate Research Program Fellowships to J.D.N. and J.H.S. The authors are also grateful for funding from the U.S. Army Research Office DURIP Equipment Program (grant #W911NF2010064) for the LC-MS/MS system. The statements and conclusions in this report are those of the investigators and not necessarily those of the California Air Resources Board, the NIH or UC Irvine. The mention of commercial products, their source, or their use in connection with material reported herein is not to be construed as actual or implied endorsement of such products.

Authors' contributions: UL co-designed the project, obtained funding, acquired, analyzed, and interpreted data, and drafted the manuscript. JL acquired and analyzed data. LO acquired and analyzed data. JDN acquired and analyzed data; JHS acquired and analyzed data. BDA acquired and analyzed data. LSL acquired and analyzed data. KL acquired and analyzed data, drafted parts of the manuscript. VP acquired and analyzed data, edited the manuscript. LW acquired and analyzed data, edited the manuscript. RJA acquired and analyzed data, drafted parts of the manuscript. BB acquired and analyzed data. DAH acquired and analyzed data. MTK co-designed the project, obtained funding, edited the manuscript.

Acknowledgments: The authors thank Irene Hasen, Samantha R. Renusch, and Amanda Ting for excellent technical support. The statements and conclusions in this report are those of the investigators and not necessarily those of the California Air Resources Board, the NIH or UC Irvine. The mention of commercial products, their source, or their use in connection with material reported herein is not to be construed as actual or implied endorsement of such products.

References

1. Velasco P. Characterization of Ambient PM10 and PM2.5 in California. California Environmental Protection Agency Air Resources Board; 2005. https://ww3.arb.ca.gov/pm/pmmeasures/pmch05/stateover05.pdf

2. Hirshfield AN. Overview of Ovarian Follicular Development: Considerations for the Toxicologist. Environ Mol Mutagen. 1997;29:10-5.

3. Findlay JK, Hutt KJ, Hickey M, Anderson RA. How Is the Number of Primordial Follicles in the Ovarian Reserve Established? Biol Reprod. 2016;93(5):111.

4. Lei L, Spradling AC. Female Mice Lack Adult Germ-Line Stem Cells but Sustain Oogenesis Using Stable Primordial Follicles. Proc Natl Acad Sci U S A. 2013;110(21):8585-90.

5. Dubey RK, Imthurn B, Barton M, Jackson EK. Vascular Consequences of Menopause and Hormone Therapy: Importance of Timing of Treatment and Type of Estrogen. Cardiovasc Res. 2005;66(2):295-306.

6. Shuster LT, Gostout BS, Grossardt BR, Rocca WA. Prophylactic Oophorectomy in Premenopausal Women and Long-term Health. Menopause Int. 2008;14(3):111-6.

7. Silva I, Mor G, Naftolin F. Estrogen and the Aging Brain. Maturitas. 2001;38(1):95-100.

8. Svejme O, Ahlborg HG, Nilsson J-Å, Karlsson MK. Early Menopause and Risk of Osteoporosis, Fracture and Mortality: A 34-Year Prospective Observational Study in 390 Women. BJOG. 2012;119(7):810-6.

9. Davis BJ, Heindel JJ. Ovarian Toxicants: Multiple Mechanisms of Action. In: Korach KS, editor. Reproductive and Developmental Toxicology. New York: Marcel Dekker, Inc.; 1998. p. 373-95.

10. Zhang T, Dai P, Cheng D, Zhang L, Chen Z, Meng X, et al. Obesity occurring in apolipoprotein E-knockout mice has mild effects on fertility. Reproduction. 2014;147(2):141-51.

11. Nicosia M, Moger WH, Dyer CA, Prack MM, Williams DL. Apolipoprotein-E messenger RNA in rat ovary is expressed in theca and interstitial cells and presumptive macrophage, but not in granulosa cells. Mol Endocrinol. 1992;6(6):978-88.

12. Polacek D, Beckmann MW, Schreiber JR. Rat ovarian apolipoprotein E: localization and gonadotropic control of messenger RNA. Biol Reprod. 1992;46(1):65-72.

13. Umemori Y, Chiba H, Tokusashi Y, Miyokawa N. [Apolipoprotein E immunoreactivities in normal human ovary and ovarian neoplasms] abstract only available in English. Rinsho Byori. 1998;46(1):69-72.

14. Bogan RL, Hennebold JD. The reverse cholesterol transport system as a potential mediator of luteolysis in the primate corpus luteum. Reproduction. 2010;139(1):163-76.

15. Zhang G, Curtiss LK, Wade RL, Dyer CA. An apolipoprotein E synthetic peptide selectively modulates the transcription of the gene for rat ovarian theca and interstitial cell P450 17alpha-hydroxylase, C17-20 lyase. J Lipid Res. 1998;39(12):2406-14.

16. Thompson JE. Airborne Particulate Matter. Human Exposure and Health Effects. J Occup Environ Med. 2018;60(5):392-423.

17. Li X, Huang S, Jiao A, Yang X, Yun J, Wang Y, et al. Association between ambient fine particulate matter and preterm birth or term low birth weight: An updated systematic review and meta-analysis. Environ Pollution. 2017;227:596-605.

18. Pope CAI, Burnett RT, Thurston GD, Thun MJ, Calle EE, Krewski D, et al. Cardiovascular Mortality and Long-Term Exposure to Particulate Air Pollution: Epidemiological Evidence of General Pathophysiological Pathways of Disease. Circulation. 2004;109(1):71-7.

19. Bleil ME, Gregorich SE, McConnell D, Rosen MP, Cedars MI. Does accelerated reproductive aging underlie premenopausal risk for cardiovascular disease? Menopause. 2013;20:1139-46.

20. Agrinier N, Cournot M, Dallongeville J, Arveiler D, Ducimetiere P, Ruidavets J-B, et al. Menopause and modifiable coronary heart disease risk factors: a population based study. Maturitas. 2010;65:237-43.

21. Matthews KA, Kuller LH, Sutton-Tyrrell K, Chang YF. Changes in cardiovascular risk factors during the perimenopause and postmenopause and carotid artery atherosclerosis in healthy women. Stroke. 2001;32(5):1104-11.

22. Bourassa P-AK, Milos PM, Gaynor BJ, Breslow JL, Aiello RJ. Estrogen Reduces Atherosclerotic Lesion Development in Apolipoprotein E-Deficient Mice. Proc Natl Acad Sci U S A. 1996;93:10022-7.

23. Meir KS, Leitersdorf E. Atherosclerosis in the Apolipoprotein E-Deficient Mouse. A Decade of Progress. Arterioscler Thromb Vasc Biol. 2004;24:1006-14.

24. Araujo JA, Barajas B, Kleinman M, Wang X, Bennett BJ, Gong KW, et al. Ambient Particulate Pollutants in the Ultrafine Range Promote Early Atherosclerosis and Systemic Oxidative Stress. Circ Res. 2008;102:589-96.

25. Sun Q, Wang A, Jin X, Natanzon A, Duquaine D, Brook RD, et al. Long-term air pollution exposure and acceleration of atherosclerosis and vascular inflammation in an animal model. JAMA. 2005;294(23):3003-10.

26. Mohallem SV, de Araújo Lobo DJ, Pesquero CR, Assunção JV, de Andre PA, Saldivo PHN, et al. Decreased Fertility in Mice Exposed to Environmental Air Pollution in the City of Sao Paolo. Environ Res. 2005;98:196-202.

27. Veras MM, Damaceno-Rodrigues NR, Guimarães Silva RM, Scoriza JN, Nascimento Saldiva PH, Garcia Caldini E, et al. Chronic Exposure to Fine Particulate Matter Emitted by Traffic Affects Reproductive and Fetal Outcomes in Mice. Environ Res. 2009;109:536-43.

28. Ogliari KS, Lichtenfels AJ, de Marchi MR, Ferreira A, Dolhnikoff M, Saldiva PH. Intrauterine Exposure to Diesel Exhaust Diminishes Adult Ovarian Reserve. Fertil Steril. 2013;99:1681-8.

29. Liao BQ, Liu CB, Xie SJ, Liu Y, Deng YB, He SW, et al. Effects of fine particulate matter (PM2.5) on ovarian function and embryo quality in mice. Environ Int. 2020;135:105338.

30. Zhou S, Xi Y, Chen Y, Zhang Z, Wu C, Yan W, et al. Ovarian Dysfunction Induced by Chronic Whole-Body PM2.5 Exposure. Small. 2020;16(33):e2000845.

31. Lewtas J. Air Pollution Combustion Emissions: Characterization of Causative Agents and Mechanisms Associated with Cancer, Reproductive, and Cardiovascular Effects. Mutat Res. 2007;636:95-133.

32. Jensen TK, Henriksen TB, Hjollund NH, Scheike T, Kolstad H, Giwercman A, et al. Adult and Prenatal Exposures to Tobacco Smoke as Risk Indicators of Fertility among 430 Danish Couples. Am J Epidemiol. 1998;148(10):992-7.

33. Soares SR, Melo MA. Cigarette Smoking and Reproductive Function. Curr Opin Obstet Gynecol. 2008;20:281-91.

34. Tuttle AM, Stampfli M, Foster WG. Cigarette Smoke Causes Follicle Loss in Mice Ovaries at Concentrations Representative of Human Exposure. Hum Reprod. 2009;24(6):1452-9.

35. Mattison DR, White NB, Nightingale MR. The Effect of Benzo(a)pyrene on Fertility, Primordial Oocyte Number, and Ovarian Response to Pregnant Mare's Serum Gonadotropin. Pediatric Pharmacology. 1980;1:143-51.

36. Mattision DR, Singh H, Takizawa K, Thomford PJ. Ovarian Toxicity of Benzo(a)pyrene and Metabolites in Mice. Reprod Toxicol. 1989;3:115-25.

37. Borman SM, Christian PJ, Sipes IG, Hoyer PB. Ovotoxicity in Female Fischer Rats and B6 Mice Induced by Low-Dose Exposure to Three Polycyclic Aromatic Hydrocarbons: Comparison through Calculation of an Ovotoxic Index. Toxicol Appl Pharmacol. 2000;167:191-8.

38. Lim J, Ortiz L, Nakamura BN, Hoang YD, Banuelos J, Flores VN, et al. Effects of Deletion of the Transcription Factor *Nrf2* and Benzo[a]pyrene Treatment on Ovarian Follicles and Ovarian Surface Epithelial Cells in Mice. Reprod Toxicol. 2015;58:24-32.

39. Archibong AE, Ramesh A, Inyang F, Niaz MS, Hood DB, Kopsombut P. Endocrine Disruptive Actions of Inhaled Benzo[a]pyrene on Ovarian Function and Fetal Survival in Fisher F344 Adult Rats. Reprod Toxicol. 2012;34:635-43.

40. Fairchild GA. Measurement of respiratory volume for virus retention studies in mice. Appl Microbiol. 1972;24(5):812-8.

41. Verma V, Cho A, Kleinman M, Shafer M, Schauer J, Sioutas C. Physicochemical and Oxidative Characteristics of Semi-Volatile Components of Quasi-Ultrafine Particles in an Urban Atmosphere. Atmos Environ. 2011;45:1025-33.

42. Keebaugh AJ, Sioutas C, Pakbin P, Schauer JJ, Mendez LB, Kleinman MT. Is atherosclerotic disease associated with organic components of ambient fine particles? Sci Total Environ. 2015;533:69-75.

43. Rogakou EP, Pilch DR, Orr AH, Ivanova VS, Bonner WM. DNA double-stranded breaks induce histone H2AX phosphorylation on serine 139. J Biol Chem. 1998;273(10):5858-68.

44. Franco S, Gostissa M, Zha S, Lombard DB, Murphy MM, Zarrin AA, et al. H2AX prevents DNA breaks from progressing to chromosome breaks and translocations. Mol Cell. 2006;21(2):201-14.

45. Fernandez-Capetillo O, Chen HT, Celeste A, Ward I, Romanienko PJ, Morales JC, et al. DNA damage-induced G2-M checkpoint activation by histone H2AX and 53BP1. Nat Cell Biol. 2002;4(12):993-7.

46. Scholzen T, Gerdes J. The Ki-67 Protein: From the Known to the Unknown. J Cell Physiol. 2000;182:311-22.

47. USEPA. NAAQS Table Washington, D.C.: U.S. Environmental Protection Agency; [Available from: https://www.epa.gov/criteria-air-pollutants/naaqs-table.]

48. Stone SL, Anderko L, Berger MF, Butler CR, Cascio WE, Clune A, et al. Wildfire Smoke: A Guide for Public Health Officials: U.S. Environmental Protection Agency; 2019.

49. Popovich N, Migliozzi B, Patanjali K, Singhvi A, Huang J. See How the World's Most Polluted Air Compares With Your City's New York, NY: New York Times; 2019 [Available from: https://www.nytimes.com/interactive/2019/12/02/climate/air-pollution-compare-ar-ul.html.]

50. Chauhan A, Singh RP. Decline in PM(2.5) concentrations over major cities around the world associated with COVID-19. Environ Res. 2020;187:109634.

51. Wichers Stanek L, Brown JS, Stanek J, Gift J, Costa DL. Air Pollution Toxicology - A Brief Review of the Role of the Science in Shaping the Current Understanding of Air Pollution Health Risks. Toxicol Sci. 2011;120(S1):S8-S27.

52. Nakane H. Translocation of particles deposited in the respiratory system: a systematic review and statistical analysis. Environ Health Prev Med. 2012;17(4):263-74.

53. Hirshfield AN. Size-Frequency Analysis of Atresia in Cycling Rats. Biol Reprod. 1988;38:1181-8.

54. Fenwick MA, Hurst PR. Immunohistochemical Localization of Active Caspase-3 in the Mouse Ovary: Growth and Atresia of Small Follicles. Reproduction. 2002;124:659-65.

55. McGee EA, Horne J. Follicle Atresia. In: Spencer T, Flaws J, editors. Female Reproduction. Encyclopedia of Reproduction. 2. 2 ed. Oxford, UK: Elsevier; 2018. p. 87-91.

56. Hussein MR. Apoptosis in the ovary: molecular mechanisms. Hum Reprod Update. 2005;11(2):162-77.

57. Spears N, Lopes F, Stefansdottir A, Rossi V, De Felici M, Anderson RA, et al. Ovarian damage from chemotherapy and current approaches to its protection. Hum Reprod Update. 2019;25(6):673-93.

58. Tsai-Turton M, Nakamura BN, Luderer U. Induction of Apoptosis by 9,10-Dimethyl-1,2-benzanthracene (DMBA) in Cultured Preovulatory Rat Follicles Is Preceded by a Rise in Reactive Oxygen Species and Is Prevented by Glutathione. Biol Reprod. 2007;77(3):442-51.

59. Kalich-Philosoph L, Roness H, Carmely A, Fishel-Bartel M, Ligumsky H, Paglin S, et al. Cyclophosphamide Triggers Follicle Activation and "Burnout"; AS101 Prevents Follicle Loss and Preserves Fertility. Sci Transl Med. 2013;5(185):185ra62.

60. Roness H, Gavish Z, Cohen Y, Meirow D. Ovarian follicle burnout: a universal phenomenon? Cell Cycle. 2013;12(20):3245-6.

61. Durlinger ALL, Kramer P, Karels B, de Jong FH, Uilenbroek JTJ, Grootegoed JA, et al. Control of Primordial Follicle Recruitment by Anti-Müllerian Hormone in the Mouse Ovary. Endocrinology. 1999;140(12):5789-96.

62. Visser JA, Themmen APN. Anti-Müllerian Hormone and Folliculogenesis. Mol Cell Endocrinol. 2005;234:81-6.

63. Mattsson A, Jernström B, Cotgreave IA, Bajak E. H2AX Phosphorylation in A549 Cells Induced by the Bulky and Stable DNA Adducts of Benzo[*a*]pyrene and Dibenzo[*a,l*]pyrene Diol Epoxides. Chem Biol Interact. 2009;177:40-7.

64. Xue W, Warshawsky D. Metabolic Activation of Polycyclic Aromatic Hydrocarbon and Heterocyclic Aromatic Hydrocarbons and DNA Damage: A Review. Toxicol Appl Pharmacol. 2005;206:73-93.

65. O'Brien TJ, Ceryak S, Patierno SR. Complexities of Chromium Carcinogenesis: Role of Cellular Response, Repair, and Recovery Mechanisms. Mutat Res. 2003;533:3-36.

66. Tam LM, Price NE, Wang Y. Molecular Mechanisms of Arsenic-Induced Disruption of DNA Repair. Chem Res Toxicol. 2020;33(3):709-26.

67. Barnhill LM, Khuansuwan S, Juarez D, Murata H, Araujo JA, Bronstein JM. Diesel Exhaust Extract Exposure Induces Neuronal Toxicity by Disrupting Autophagy. Toxicol Sci. 2020;176(1):193-202.

68. Mattison DR, Thorgeirsson SS. Ovarian Aryl Hydrocarbon Hydroxylase Activity and Primordial Oocyte Toxicity of Polycyclic Aromatic Hydrocarbons in Mice. Cancer Res. 1979;39:3471-5.

69. Ahn RW, Barrett SL, Raja MR, Jozefik JK, Spaho L, Chen H, et al. Nano-encapsulation of arsenic trioxide enhances efficacy against murine lymphoma model while minimizing its impact on ovarian reserve in vitro and in vivo. PLoS One. 2013;8(3):e58491.

70. Banu SK, Samuel JB, Arosh JA, Burghardt RC, Aruldhas MM. Lactational Exposure to Hexavalent Chromium Delays Puberty by Impairing Ovarian Development, Steroidogenesis, and Pituitary Hormone Synthesis in Developing Wistar Rats. Toxicol Appl Pharmacol. 2008;232:180-9.

71. Stanley JA, Sivakumar KK, Nithy TK, Arosh JA, Hoyer PB, Burghardt RC, et al. Postnatal Exposure to Chromium through Mother's Milk Accelerates Follicular Atresia in F1 Offspring through Increased Oxidative Stress and Depletion of Antioxidant Enzymes. Free Radic Biol Med. 2013;61:179-96.

72. Wilde E, Aubdool AA, Thakore P, Baldissera L, Jr., Alawi KM, Keeble J, et al. Tail-Cuff Technique and Its Influence on Central Blood Pressure in the Mouse. J Am Heart Assoc. 2017;6(6):e005204.

73. Padmanabhan V, Puttabyatappa M, Cardoso R. Hypothalamus-Pituitary-Ovary Axis. In: Spencer T, Flaws J, editors. Female Reproduction. Encyclopedia of Reproduction. 2. 2 ed. Oxford, UK: Elsevier; 2018. p. 121-9.

74. Legro RS, Sauer MV, Mottla GL, Richter KS, Li X, Dodson WC, et al. Effect of air quality on assisted human reproduction. Hum Reprod. 2010;25(5):1317-24.

75. Mahalingaiah S, Hart JE, Laden F, Farland LV, Hewlett MM, Chavarro J, et al. Adult air pollution exposure and risk of infertility in the Nurses' Health Study II. Hum Reprod. 2016;31(3):638-47.

76. Carré J, Gatimel N, Moreau J, Parinaud J, Léandri R. Does air pollution play a role in fertility?: A systematic review. Environ Health. 2017;16:82.

77. Erickson GF, Nakatani A, Ling N, Shimasaki S. Insulin-Like Growth Factor Binding Protein-3 Gene Expression Is Restricted to Involuting Corpora Lutea in Rat Ovaries. Endocrinology. 1993;133(3):1147-57.

78. Gai HF, An JX, Qian XY, Wei YJ, Williams JP, Gao GL. Ovarian Damages Produced by Aerosolized Fine Particulate Matter (PM2.5) Pollution in Mice: Possible Protective Medications and Mechanisms. Chin Med J (Engl). 2017;130(12):1400-10.

79. Bourdon M, Torres-Rovira L, Monniaux D, Faure C, Levy R, Tarrade A, et al. Impact of a gestational exposure to diesel exhaust on offspring gonadal development: experimental study in the rabbit. J Dev Orig Health Dis. 2018;9(5):519-29.

80. Miller PB, Charleston JS, Battaglia DE, Klein NA, Soules MR. An Accurate, Simple Method for Unbiased Determination of Primordial Follicle Number in the Primate Ovary. Biol Reprod. 1997;56:909-15.

81. Myers M, Britt KL, Wreford NGM, Ebling FJP, Kerr JB. Methods for quantifying follicular numbers within the mouse ovary. Reproduction. 2004;127(5):569-80.

82. Chen T, Jia G, Wei Y, Li J. Beijing ambient particle exposure accelerates atherosclerosis in ApoE knockout mice. Toxicol Lett. 2013;223(2):146-53.

83. Zhang G, Li C, Zhu N, Chen Y, Yu Q, Liu E, et al. Sex differences in the formation of atherosclerosis lesion in apoE(-/-)mice and the effect of 17β-estrodiol ſon protein S-nitrosylation. Biomed Pharmacother. 2018;99:1014-21.

84. Piedrahita JA, Zhang SH, Hagaman JR, Oliver PM, Maeda N. Generation of mice carrying a mutant apolipoprotein E gene inactivated by gene targeting in embryonic stem cells. Proc Natl Acad Sci U S A. 1992;89(10):4471-5.

85. Souza VR, Mendes E, Casaro M, Antiorio ATFB, Oliveira FA, C.M. F. Description of Ovariectomy Protocol in Mice. In: Guest PC, editor. Pre-Clinical Models: Techniques and Protocols. Methods in Molecular Biology: Springer Science+Business Media, LLC; 2019.

86. Rowan WH, 3rd, Campen MJ, Wichers LB, Watkinson WP. Heart rate variability in rodents: uses and caveats in toxicological studies. Cardiovasc Toxicol. 2007;7(1):28-51.

87. Thireau J, Zhang BL, Poisson D, Babuty D. Heart rate variability in mice: a theoretical and practical guide. Exp Physiol. 2008;93(1):83-94.

88. Kleinman MT, Sioutas C, Froines JR, Fanning E, Hamade A, Mendez L, et al. Inhalation of Concentrated Ambient Particulate Matter Near a Heavily Trafficked Road Stimulates Antigen-Induced Airway Responses in Mice. Inhal Toxicol. 2007;19(Suppl 1):117-26.

89. Kim S, Jaques PA, Chang M, Barone T, Xiong C, Friedlander SK, et al. Versatile Aerosol Concentration Enrichment System (VACES) for Simultaneous in Vivo and in Vitro Evaluation of Toxic Effects of Ultrafine, FIne, and Coarse Ambient Particles Part II: Field Evaluation. J Aerosol Sci. 2001;32:1299-314.

90. Kim S, Jaques PA, Chang M, Froines JR, Sioutas C. Versatile Aerosol Concentration Enrichment System (VACES) for Simultaneous in Vivo and in Vitro Evaluation of Toxic Effects of Ultrafine, Fine, and Coarse Ambient Particles Part I: Development and Laboratory Characterization. J Aerosol Sci. 2001;32(11):1281-97.

91. Oldham M, Phalen RF, Robinson RJ, Kleinman MT. Performance of a Portable Whole-Body Mouse Exposure System. Inhal Toxicol. 2004;16:657-62.

92. Goldman JM, Murr AS, Cooper RL. The Rodent Estrous Cycle: Characterization of Vaginal Cytology and Its Utility in Toxicological Studies. Birth Defects Res (Part B). 2007;80:84-97.

93. Charleston JS, Hansen KR, Thyer AC, Charleston LB, Gougeon A, Siebert JR, et al. Estimating Human Ovarian Non-growing Follicle Number: The Application of Modern Stereology Techniques to an Old Problem. Hum Reprod. 2007;22(8):2103-10.

94. Lopez SG, Luderer U. Effects of Cyclophosphamide and Buthionine Sulfoximine on Ovarian Glutathione and Apoptosis. Free Radic Biol Med. 2004;36:1366-77.

95. Plowchalk DR, Smith BJ, Mattison DR. Assessment of Toxicity to the Ovary Using Follicle Quantitation and Morphometrics. In: Heindel JJ, Chapin RE, editors. Female Reproductive Toxicology. Methods in Toxicology. 3B. San Diego, CA: Academic Press; 1993. p. 57-68.

96. Lim J, Lawson GW, Nakamura BN, Ortiz L, Hur JA, Kavanagh TJ, et al. Glutathione-Deficient Mice Have Increased Sensitivity to Transplacental Benzo[a]pyrene-Induced Premature Ovarian Failure and Ovarian Tumorigenesis. Cancer Res. 2013;73(2):908-17.

97. Desmeules P, Devine PJ. Characterizing the Ovotoxicity of Cyclophosphamide Metabolites on Cultured Mouse Ovaries. Toxicol Sci. 2006;90(2):500-9.

98. Keksi-Rahkonen P, Desai R, Jimenez M, Harwood DT, Handelsman DJ. Measurement of Estradiol in Human Serum by LC-MS/MS Using a Novel Estrogen-Specific Derivatization Reagent. Anal Chem. 2015;87:7180-6.

99. McNamara KM, Harwood DT, Simanainen U, Walters KA, M. J, Handelsman DJ. Measurement of Sex Steroids in Murine Blood and Reproductive Tissues by Liquid Chromatography-Tandem Mass Spectrometry. J Steroid Biochem Mol Biol. 2010;121:611-8.

100. Pasternack BS, Shore RE. Analysis of Dichotomous Response Data from Toxicological Experiments Involving Stable Laboratory Mouse Populations. Biometrics. 1982;38:1057-67.

101. NRC. Guide for the Care and Use of Laboratory Animals. 8 ed. Washington, DC: National Research Council, National Academy of Sciences, National Academies Press; 2011.

Chapter 4

In Chapter 4, we focus on oxidative stress and assess its role in decreasing oocyte developmental competence. GSH is a crucial antioxidant to the reproductive system, we have previously shown that *Gclm -/-* mice are GSH-deficient in the ovaries and oocytes [49]. Additionally, we reported that GSH is important in preventing ovotoxicity of PAHs [89,92]. The studies described in this chapter sought to characterize how the altered the cellular redox state of *Gclm -/-* oocytes would impact the oocyte developmental competence. To this end, we superovulated *Gclm +/+*, *Gclm +/-*, *Gclm -/-* pubertal female mice to measure markers of oxidative stress and explore downstream effects on oocyte maturation.

We observed that *Gclm -/-* oocytes had increased levels of ROS and superoxide as well as decreased mitochondrial membrane potential ($\Delta\Psi m$) compared with *Gclm +/+*; however, interestingly *Gclm* -/- oocytes showed no differences in lipid peroxidation levels compared with the other two genotypes. Previous reports have indicated that *Gclm -/-* mice appear to have dysregulated lipid metabolism [115], and our own findings show that *Gclm* deficiency is protective against BaP-induced hepatic steatosis [116]. We explored neutral lipid droplet (LD) and mitochondrial content and observed that *Gclm -/-* oocytes had significantly decreased LD content compared with wildtypes. This was supported by serum lipidomics analysis using UHPLC-MS/MS which showed significantly distinct serum lipid populations in *Gclm -/-* mice compared with *Gclm +/-* and *Gclm +/+*. Although no differences were observed in total mitochondria or mitochondria colocalization with LDs, *Gclm -/-* oocytes did show significantly decreased mitochondrial clustering in the subcortical region. Together these data demonstrate that decreased oocyte developmental competence of *Gclm -/-* oocytes is likely attributable to increased oxidative stress driven by the mitochondria and subsequent

dysregulation of lipid metabolism globally and storage in the oocyte. These data are consistent with our finding that gestational BaP exposure induced oxidative stress and dysregulation of lipid storage in the F1 oocytes.

Primary Research Article

Glutathione Deficiency Decreases Lipid Droplet Stores and Increases Reactive Oxygen Species in Mouse Oocytes

Kelli F Malott[1], Samantha Reshel[2], Laura Ortiz[3], Ulrike Luderer[1,2,3,4,5,6]

[1]Environmental Health Sciences Graduate Program,

[2]Department of Environmental and Occupational Health,

[3]Department of Developmental and Cell Biology,

[4]Department of Medicine, University of California, Irvine, Irvine, Ca 92617

[5]Grant Support: National Institutes of Health (NIH) R01ES020454 and R21HD097541 to U.L. Tobacco Related Diseases Research Program Predoctoral Fellowship T30DT0816 to K.F.M. The authors wish to acknowledge the support of the UC Irvine Chao Family Comprehensive Cancer Center Optical Biology Shared Resource, supported by the National Cancer Institute of the NIH under award number P30CA062203. West Coast Metabolomics Center, University of California, Davis, supported by NIH U2CES030158.

The content is solely the responsibility of the authors and does not necessarily represent the official views of the National Institutes of Health.

[6]Correspondence: Dr. Ulrike Luderer
Center for Occupational and Environmental Health
100 Theory Drive, Suite 100
Irvine, CA 92617, U.S.A
Tel: 949-824-8641
Email: uluderer@uci.edu

Short Title: Glutathione deficiency and oocyte competence

Summary Sentence: Glutathione deficiency leads to increased oocyte oxidative stress, reduced mitochondrial membrane potential, and aberrant lipid storage, reducing oocyte competence.

Keywords: oocyte, mitochondria, lipid droplets, glutathione, oxidative stress, lipidomics

Abstract

Glutathione (GSH) is a tripeptide thiol antioxidant that has been shown to be important to overall reproductive health. Glutamate cysteine ligase, the rate-limiting enzyme in GSH synthesis consists of a catalytic and a modifier (GCLM) subunit. We previously showed that oxidative stress in the ovary and oocytes of *Gclm -/-* mice is associated with accelerated age-related decline in ovarian follicles and decreased female fertility due to preimplantation embryonic mortality. Mammalian preimplantation development is a highly regulated and energy intensive process that primarily relies on coordination between lipid droplets (LDs) and mitochondria to maintain cellular homeostasis. In this study we hypothesized that GSH-deficiency in oocytes increases oxidative stress, leading to increased mitochondrial dysfunction and decreased LD consumption, therefore decreasing oocyte developmental competence. We observed that *Gclm* -/- oocytes have increased oxidative stress, primarily in the form of mitochondrial superoxide and decreased subcortical mitochondrial clusters. Further, *Gclm* -/- oocytes have decreased mitochondrial membrane potential (ΔΨm) compared with *Gclm* +/+. We surmise this is likely due to the decreased availability of LDs, as we observed a significant decrease in LD content in *Gclm -/-* oocytes compared with *Gclm +/+.* The decreased oocyte LD content is likely related to an altered serum lipidome, with *Gclm -/-* serum having relatively lower unsaturated fatty acids and triglycerides compared to *Gclm +/+* and *Gclm +/-* females*.* Altogether these data support that decreased LDs and increased oxidative stress are primary drivers of decreased oocyte developmental competence in GSH-deficient oocytes.

Introduction

Glutathione (GSH) is an important tripeptide and thiol antioxidant that is produced through two ATP-dependent reactions. The first, mediated by the enzyme glutamate cysteine ligase (GCL), is the rate-limiting reaction [6]. GCL is composed of two subunits, the catalytic and modifier subunits, GCLC and GCLM, respectively [7]. Deletion of *Gclc* is embryonic lethal [8]. *Gclm -/-* mice, however, have apparently normal lifespans despite tissue GSH concentrations that are about 75-90% lower than levels in *Gclm +/+* mice [1,2,5,9].

Mammalian preimplantation development is a highly regulated process that requires oocyte developmental competence, as the preimplantation embryo relies almost entirely on the oocyte for successful development [10]. The mature oocyte has among the highest GSH concentrations of any cell type, around 10 mM [11,12]. GSH stores in the oocyte have been shown to be important for sperm nuclear decondensation, male pronuclear formation, and the formation of the meiotic spindle during meiosis II [11,13–15]. Previously, we observed that female *Gclm -/-* and *Gclm +/+* mice produced equal numbers of litters, but the *Gclm -/-* females produced significantly fewer pups [1]. The decreased offspring production was not caused by increased post-implantation death, as no increases in uterine resorption sites or number of dead fetuses were observed [1]. Instead, we observed increased preimplantation mortality. Oocytes and conceptuses derived from *Gclm -/-* females progressed to the two pronuclei stage and to the blastocyst stage in vivo and in vitro at much lower rates than conceptuses from *Gclm +/-* and *Gclm +/+* females [1]. These data taken together show that the normally high oocyte GSH concentration is important to preimplantation development. Further, we have previously demonstrated that *Gclm -/-* ovaries undergo increased oxidative stress in the form of increased lipid peroxidation marker, 4-hydroxynonenal (4-HNE), and

increased protein oxidative damage marker nitrotyrosine, in both pubertal and adult ovaries compared with *Gclm +/+* [16]. Prepubertal *Gclm -/-* ovaries displayed increased percentages of transitional/primary follicles with mitotic granulosa cells, suggesting increased recruitment into the growing follicle pool. These data combined with the observation of accelerated age-related decline in ovarian follicle numbers in *Gclm -/-* compared with *Gclm +/+* mice all suggest that GSH is an important antioxidant for maintaining a healthy ovarian reserve and preventing accelerated age-related ovarian failure [16]. Left unaddressed in these inquiries was how GSH deficiency alters oocyte developmental competence in the mature MII oocyte.

Oogenesis is the progressive process through which the female germ cell acquires the ability to successfully complete meiosis, ensure monospermic fertilization, decondense the sperm head, and undergo preimplantation development [17,18]. This developmental competence is achieved through nuclear maturation, including nuclear envelope breakdown, meiotic spindle formation, and 1st polar body extrusion upon ovulation [19]; and cytoplasmic maturation, including stockpiling organelles such as endoplasmic reticula, mitochondria, and lipid droplets (LDs), as well as small molecules such as mRNA, ATP, and GSH [19].

Mitochondria are among the most abundant organelles in a healthy, mature oocyte, with each murine oocyte possessing roughly 100,000 mitochondria [20–23]. It is hypothesized that oocyte mitochondria are maintained in a less active state [24] to reduce reactive oxygen species (ROS) production by active oxidative phosphorylation, while still supplying enough ATP to meet the needs of the oocyte, primarily through pyruvate oxidation up until ovulation [25–27]. Mitochondria are the primary source of ROS in cells, converting

0.2-2% oxygen taken up by the oocyte into ROS [28]. Proteins along the electron transport chain partially reduce molecular oxygen, producing the highly reactive superoxide anion radical ($O_2^{-\bullet}$), which is readily converted to hydrogen peroxide and other ROS [20,28]. ROS are well characterized cell signaling molecules, but in excess, ROS can shift the redox state of the cell causing oxidative stress [17,20,29].

Lipid droplets (LDs) are ubiquitous organelles, composed of a neutral, primarily, triacylglycerol core enclosed in a monophospholipid layer [30,31]. Oocytes possess LDs that are composed of triacylglycerols formed from free fatty acids taken up from the follicular fluid, supplied through the blood serum [18,30]. Triacylglycerols and free fatty acids are present in the follicular fluid of several mammalian species, including mice and humans [30,31]. Lipids in the oocyte can be taken up from the follicular fluid or broken down from endogenous cellular lipid to be stored in LDs [17]. LDs are multi-faceted organelles that supply secondary signaling molecules [30,34], supply phospholipids for cellular membrane maintenance [31,34], and provide lipoic acid, an important cofactor for mitochondrial dehydrogenases, that generate NADH to regulate cellular homeostasis [35]. LDs and mitochondria have been demonstrated to colocalize in porcine oocytes using fluorescence / Forster resonance energy transfer [36]. Triacylglycerol stored within oocyte LDs can also be hydrolyzed by lipases to provide free fatty acids for mitochondrial fatty acid β-oxidation, which is required for oocyte nuclear maturation and developmental competence [33,37,38]. Inhibition of mitochondrial fatty acid uptake by the carnitine palmitoyl transferase I inhibitor, etomoxir, hindered mouse oocyte maturation and reduced the rate of blastocyst formation [39,40]. Moreover, delipidated MII oocytes will expend precious resources to rebuild LDs through de novo lipogenesis to support fertilization [41].

In the current study, we used our *Gclm -/-* mouse model to explore the effects of low oocyte GSH concentrations on oocyte quality. We hypothesized that oocytes derived from *Gclm -/-* females have increased ROS levels due to low GSH concentrations, which results in mitochondrial dysfunction, lipid oxidation, and telomere shortening, a hallmark of aging. We further hypothesized that oocytes from *Gclm -/-* females contain fewer LDs.

Materials and Methods

Animals

Gclm null mice were generated by disrupting the *Gclm* gene by replacing exon 1 with a beta-galactosidase/neomycin phospho-transferase fusion minigene [1,9]. The mice have been backcrossed 10 times onto a C57BL/6J genetic background (B6.129-*Gclm*^{tm1Tjka}; hereafter referred to as *Gclm* −/−). Mice for these experiments were generated at the University of California Irvine (UC Irvine) and housed in an American Association for the Accreditation of Laboratory Animal Care-accredited facility, with free access to deionized water and soy-free laboratory chow (Harlan Teklad 2919) on a 14:10h light-dark cycle. Offspring were genotyped by Transnetyx (Cordova, TN) by PCR using primers for both the native *Gclm* sequence and the β-Geo sequence on DNA extracted from toe snips as previously described [1]. Temperature was maintained at 21–23°C. The experimental protocols were carried out in accordance with the Guide for the Care and Use of Laboratory Animals [42] and were approved by the Institutional Animal Care and Use Committee at UC Irvine.

Superovulation

Postnatal day (PND) 35-45 *Gclm +/+, Gclm +/-,* and *Gclm -/-* females were primed to produce a large cohort of preovulatory follicles by i.p. injection with 5 IU equine chorionic

gonadotropin (eCG) (Prospec Protein Specialists, Israel) at 1800 h; 46 h later ovulation was induced by an i.p. injection with 5 IU human chorionic gonadotropin (hCG) (Sigma Aldrich, St. Louis, MO). Twelve to 14 h later, cumulus-oocyte-complexes were harvested, following CO_2 euthanasia, from the ampullae of the oviducts into flushing and holding medium (FHM) (Neta Scientific, Hainesport, NJ). Oocytes were dissociated from the cumulus clouds by incubation in 0.3 mg/ml of hyaluronidase (Thermo Fisher Scientific) for no more than 5 minutes, then immediately transferred to FHM under mineral oil (Sigma-Aldrich, St. Louis, MO) for assessment. Morphologically healthy oocytes were defined as having clear, granular cytoplasm; small perivitelline space; first polar body; colorless zona pellucida; not fragmented. For the following experiments, one *Gclm* -/- female and age-matched *Gclm* +/+ and/or *Gclm* +/- female were superovulated at the same time per experimental replicate.

Measurement of Reactive Oxygen Species

To measure oocyte ROS levels, 2-3 morphologically healthy oocytes from *Gclm -/-* and *Gclm +/+* females per experimental replicate were incubated in 10 μM H_2-DCFDA (2',7'-dichlorofluorescin diacetate) (Thermo Fisher Scientific, Waltham, MA) in FHM under mineral oil at 37°C and 5% CO_2 for 15 minutes. Two oocytes from each genotype were incubated with 0.003% hydrogen peroxide plus H_2-DCFDA as positive control oocytes and two oocytes from each genotype were incubated with FHM alone as negative controls. Upon entering the cell, H_2-DCFDA is deacetylated by cellular esterases, yielding a nonfluorescent compound, which is oxidized by ROS into a highly fluorescent compound. Oocytes were then washed through three droplets of FHM under mineral oil and imaged in a glass-bottomed petri dish in 50 μL droplets of FHM without phenol red under mineral oil. Oocytes were

imaged using a Zeiss Axiovert 200M microscope (Zeiss, Oberkochen, Germany) at 40X objective with FITC excitation. Images were captured using an Axiovision camera and fluorescence intensity was quantified using ImageJ software to estimate levels of ROS. Specifically, the Corrected Total Cell Fluorescence (CTCF) was obtained by subtracting the product of area of the selected cell and the fluorescence of background measurements from the integrated density of the selected oocyte (CTCF=Integrated Density-[Area of selected cell x Background fluorescence]) [43]. On every experimental day oocytes from *Gclm -/-* and *Gclm +/+* mice were imaged, and the fluorescence intensity for each experimental oocyte of each genotype was expressed as fold the average fluorescence in the respective positive control oocytes from the same experimental day. This allowed for normalization across experimental days.

Measurement of Neutral and Oxidized Lipid Droplets

To measure the ratio of oxidized:unoxidized lipids, 2-3 morphologically healthy oocytes per genotype per experimental replicate were incubated in 10 μM BODIPY 581/591 C11 (Thermo Fisher Scientific, D3861) at 37ºC and 5% CO_2 for 30 minutes under mineral oil, then subsequently washed through three droplets of FHM. Oocytes were imaged in glass-bottomed petri dishes in 50 μL droplets of FHM without phenol red under mineral oil. BODIPY 581/591 C11 colocalizes with fatty acids inside the cell; upon oxidation of the polyunsaturated butadienyl portion, the fluorescence emissions peak shifts from ~590 nm to ~510 nm, this red-to-green fluorescence shift allows for the use of green:red ratio reporting of oxidized lipids.

To measure the total neutral lipid content, 2-3 morphologically healthy oocytes per genotype per experimental replicate were fixed with 4% paraformaldehyde for 1 h at room temperature, then washed through three droplets of 1X phosphate-buffered saline (PBS) with 3 mg/mL of polyvinyl-pyrrolidine (PVP) (Thermo Fisher Scientific, P0930). Fixed oocytes were incubated in 3.82 μM of BODIPY 493/503 (4,4-difluoro-1, 3, 5, 7, 8-pentamethyl-4-bora-3a,4a-diaz-s-indacene) (Thermo Fisher Scientific, D3922) for 1 h at room temperature under mineral oil, washed through three droplets of 1X PBS with 3 mg/mL PVP then imaged in glass-bottomed petri dishes in 50 μL droplet of 1X PBS under mineral oil. BODIPY 493/503 is a nonpolar lipid stain. Total lipid droplet content per oocyte was estimated by the sum fluorescence per cell.

Measurement of Mitochondrial Membrane Potential and Superoxide Production

To assess mitochondrial membrane potential (ΔΨm), we used the JC-1 (5,5',6,6'-tetrachloro-1,1',3,3'-tetraethyl-benzimidazolylcarbocyanine iodide) probe (Thermo Fisher Scientific, T3168). One to three Morphologically healthy oocytes per genotype per experimental replicate were incubated in 5 μM of JC-1 for 15 minutes at 37ºC and 5% CO_2 under mineral oil, subsequently washed through three consecutive droplets of FHM, prior to imaging on a glass-bottomed petri dish in 50 μL droplet of FHM under mineral oil. Positive control oocytes were incubated in 1 μM of CCCP (carbonyl cyanide 3-chlorophenylhydrazon) (Millipore Sigma, C2759) under mineral oil for 15 minutes at 37º C at 5% CO_2 prior to incubation with JC-1. CCCP is a known mitochondrial uncoupler, which breaks down the ΔΨm by transporting protons across the inner mitochondrial membrane [44]. JC-1 is a cationic carbocyanine dye that accumulates in the mitochondria. In low concentrations, the

dye stays in its j-monomer form and will fluoresce green; however, in high concentrations the dye will form j-aggregates that fluoresce red. Due to its cationic nature, the concentration of JC-1 per organelle is dependent on the ΔΨm, thus, lower ΔΨm will fluoresce green and high ΔΨm, red. Total ΔΨm per oocyte is reported as the total sum fluorescence ratio of red:green.

MitoSOX (Thermo Fisher Scientific, M36008) was used to assess specifically mitochondrial superoxide production in live oocytes. One to three morphologically healthy oocytes per genotype per experimental replicate were incubated in 5 μM of MitoSOX for 30 minutes at 37°C and 5% CO_2 under mineral oil, then washed through three droplets of FHM prior to imaging on a glass-bottomed petri dish in 50 μL droplet of FHM under mineral oil. Positive control oocytes were incubated with 1 μM of CCCP for 15 minutes at 37°C and 5% CO_2 prior to MitoSOX incubation. MitoSOX is fluorogenic dye targeted to the mitochondria. Once in the mitochondria, it will be immediately oxidized by superoxide if present, emitting red fluorescence. Mitochondrial superoxide production was estimated by total red fluorescence per oocyte divided by the mean red fluorescence of *Gclm -/-* oocytes analyzed on the same day.

Measurement of Mitochondria and Lipid Droplet Colocalization

One to three morphologically healthy oocytes per genotype per experimental replicate were incubated in 300 nM of MitoTracker Deep Red (Thermo Fisher Scientific, M22426) at 37°C and 5% CO_2 for 30 minutes under mineral oil, then washed through three droplets of FHM, and fixed in 4% paraformaldehyde at room temperature for 1 h in darkness. Following fixation, oocytes were washed through three small droplets of 1X PBS with 3

mg/mL PVP then incubated in 3.82 μM BODIPY 493/503 under mineral oil for 1 h at room temperature in darkness. Following that incubation, oocytes were washed through three small droplets of 1X PBS with 3 mg/mL PVP. Oocytes were immediately imaged using confocal microscopy; mitochondria were visualized using 644/665 (ex/em) and LDs were visualized using 493/503 (ex/em).

Confocal Imaging and Image Analysis

Unless otherwise stated, z-stack imaging was performed on a Zeiss two-photon laser scanning microscope 780 (ZEISS Research Microscopy Solutions), and all imaging analysis was performed using Imaris imaging software (Oxford Instruments) or FIJI ImageJ (NIH). Analysis of ΔΨm, mitochondria, and LDs were performed in Imaris by using a 3-dimensional (3D) rendering of the z-stack images. The raw fluorescence for each channel was used to render volumes specific to the fluorescence wavelength. Volumes in Imaris are 3D models computed from 3D images. The mean fluorescence of each individual volume was calculated and the sum fluorescence for the whole oocyte was calculated. Mitochondrial clustering was assessed in Imaris using volumes created in the 3D rendered oocyte from z-stack. Clusters were defined as overlapping mitochondrial surfaces having a combined volume of greater than 10 μm^3. Any mitochondrial surface, individual or clustered, located within 8 μm of the plasma membrane was defined as subcortical.

Mitosox fluorescence was analyzed in ImageJ FIJI by compressing the z-stack into a z-stack maximum intensity projection, subtracting background fluorescence, then measuring the fluorescence in a region of interest encompassing the oocyte.

qPCR for Telomere Length

Mice were superovulated, and oocytes were collected and washed through drops of FHM as described above. Oocytes were then transferred to 1X PBS with 3 mg/mL PVP and frozen at -80°C. On the day of DNA extraction, oocytes were thawed and pooled, with 20 oocytes of good morphology (clear, granular cytoplasm; small perivitelline space; first polar body; colorless zona pellucida; not fragmented) of the same genotype per pool and with each pool containing oocytes from 1 to 3 mice. Genomic DNA was extracted from oocytes following QIAmp DNA Micro Handbook according to "Isolation of Genomic DNA from Tissues" protocol with a few modifications. Briefly, oocytes were suspended in 180 µL Buffer ATL and equilibrated to room temperature then proteinase K was added to each sample and incubated overnight at 56° C. 200 µL of Buffer AL was added to all samples followed by 200 µL of 95% EtOH, mixed and incubated for 5 min at room temperature. Samples were briefly centrifuged, and lysates were eluted using QIAamp MinElute column. Columns were washed with 80% EtOH following standard column wash steps then centrifuged at full speed for 3 min to dry the membrane. Following centrifugation, ultrapure water was warmed to 65° C, then applied to the column and allowed to incubate for 10 min. Eluted genomic DNA was quantified using NanoDrop. Relative average length of telomeres was assessed by qPCR according to previously described methods [45]. This method quantifies telomeric DNA using forward and reverse primers 5′ CGG TTT GTT TGG GTT TGG GTT TGG GTT TGG GTT TGG GTT 3′ and 5′ GGC TTG CCT TAC CCT TAC CCT TAC CCT TAC CCT TAC CCT 3′ respectively. That amount is then divided by the quantity of a single copy gene, the ribosomal protein, large, P0 (RPLP0, also known as 36B4) gene (Forward and reverse primers were 5′ ACT GGT CTA GGA CCC GAG AAG 3′ and 5′ TCA ATG GTG CCT CTG GAG ATT 3′, respectively) providing an average telomere length ratio. Reactions were run in triplicate with 25 µL total (12.5 µL

Sybr Green PCR Master Mix, 300 nM forward primer, 500 nM reverse primer, 20 ng genomic DNA, and ultrapure water). A standard curve was generated using a 2X dilution series of gDNA from 0.156 ng/μL-0.00061 ng/μL. PCR amplification of telomeres was performed on a BioRad CFX Connect Thermal Cycler using the following program: 1) initial incubation at 95° C for 10 min; 2) each cycle (total of 40 cycles) at 95° C for 15 sec, followed by incubation at an average annealing temperature of forward and reverse primers at 61° C for 1 min; 3) final elongation step at 55° C for 5 sec. Relative telomere length was calculated using the Pfaffl method [46].

Serum Lipidomics

Serum lipidomics were carried out on superovulated *Gclm* +/+, *Gclm* +/-, and *Gclm* -/- mice as well as unsuperovulated *Gclm* +/- females, by the NIH West Coast Metabolomics Center at the University of California, Davis using the following protocol. Blood serum was extracted following the protocols first published in Matyash V. et al. 2008 [47]. Data were acquired using the following chromatographic parameters. Waters Acquity UPLC CSH C18 column (100 mm length x 2.1 mm internal diameter; 1.7 μm particles) was heated to 65°C and protected by a guard column. Mobile phase flow-rate was 0.6 mL/min, and samples were injected at volume of 1.67 μL for ESI(+) and 5 μL for ESI(−) at injection temperature of 4°C. Mobile phases for positive mode were as follows, mobile phase A: 60:40 v/v acetonitrile:water + 10 mM ammonium formate + 0.1% formic acid and mobile phase B: 90:10 v/v isopropanol:acetonitrile + 10 mM ammonium formate + 0.1% formic acid. Mobile phases for negative mode were as follows, mobile phase A: 60:40 v/v acetonitrile:water + 10 mM ammonium acetate and mobile phase B: 90:10 v/v isopropanol:acetonitrile + 10 mM

ammonium acetate. The gradient was the same for both positive and negative modes as follows: 0 min 15% (B), 0–2 min 30% (B), 2–2.5 min 48% (B), 2.5–11 min 82% (B), 11–11.5 min 99% (B), 11.5– 12 min 99% (B), 12–12.1 min 15% (B), 12.1–15 min 15% (B). ESI capillary voltage was ESI(+): +3.5 kV; ESI(–): –3.5 kV. Precursor/product isolation width set for 4 Da. Collision energy was set at 25 eV for ESI(+); 25 eV for ESI(–). Scan range for positive mode was m/z 120 – 1200 Da and scan range negative mode was m/z 60–1200 Da. Spectral acquisition speed: 2 spectra/s. Mass resolution was set at 10,000 for ESI(+) on an Agilent 6530 QTOF MS; 20,000 for ESI(–) on an Agilent 6550 QTOF MS.

Lipidomics peak intensity data were analyzed using MetaboAnalyst 5.0 (NIH and GenomeCanada; [48]). No data were filtered, all values were normalized to the mean of *Gclm* -/- serum; the data were found to be skewed so a log10 transformation was used along with pareto scaling. Univariate analyses utilized ANOVA with Fisher's Least Significant Difference tests for intergroup comparisons. Multivariate Principal Component Analysis (PCA) was performed. Hierarchical clustering analysis using a Euclidean distance measure and Ward clustering algorithm was performed on the lipid species that were found to have an ANOVA FDR adjusted p-value of less than 0.02. Random Forest supervised classification and feature selection was also performed. Random Forest is a supervised learning algorithm that uses a group of classification trees. A bootstrap subset of the whole data set from which random features were selected at each branch was used to grow the group. Class prediction was based on the majority vote of the group. During tree construction, about one-third of the samples were left out of the bootstrap set. This (out of bag) OOB data was then used as a test sample to obtain an unbiased estimate of the classification error (OOB error). Variable

importance was evaluated by measuring the increase of the OOB error when it was permuted.

Statistical Analyses

Data are displayed as means +/- SEM unless otherwise noted. The reported Ns in this study are representative of the number of animals per genotype for each endpoint. The effect of *Gclm* genotype on the average oocyte DCF fluorescence levels for multiple oocytes from the same mouse was analyzed by t-test. The effects of *Gclm* genotype on all other oocyte endpoints were analyzed using the Generalized Estimating Equation (GEE) form of General Linear Model to account for repeated measures within animals (the same endpoint was measured in multiple oocytes from the same mouse). GEE models utilized exchangeable correlation matrices. IBM SPSS Statistics 25 for Macintosh was used for statistical analyses.

Results

Gclm -/- oocytes have increased ROS levels, likely attributed to increased mitochondrial superoxide.

We observed no differences in the numbers of morphologically healthy oocytes ovulated across genotypes (Figure 4.1A). On average, *Gclm +/+* ovulated 19 ± 3 (N=13), *Gclm* +/- ovulated 15 ± 2 (N=21), *Gclm -/-* ovulated 17 ± 2 (N=31). ROS levels were measured in superovulated oocytes of *Gclm* -/- and *Gclm* +/+ mice using H_2DCF-DA. Relative ROS was measured as fluorescence intensity in experimental oocytes compared to fluorescence intensity in 0.003% hydrogen peroxide treated positive control oocytes of the same genotype on the same day. Relative ROS concentrations in *Gclm -/-* oocytes were significantly higher compared with *Gclm +/+* counterparts (P=0.008, *t*-test) (Figure 4.1B). Mitochondria

are the primary source of ROS in oocytes even though the mitochondria of oocytes are relatively quiescent [23,29,49]. H_2DCF-DA fluorescence assays are non-specific, reacting with any reactive oxygen species to fluoresce green. Therefore, we measured mitochondrial superoxide using the fluorescent probe MitoSOX to determine the average fold red fluorescence of *Gclm +/+*, *Gclm +/-,* and *Gclm -/-* oocytes. We observed that *Gclm -/-* oocytes have increased mitochondrial superoxide compared with both *Gclm +/+* and *Gclm +/-* oocytes (P=0.045, GEE) suggesting that the lack of GSH in the mitochondria of the *Gclm -/-* oocytes is the primary cause for increased oxidative stress and that GSH is the primary antioxidant that maintains this balance in oocyte mitochondria (Figure 4.1C).

No difference in telomere length between Gclm -/- and Gclm +/+ oocytes.

Telomeres are tandem repeats of TTAGGG at the end of chromosomes. They are thought to prevent chromosome ends from being recognized as DNA double strand breaks. However, due to their high guanine content, telomeres are especially susceptible to oxidative damage [50,51]. Previously we have shown that *Gclm -/-* mice undergo accelerated age-related decreases in ovarian follicle numbers [16]. Shortened telomere length is considered to be a hallmark of aging [52]. To assess if increased ROS in *Gclm -/-* oocytes lead to decreased telomere length and therefore advanced aging in the *Gclm -/-* oocyte, telomere length was compared in oocyte DNA from *Gclm -/-* and *Gclm +/+* mice. The relative telomere lengths did not differ significantly between the two genotypes for oocytes with normal morphology (Figure 4.1D). These data suggest that increased ROS in the oocyte does not cause a statistically significant difference in oocyte telomere length in peripubertal mice.

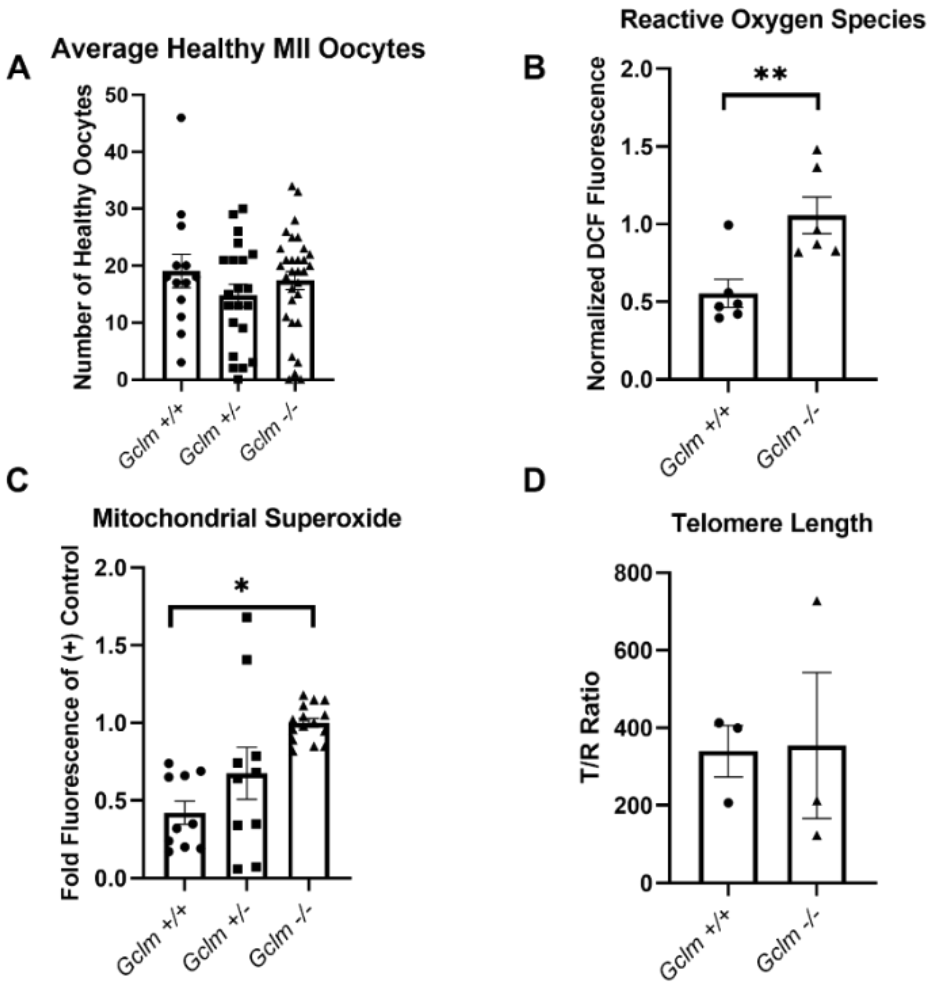

Figure 4.1: *Gclm -/-* oocytes have increased levels of ROS compared to *Gclm +/+* oocytes. A) No difference among genotypes in the number of morphologically healthy oocytes ovulated (N=13-31 females/genotype). **B)** Mean ± SEM green fluorescence of experimental oocytes relative to mean fluorescence of 0.003% hydrogen peroxide-treated, positive control oocytes of same genotype on the same experimental day (**P=0.008, T-test, N= 6 females/genotype; superimposed filled circles, squares and triangles show values for individual oocytes in this and subsequent figures). **C)** *Gclm -/-* oocytes have increased levels of mitochondrial superoxide, as estimated by fold *Gclm -/-* fluorescence of oocytes analyzed on the same day (*P=0.045, GEE, N=5-8 females/genotype) **D)** There was no statistically significant difference in telomere length between genotypes (N=3 pools of 20 oocytes each from 1-2 females/genotype)

Gclm -/- oocytes have decreased mitochondrial membrane potential and decreased subcortical mitochondrial clustering

We observed an increase in superoxide production in *Gclm -/-* oocytes (Figure 4.1B). Mitochondrial superoxide is produced during the reduction of oxygen in the electron transport chain [53,54]. Typically, the increase in SO production implicates mitochondrial respiratory dysfunction [53,54]. Electrons are carried along the electron transport chain and used to pump protons into the intermembrane space of the mitochondrion, generating an electrochemical gradient. This gradient is referred to as mitochondrial membrane potential (ΔΨm) and is an important indicator of mitochondrial activity. We assessed ΔΨm of *Gclm +/+, Gclm +/-,* and *Gclm -/-* oocytes and observed that *Gclm -/-* and *Gclm +/-* oocytes had significantly lower ΔΨm than *Gclm +/+* counterparts (P=0.032, effect of genotype, GEE) (Figure 4.2A, B). Next, we explored differences in mitochondrial clustering among genotypes and found that although there was no difference in mitochondrial clustering in the whole oocyte, *Gclm -/-* oocytes had significantly less mitochondrial clusters in the more oxygenated subcortical region of the oocyte than *Gclm+/-* and *Gclm+/+* oocytes (Figure 4.2D, E). Together these data demonstrate a potential compensatory mechanism exhibited by *Gclm -/-* oocyte mitochondria to accommodate higher levels of oxidative stress.

No difference in oocyte lipid peroxidation across genotypes

ROS are highly reactive and stochastically react with and oxidize the first macromolecules (lipids, DNA, proteins) with which they come in contact; in the case of free fatty acids and other lipids this can create lipotoxic conditions that degrade the health of the cell further [55]. Under homeostatic conditions, oxidized lipids and other macromolecules

would be reduced by GSH, with the help of glutathione peroxidase [29]. To characterize how GSH-deficiency impacts the oxidation state of this crucial energy source in mature oocytes, we utilized the fluorophore BODIPY 581/591 C11. We measured the fold difference of oxidized (green) to unoxidized (red) fluorescence ratio compared with *Gclm -/-* oocytes and observed no statistical difference among all genotypes in lipid peroxidation levels (Figure 4.2C). Even though there is a significant increase in ROS, specifically superoxide (Figure 4.1A, B), there is no effect on lipid peroxidation levels in *Gclm -/-* oocytes. Given that ROS reactivity with cellular macromolecules is stochastic in nature, this suggests that *Gclm -/-* oocytes have fewer lipids overall therefore reducing the probability that a ROS molecule will react with a lipid before a protein or other macromolecules.

Table 4.1: Random Forest Classification Performance

	Gclm -/-	***Gclm +/-***	***Gclm +/+***	**unsuper-ovulated**	**classification error**
Gclm -/-	9.00	0.00	0.00	0.00	0.00
Gclm +/-	2.00	1.00	1.00	1.00	0.80
Gclm +/+	0.00	4.00	0.00	0.00	1.00
unsuper-ovulated	0.00	0.00	0.00	4.00	0.00

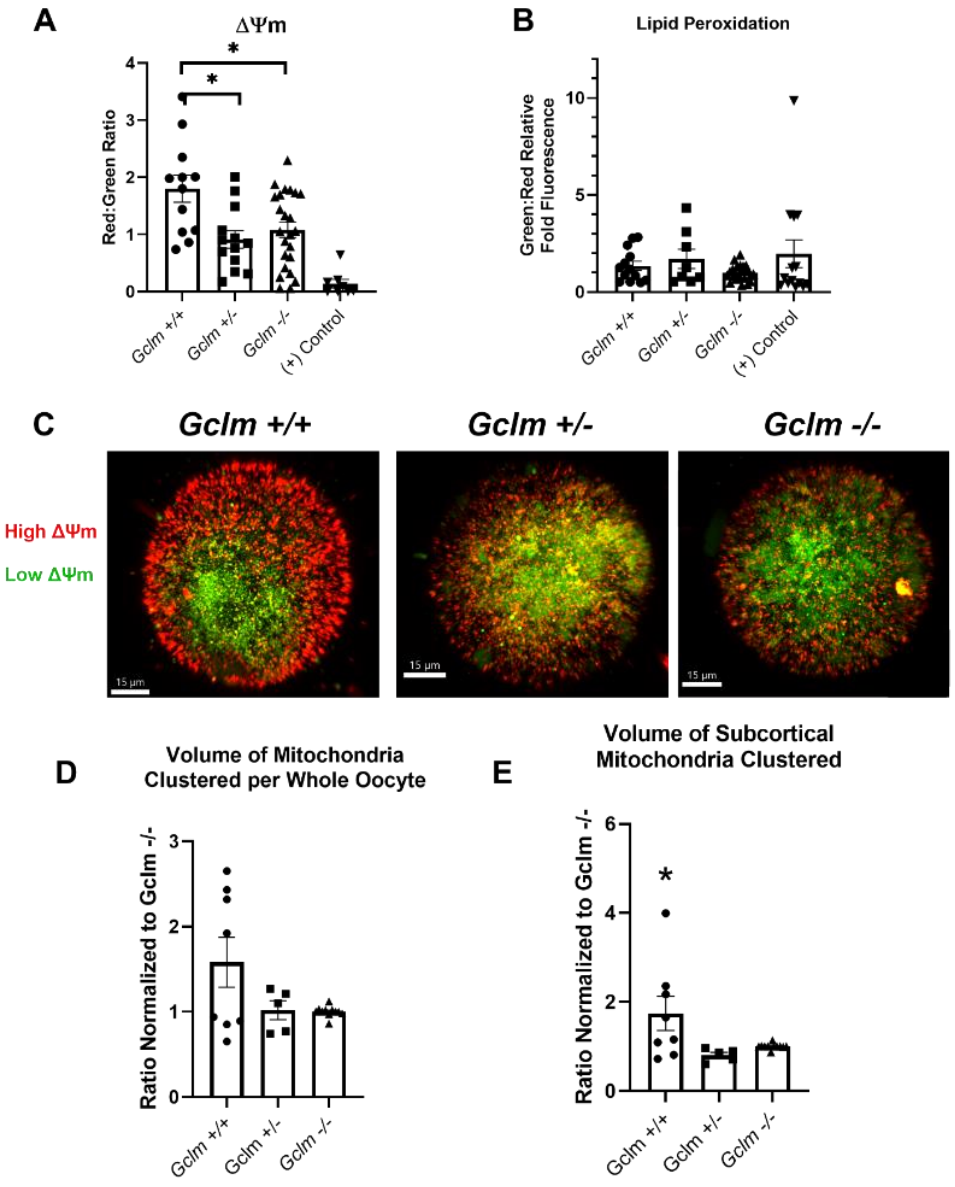

Figure 4.2: *Gclm -/-* oocytes have decreased ΔΨm but no difference in lipid peroxidation compared with *Gclm +/+* oocytes. A) Total mean red:green fluorescence ratio measured using JC-1, where red is indicative of highly polarized mitochondria and green is indicative of less polarized mitochondria (*P<0.05, GEE, N=5-11 females/genotype). **B)** Representative confocal images of JC-1 ΔΨm measurement (red= high ΔΨm, green= low ΔΨm). **C)** Total mean green:red fluorescence ratio as measured by BODIPY 581/591 C11, excitation at 581 nm and emission at 591 nm (red) which will shift to 510 nm (green) when oxidized. (N=4-9 females/genotype). **D)** Total mitochondria clusters per whole oocyte (N=3-7 females/genotype) **E)** Ratio of mitochondria clustered in the subcortical region (N=3-7 females/genotype, *P<0.05, GEE). Superimposed filled symbols show values for individual oocytes in all graphs in this Figure.

Gclm -/- mice have altered serum lipid profiles compared with Gclm +/- and Gclm +/+

It is understood that follicular fluid is sourced from the serum and provides essential metabolites to growing follicles [21,34]. We have previously demonstrated that *Gclm* -/- mice have decreased adipogenesis and are therefore protected from increased risk of hepatic steatosis following in utero exposure to benzo(a)pyrene [5]. Since we observed no difference in the lipid peroxidation of ovulated oocytes among genotypes, we explored if there was a *Gclm* genotype-associated difference in serum lipids using high performance liquid chromatography-mass spectrometry.

We observed distinct differences among genotypes, with superovulated *Gclm -/-* females possessing a distinct serum lipid population from superovulated *Gclm +/+* and *Gclm +/-* females by hierarchical cluster analysis, PCA, and Random Forest analyses (Figure 4.3A, B, C, Table 4.1). Serum from superovulated *Gclm +/+* and *Gclm +/-* mice was enriched in mono- and poly-unsaturated fatty acids (linolenic, eicosenoic, eicosatrienoic, and FA 22:4) and triacylglycerols compared with *Gclm -/-* serum (Figure 4.3A; Figure 4.4A, B; Supplemental Table S1). Further, serum from superovulated *Gclm -/-* mice was observed to be enriched in sphingomyelins and had increased levels of cholesterol compared with the other genotypes (Figure 4.3A; Figure 4.4D, Supplemental Table S1). Interestingly, serum from unsuperovulated *Gclm +/-* females had a distinct lipid profile from superovulated females of all genotypes (Figure 4.3A, B, C; Figure 4.4C). This group was found to be enriched in phospholipids and sphingomyelins, and deficient in triacylglycerols as well as ceramides (Figure 4.3A; Figure 4.4B, C, D; Supplemental Table S1). Together these data show that *Gclm*

-/- serum carries decreased levels of the lipids that are ultimately required for oocyte competence.

Gclm +/- and Gclm -/- oocytes have fewer lipid droplets

It is well established that LDs are important for oocyte developmental competence, playing several crucial roles in maintenance of the oocyte and preimplantation embryonic development [20,21,34,40,41,56]. Above we found that the serum lipid profile in *Gclm* -/- mice was distinctly different from the serum lipid profiles of the other two genotypes (Figure 4.3A, B, C). Therefore, we assessed the lipid stores in ovulated oocytes in all three genotypes. We found both *Gclm +/-* and *Gclm -/-* oocytes have significantly lower LD content than *Gclm +/+* oocytes (P=0.001, effect of genotype, GEE) (Figure 4.5A, D). The average volume of a single LD was significantly lower in *Gclm -/-* oocytes compared to *Gclm +/-* and *Gclm +/+* oocytes (P<0.001, effect of genotype, GEE) (Figure 4.5C). However, there was no significant difference in the proportion of mitochondria colocalized with LDs amongst genotypes (Figure 4.5B). Together these data show that the decreased levels of triacyglycerols and free fatty acids in *Gclm -/-* serum are correlated with decreased LD content and smaller LDs, but the ability for those oocytes to metabolize fatty acids is likely equivalent amongst genotypes.

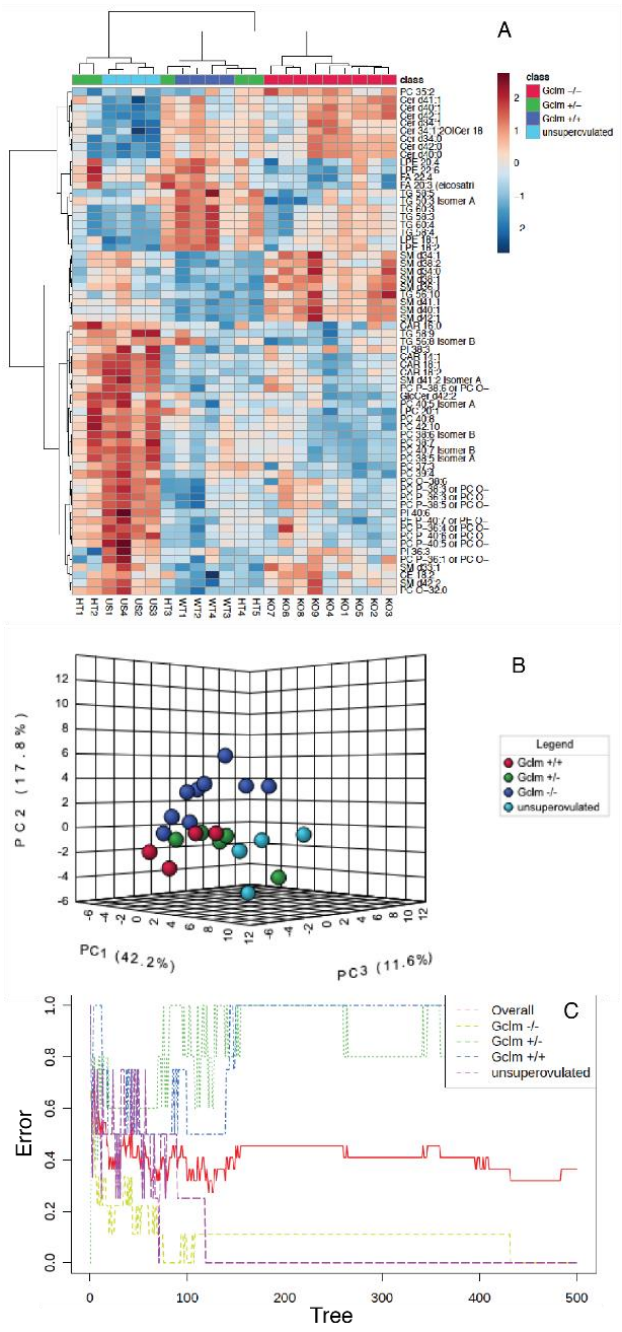

Figure 4.3: Serum lipidomics demonstrate altered lipid profile in superovulated *Gclm -/-* mice compared to superovulated *Gclm +/-* and *Gclm +/+* mice and unsuperovulated *Gclm+/-* mice. A) Hierarchical cluster analysis of serum lipid concentrations shows distinct clusters of *Gclm -/-* and unsuperovulated *Gclm+/-*. **B)** Principal component analysis similarly shows that *Gclm -/-* females have distinct serum lipid profile compared with other genotypes. **C)** The Random Forest classification shows the cumulative classification error rates for each experimental group, as well as the overall error rate, as the group of classification trees is grown by random feature selection from a bootstrap sample. The analysis shows that *Gclm-/-* and unsuperovulated mice have distinct serum lipid profiles, which allow them to be reliably separated with zero error rates from the other experimental groups, while *Gclm +/-* and *Gclm +/+* mice do not. (N=4-9 females/group)

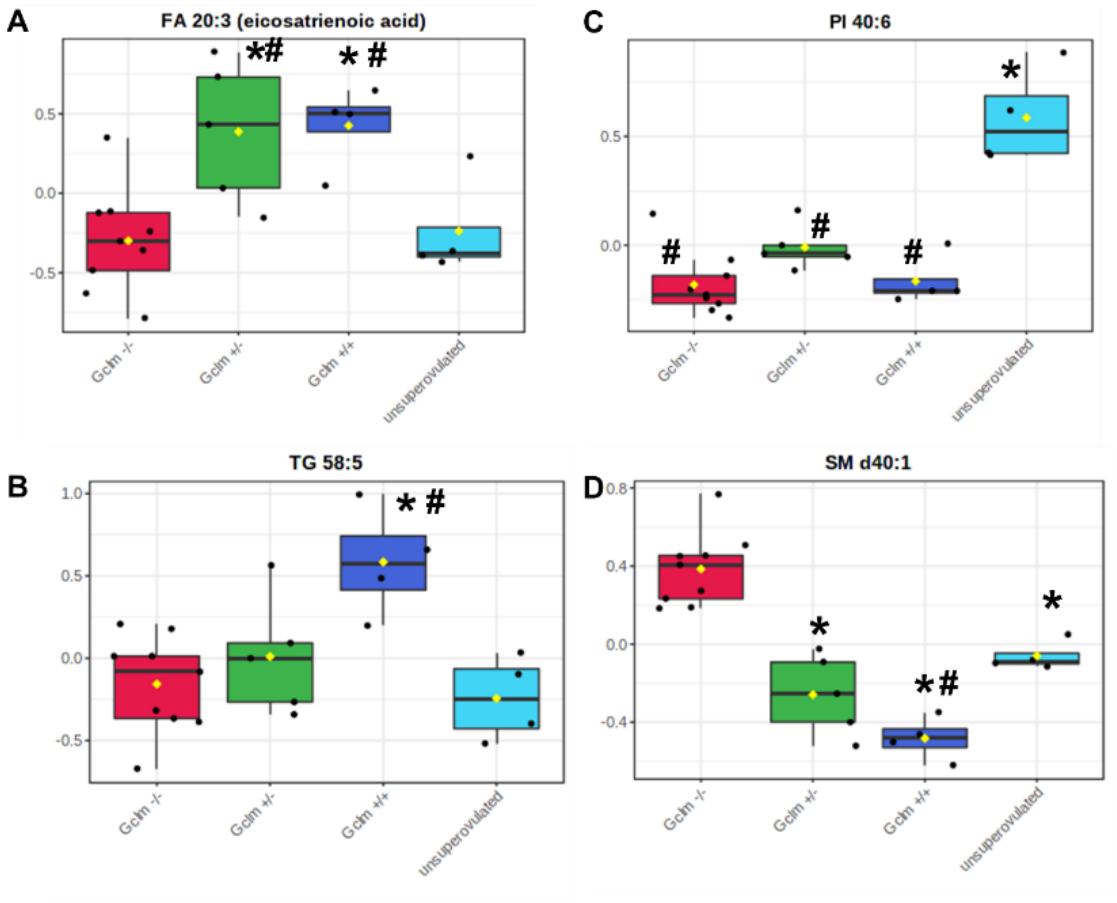

Figure 4.4: Representative differences in serum fatty acids, triacylglycerols, phosphoslipids, and sphingomyelins among *Gclm* genotypes. A-D) Representative box-and-whisker plots from serum lipidomics analysis described in Figure 3 showing significantly different concentrations of representative (A) fatty acids (FDR p-value=0.015), (B) triacylglycerols (FDR p-value=0.004), (C) phospholipids (FDR p-value=0.0001), and (D) sphingomyelin (FDR p-value=7.43E-05) among experimental groups. * Significantly different ($p<0.05$) from *Gclm-/-* by Fisher's LSD test; # significantly different ($p<0.05$) from unsuperovulated by Fisher's LSD test. (N=4-9 females/group)

Discussion

In this study we explored possible underlying changes in oocyte quality, which may explain why embryos derived from *Gclm -/-* oocytes, possessing <20% of the average *Gclm +/+* oocyte GSH concentration, have increased preimplantation mortality compared with *Gclm* +/+ oocytes [1]. We observed that *Gclm -/-* oocytes have increased cellular ROS and mitochondrial superoxide in comparison to their wildtype counterparts. Consistent with

this, we found that *Gclm -/-* and *Gclm +/-* oocytes had decreased ΔΨm and decrease subcortical mitochondrial clustering in comparison to *Gclm +/+* oocytes. This increase in ROS and decreased ΔΨm did not, however, result in an increase in oocyte lipid peroxidation; we surmise this is likely because *Gclm -/-* oocytes possess significantly less LD content than *Gclm +/+* oocytes. Lipids stored in LDs are derived, in part, from serum. When we assessed the serum lipid profiles for the three genotypes, we found *Gclm -/-* serum to be deficient in triacylglycerols and fatty acids compared with *Gclm +/-* and *Gclm +/+* serum.

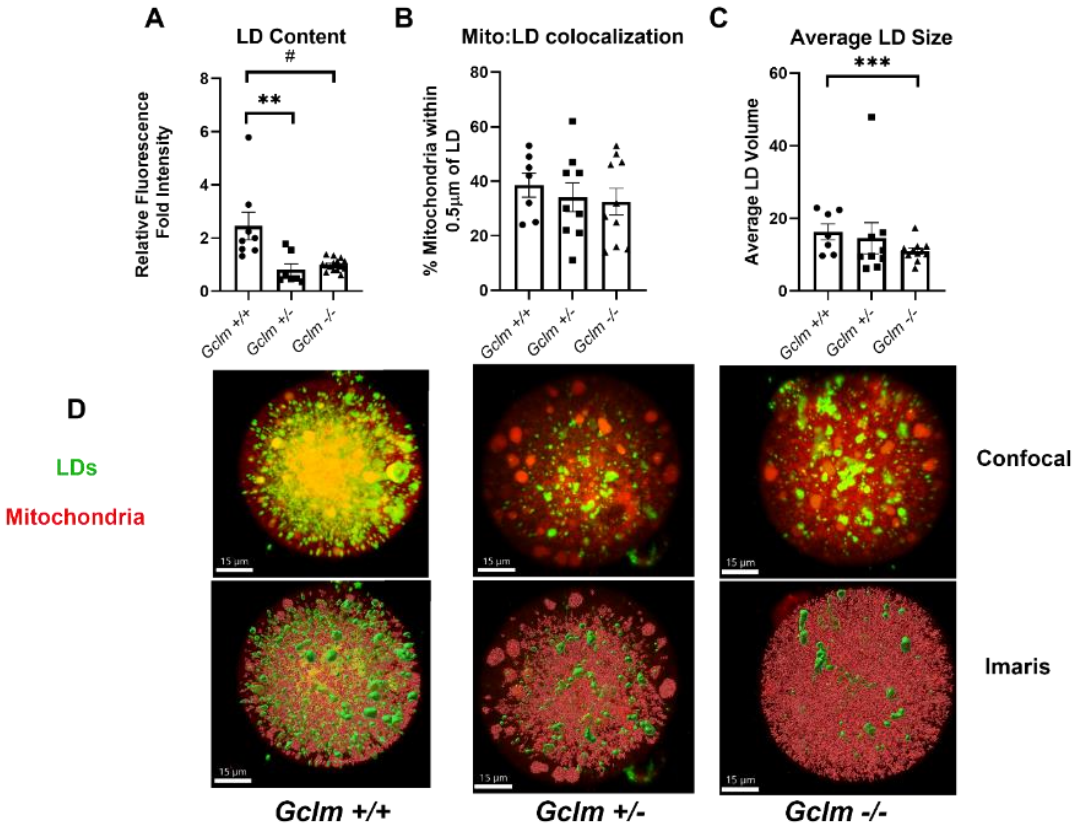

Figure 4.5: *Gclm -/-* oocytes have fewer LDs than *Gclm +/+* oocytes. **A)** Relative green fluorescence fold intensity as measured using BODIPY 493/503 (#P-value=0.083, **P-value=0.007, by generalized estimating equation, N=3-6 females/genotype) **B)** No differences in mitochondria colocalization with LDs in *Gclm -/-* oocytes as measured using Mitotracker Deep Red and BODIPY 493/503 (N= 5-6 females/genotype). **C)** Volume measurements rendered in Imaris imaging software using BODIPY 493/503 fluorescence shows *Gclm -/-* oocytes have smaller LDs on average compared with *Gclm +/+* (***P-value<0.001, generalized estimating equation N= 5-6 females/genotype). Superimposed filled symbols show values for individual oocytes in all graphs in this Figure.

The oxidative state of the oocyte, and therefore its developmental competence, is very sensitive to any perturbations [24,57]. GSH plays a crucial role in maintaining the redox state of the ovary [29] and oocyte [1,16]. Mice deficient in GSH undergo accelerated age-related ovarian failure [16], and the embryos derived from oocytes of GSH-deficient mice have a higher incidence of preimplantation mortality [1]. Therefore it could be surmised that *Gclm -/-* oocytes, with GSH concentrations <20% those of *Gclm* +/+ oocytes [1], would have a drastic shift in their cellular redox state to be more oxidized [29] and possibly show signs of accelerated aging. In this study we observed an increase in ROS in *Gclm -/-* oocytes (Figure 4.1B), most likely driven by an increase in mitochondrial superoxide (Figure 4.1B). However, we did not observe telomere shortening in the *Gclm -/-* oocytes compared with *Gclm* +/+ (Figure 4.1C). It is likely that the mice used in this experiment were too young to begin to see an effect of oxidative stress on oocyte telomere length. The mice used in this study were between PND 35-45. In contrast, the youngest age at which we previously observed significantly lower ovarian follicle numbers in *Gclm -/-* mice compared to *Gclm +/+* mice was 2 months of age, and the difference became more pronounced with increasing age thereafter [16]. Given the highly oxidized state of the *Gclm -/-* oocytes, it is possible that we would observe shortening of telomeres in older mice, and later studies should explore this. This more highly oxidized state could lead to shifts in the delicately balanced mitochondrial functions within the oocytes [29,58,59].

Oocyte mitochondria are small and round, possessing relatively few cristae, and an electron-dense matrix, as opposed to rod-like somatic cell mitochondria, which contain many cristae and a less electron-dense matrix [10,20,21]. However, even though they are relatively quiescent, the mitochondria are the primary source of ATP for the mature,

ovulated oocyte [21,24,25]. After fertilization until the compacted morula stage, the mammalian embryo is entirely dependent on the mitochondria contributed from the ovulated oocyte, roughly 100,000 mitochondria per murine oocyte. The early embryo relies primarily on pyruvate oxidation and fatty acid β-oxidation to survive until the compacted morula commences glycolysis [20,25]. We observed that *Gclm* -/- oocytes have decreased ΔΨm compared with *Gclm +/-* and *Gclm +/+* oocytes (Figure 4.2A). From this we can conclude that mitochondria in *Gclm* -/- oocytes, undergoing higher levels of oxidative stress, have downregulated activity of oxidative phosphorylation to avoid further production of ROS and propagation of a vicious cycle [49,55]. These observations are corroborated by *Gclm -/-* oocytes having less mitochondria clusters in the subcortical region of the oocyte compared to *Gclm +/+* (Figure 4.2D). Although oocyte mitochondria are generally fragmented and smaller [61], they still have been documented to aggregate [62]. Sturmey et al. observed that in pig oocytes, peripheral or subcortical mitochondrial clustering was correlated with higher oxygen availability [36]. Redox homeostasis and structural mitochondrial dynamics have been exhaustively studied in somatic cells and have reproducibly shown that exposure to increased ROS triggers ΔΨm depolarization alongside mitochondrial fragmentation [63], while clustered or fused mitochondria consume oxygen for ATP production [64]. Together these data demonstrate that increased oxidative stress in the absence of GSH, depolarizes oocyte mitochondria. But in a compensatory mechanism, *Gclm -/-* oocytes cluster mitochondria away from the subcortical region to maintain similar levels of metabolism while avoiding the potential for even more production of ROS.

Gclm -/- mice also have decreased lipid biosynthesis and decreased weight gain on a high-fat diet [4]. We have observed that *Gclm -/-* female mice have about 50% lower visceral

adipose tissue weights than *Gclm* +/+ littermates [5]. We hypothesized that the previously observed decreased lipid biosynthesis in *Gclm -/-* mice would have implications for mature oocyte health, given the important role LDs play in embryo development. To this end, we used LC-MS to assess serum lipidomics across all three genotypes. We observed different serum lipid populations among the genotypes, with *Gclm* -/- being the most distinct from *Gclm +/+* and *Gclm +/-* assessed by hierarchical clustering analysis, PCA, and Random Forest analysis (Figure 4.3A, B, C; Table 4.1). Specifically, we observed a decrease in serum triacylglycerols in *Gclm -/-* serum (Figure 4.4A, B, Supplemental Table S1). Serum metabolites and macromolecules populate the follicular fluid in the ovary, and optimal composition of the follicular fluid is required for normal cumulus cell and oocyte function [17,65]. Triacylglycerols are the primary components of the neutral lipid core of LDs in all cell types [66,67]. Whether these are primarily sourced from the follicular fluid or synthesized intracellularly has not been fully explored, but it is likely a combination of sources. Having observed decreased serum triacylglycerol content in *Gclm -/-* females, we hypothesized that *Gclm -/-* oocytes have less LD content than the other genotypes.

Lipid composition of ovarian follicular fluid differs significantly between older and young ovaries, with older patients possessing less arachidonate and certain lysophosphatidylcholines [32], which all play a part in follicular development and oocyte competence. The most interesting differences we observed in serum were decreased concentrations of polyunsaturated fatty acids in *Gclm -/-* serum (Figure 4.3, Figure 4.4A; Supplemental Table S1). Li et al., recently characterized the metabolic patterns of mouse oocytes during meiotic maturation and demonstrated that polyunsaturated fatty acids decline sharply in the oocyte from germinal vesicle to MII stage [68]. Their data further

suggest that polyunsaturated fatty acid signaling plays an inhibitory role in oocyte maturation, and that it must be downregulated for oocyte maturation to proceed [68]. Polyunsaturated fatty acids have been previously suggested to improve oocyte quality of various mammalian species; most commonly their benefit has been attributed to the production of prostaglandins [69–72]. However, other studies have shown that periconception diet supplementation with long chain *n*-3 polyunsaturated fatty acids resulted in altered mitochondrial distribution and increased ROS in the oocyte along with a reduction in normal embryo development [73]. Therefore, it is likely that oocyte competence is dependent on a balance of polyunsaturated fatty acids.

LDs are a source of ATP for oocyte mitochondria post-ovulation and during preimplantation development [21,24,33,41]. They also supply important signaling molecules [30,34], contribute to generation of plasma membranes for the growing embryo [31,34], and play an important role in regulation of cellular stress by lending lipoic acid as a cofactor for mitochondrial dehydrogenases, thus increasing NADH levels for maintenance of redox balance [35]. We observed that *Gclm -/-* oocytes possessed significantly fewer and smaller LDs than *Gclm +/+* counterparts (Figure 4.5A, C). These data are supported by Mok et al., who compared lipidome changes in MII oocytes from 4-week and 42 to 50-week-old mice and H_2O_2-treated oocytes from 4-week-old mice [74]. H_2O_2-treated and aged oocytes were observed to have decreased LD content compared with young oocytes [74], similar to the decreased LD content we observed in *Gclm* -/- oocytes (Figure 4.5A).

To characterize if the absence of a preferential energy resource contributed to decreased $\Delta\Psi m$ in *Gclm* -/- oocytes we analyzed mitochondria:LD colocalization to calculate

the percentage of peridroplet mitochondria and found there to be no difference in colocalization of mitochondria and LDs among genotypes (Figure 4.5B). Interestingly, the average volume of a single LD was smaller in *Gclm -/-* oocytes (Figure 4.5C). This is possibly driven, in part, by the *Gclm -/-* serum having decreased levels of triacylglycerols (Figure 4.3, Supplemental Table S1). Depending on the cell type, mitochondria colocalized with LDs can either be predominantly active in building LDs (lipogenesis), or utilizing LDs for ATP (fatty acid β-oxidation) [75]. Though there is only a little evidence to support this, it is currently accepted by the field that, in oocytes, mitochondria colocalized with LDs are primarily active in ATP production using fatty acid β-oxidation [20]. However, recent findings in hepatocytes show that peridroplet mitochondria, colocalized with LDs, actually produce and consume ATP through pyruvate oxidation to build LDs [76]. Given that MII ovulated oocytes preferentially oxidize pyruvate or fatty acids to yield ATP, further characterization of the bioenergetics of distinct peridroplet mitochondria in oocytes should be explored with more sensitive tools.

Recent findings have further expanded on the necessary role that LDs play in oocyte competence. MII oocytes were shown to immediately start producing new LDs de novo following delipidation, and delipidation had no impact on early embryo development up to the 8-cell stage, attributed to de novo lipid synthesis [41]. Our previous study documented that superovulated *Gclm -/-* mice generated significantly fewer blastocysts at 3.5 days post coitum compared to *Gclm +/+,* due to arrest at earlier stages [1]. Together these data suggest that decreased LD content in ovulated *Gclm -/-* oocytes could activate de novo lipogenesis pathways to support fertilization, creating an abundance of free fatty acids. Higher levels of ROS in *Gclm -/-* embryos may then compromise cellular integrity by oxidizing free fatty acids,

leading to arrest and preimplantation mortality. While the current study observed no differences in MII oocyte lipid peroxidation among genotypes, we did not assess lipid peroxidation in embryos. Doing so is beyond the scope of this study and should be investigated in future studies.

This study has also demonstrated a significant distinction between the lipid populations in the serum of the experimental *Gclm +/-* mice which were superovulated and those that were not. In many ways the serum of the unsuperovulated females was more similar to the *Gclm -/-* superovulated serum, having increased concentrations of cholesterol and sphingomyelins, and decreased concentrations of triacylglycerols (Figure 4.3). However, the unsuperovulated serum was even more distinct, having decreased concentrations of ceramides and increased concentrations of phospholipids compared with the superovulated *Gclm +/-* serum (Figure 4.3, Supplemental Table S1). To our knowledge, this is the first study to characterize the serum lipidome comparing superovulated and unsuperovulated mice. These data support that PMSG and hCG acutely alter the serum lipidome and should be explored further.

In summary, we demonstrated that GSH-deficient oocytes have increased oxidative stress, but this is likely only one contributor to the previously observed increased preimplantation mortality in *Gclm -/-* females [5]. Increased ROS and mitochondrial superoxide, as well as decreased ΔΨm and subcortical mitochondrial clustering were observed in *Gclm -/-* oocytes compared with *Gclm +/-* and *Gclm +/+* oocytes. Additionally, we observed that *Gclm -/-* females possess a distinct serum lipid profile from their *Gclm +/-* and *Gclm +/+* counterparts, being less enriched in triacylglycerols and polyunsaturated fatty

acids. We conclude this decrease in serum triacylglycerols and polyunsaturated fatty acids leads to our observation that *Gclm -/-* oocytes have severely diminished LD content, the primary source of energy, signaling molecules, phospholipids for cellular membranes, and regulator of cellular stress. However, the current study was unable to demonstrate a clear mechanistic link between differing serum lipidome and altered LD content in oocytes among genotypes. Future studies should assess LD content, mitochondrial co-localization, and oxygen consumption rate in granulosa cells and developing embryos. Lipid profiles of the follicular fluid among *Gclm -/-, Gclm +/-,* and *Gclm +/+* mice should also be assessed.

Acknowledgements

This research would not have been possible without the University of California, Irvine Optical Biology Core for providing training on and access to the LSM780 confocal microscope used to image live and fixed oocytes and for Imaris imaging software. We also acknowledge the time, effort, and expertise of the West Coast Metabolomics Center at University of California, Davis. We also thank Dr. David Keefe and Dr. Fang (Helen) Wang of New York University Langone Medical Center for assistance in adapting their oocyte telomere length assay for our study.

Conflict of Interest

The authors have no conflicts of interest to declare.

Author Contributions

KFM designed and performed experiments, analyzed data, drafted manuscript. SR performed experiments, analyzed data, reviewed the manuscript. LO performed experiments, analyzed data. UL conceived of overall idea, obtained funding, analyzed data, edited the manuscript.

Data Availability

The data underlying this article will be shared on reasonable request to the corresponding author.

References

1. Nakamura BN, Fielder TJ, Hoang YD, et al. Lack of maternal glutamate cysteine ligase modifier subunit (Gclm) decreases oocyte glutathione concentrations and disrupts preimplantation development in mice. *Endocrinology*. 2011;152(7):2806-2815.

2. Lim J, Lawson GW, Nakamura BN, et al. Glutathione-deficient mice have increased sensitivity to transplacental benzo[a]pyrene-induced premature ovarian failure and ovarian tumorigenesis. *Cancer Res*. 2013;73(2):908-917.

3. Lim J, Luderer U. Glutathione deficiency sensitizes cultured embryonic mouse ovaries to benzo[a]pyrene-induced germ cell apoptosis. *Toxicol Appl Pharmacol*. 2018;352(February):38-45.

4. Kendig EL, Chen Y, Krishan M, et al. Lipid metabolism and body composition in Gclm(-/-) mice. *Toxicol Appl Pharmacol*. 2011;257(3):338-348.

5. Ortiz L, Nakamura B, Li X, Blumberg B, Luderer U. In utero exposure to benzo[a]pyrene increases adiposity and causes hepatic steatosis in female mice, and glutathione deficiency is protective. *Toxicol Lett*. 2013;223(2):1-7.

6. Franklin CC, Backos DS, Mohar I, White CC, Forman HJ, Kavanagh TJ. Structure, function, and post-translational regulation of the catalytic and modifier subunits of glutamate cysteine ligase. *Mol Aspects Med*. 2009;30(1-2):86-98.

7. Shi ZZ, Osei-Frimpong J, Kala G, et al. Glutathione synthesis is essential for mouse development but not for cell growth in culture. *Proc Natl Acad Sci U S A*. 2000;97(10):5101-5106.

8. Dalton TP, Dieter MZ, Y Y, Shertzer HG, Nebert DW. Knockout of the mouse glutamate cysteine ligase catalytic subunit (Gclc) gene: embryonic lethal when homozygous, and proposed model for moderate glutathione deficiency when heterozygous. *Biochem Biophys Res Commun*. 2000;279(2):324-329.

9. Mcconnachie LA, Mohar I, Hudson FN, et al. Glutamate cysteine ligase modifier subunit deficiency and gender as determinants of acetaminophen-Induced hepatotoxicity in mice. *Toxicol Sci*. 2007;99(2):628-636.

10. Van Blerkom J. Mitochondrial function in the human oocyte and embryo and their role in developmental competence. *Mitochondrion*. 2011;11(5):797-813.

11. Calvin HI, Grosshans K, Blake EJ. Estimation and manipulation of glutathione levels in prepuberal mouse ovaries and ova: Relevance to sperm nucleus transformation in the fertilized egg. *Gamete Res*. 1986;14(3):265-275.

12. Perreault SD, Barbee RR, Slott VL. Importance of glutathione in the acquisition and maintenance of sperm nuclear decondensing activity in maturing hamster oocytes. *Dev Biol*. 1988;125(1):181-186.

13. Perreault S, Barbee R, Slott V. Importance of glutathione in the acquisition and maintenance of sperm nuclear decondensing activity in maturing hamster oocytes. *Dev Biol*. 1988;125(1):181-186.

14. Gardiner CS, Reed DJ. Status of glutathione during oxidant-induced oxidative stress in the preimplantation mouse embryo. *Biol Reprod*. 1994;51(6):1307-1314.

15. Yoshida M, Ishigaki K, Nagai T, Chikyu M, Pursel VG. Glutathione concentration during maturation and after fertilization in pig oocytes: relevance to the ability of oocytes to form male pronucleus. *Biol Reprod*. 1993;49(1):89-94.

16. Lim J, Nakamura BN, Mohar I, Kavanagh TJ, Luderer U. Glutamate cysteine ligase modifier subunit (Gclm) null mice have increased ovarian oxidative stress and accelerated age-related ovarian failure. *Endocrinology*. 2015;156(9):3329-3343.

17. Dumesic DA, Meldrum DR, Katz-Jaffe MG, Krisher RL, Schoolcraft WB. Oocyte environment: Follicular

fluid and cumulus cells are critical for oocyte health. *Fertil Steril*. 2015;103(2):303-316.

18. Ramalho-Santos J, Varum S, Amaral S, Mota PC, Sousa AP, Amaral A. Mitochondrial functionality in reproduction: From gonads and gametes to embryos and embryonic stem cells. *Hum Reprod Update*. 2009;15(5):553-572.

19. Coticchio G, Sereni E, Serrao L, Mazzone S, Iadarola I, Borini A. What criteria for the definition of oocyte quality ? 2004;144:132-144.

20. Bradley J, Swann K. Mitochondria and lipid metabolism in mammalian oocytes and early embryos. *Int J Dev Biol*. 2019;63(3-4-5):93-103.

21. Collado-Fernandez E, Picton HM, Dumollard Ré. Metabolism throughout follicle and oocyte development in mammals. *Int J Dev Biol*. 2012;56(10-12):799-808.

22. Cotterill M, Harris SE, Fernandez EC, et al. The activity and copy number of mitochondrial DNA in ovine oocytes throughout oogenesis in vivo and during oocyte maturation in vitro. *Mol Hum Reprod*. 2013;19(7):444-450.

23. Wang LY, Wang DH, Zou XY, Xu CM. Mitochondrial functions on oocytes and preimplantation embryos. *J Zhejiang Univ Sci B*. 2009;10(7):483-492.

24. Dumollard R, Carroll J, Duchen MR, Campbell K, Swann K. Mitochondrial function and redox state in mammalian embryos. *Semin Cell Dev Biol*. 2009;20(3):346-353.

25. Dumollard R, Campbell K, Halet G, Carroll J, Swann K. Regulation of cytosolic and mitochondrial ATP levels in mouse eggs and zygotes. *Dev Biol*. 2008;316(2):431-440.

26. Harris SE, Leese HJ, Gosden RG, Picton HM. Pyruvate and oxygen consumption throughout the growth and development of murine oocytes. *Mol Reprod Dev*. 2009;76(3):231-238.

27. Yu Y, Dumollard R, Rossbach A, Lai FA, Swann K. Redistribution of mitochondria leads to bursts of ATP production during spontaneous mouse oocyte maturation. 2010;672-680.

28. Guérin P, El Mouatassim S, Ménézo Y. Oxidative stress and protection against reactive oxygen species in the pre-implantation embryo and its surroundings. *Hum Reprod Update*. 2001;7(2):175-189.

29. Devine PJ, Perreault SD, Luderer U. Roles of reactive oxygen species and antioxidants in ovarian toxicity. *Biol Reprod*. 2012;86(2):1-10.

30. Walther TC, Farese R V. The life of lipid droplets. *Biochim Biophys Acta - Mol Cell Biol Lipids*. 2009;1791(6):459-466.

31. Walther TC, Farese R V. Lipid Droplets and Cellular Lipid Metabolism. *Annu Rev Biochem*. 2012;81(1):687-714.

32. Zhang X, Wang T, Song J, Deng J, Sun Z. Study on follicular fluid metabolomics components at different ages based on lipid metabolism. *Reprod Biol Endocrinol*. 2020;18(1):1-8.

33. Dunning KR, Russell DL, Robker RL. Lipids and oocyte developmental competence: the role of fatty acids and β-oxidation. *Reproduction*. 2014;148(1):R15-R27.

34. Prates EG, Nunes JT, Pereira RM. A role of lipid metabolism during cumulus-oocyte complex maturation: Impact of lipid modulators to improve embryo production. *Mediators Inflamm*. 2014;2014.

35. Jarc E, Petan T. Lipid droplets and the management of cellular stress. *Yale J Biol Med*. 2019;92(3):435-452.

36. Sturmey RG, O'Toole PJ, Leese HJ. Flourescence resonance energy transfer analysis of mitochondrial: Lipid association in the porcine oocyte. *Reproduction*. 2006;132(6):829-837.

37. Paczkowski M, Schoolcraft WB, Krisher RL. Fatty acid metabolism during maturation affects glucose uptake and is essential to oocyte competence. *Reproduction*. 2014;148(4):429-439.

38. Valsangkar D, Downs SM. A Requirement for fatty acid oxidation in the hormone-induced meiotic maturation of mouse oocytes. *Biol Reprod*. 2013;89(2):1-9.

39. Dunning KR, Akison LK, Russell DL, Norman RJ, Robker RL. Increased beta-oxidation and improved oocyte developmental competence in response to l-carnitine during ovarian in vitro follicle development in mice. *Biol Reprod*. 2011;85(3):548-555.

40. Dunning KR, Cashman K, Russell DL, Thompson JG, Norman RJ, Robker RL. Beta-oxidation is essential for mouse oocyte developmental competence and early embryo development. *Biol Reprod*. 2010;83(6):909-918.

41. Aizawa R, Ibayashi M, Tatsumi T, et al. Synthesis and maintenance of lipid droplets are essential for mouse preimplantation embryonic development. *Dev*. 2019;146(22).

42. NRC. Guide for the Care and Use of Laboratory Animals 8 ed. *National Acadmey of Sciences* 2011;National Academies Press.

43. Hammond L. Measuring cell fluorescence with ImageJ. 2014.

44. Kasianowicz J, Benz R, McLaughlin S. The kinetic mechanism by which CCCP (carbonyl cyanide m-Chlorophenylhydrazone) transports protons across membranes. *J Membr Biol*. 1984;82(2):179-190.

45. Callicott RJ, Womack JE. Real-time PCR assay for measurement of mouse telomeres. *Comp Med*. 2006;56(1):17-22.

46. Pfaffl MW. A new mathematical model for relative quantification in real-time RT-PCR. *Nucleic Acids Res*. 2001;29(9):16-21.

47. Matyash V, Liebisch G, Kurzchalia T V., Shevchenko A, Schwudke D. Lipid extraction by methyl-terf-butyl ether for high-throughput lipidomics. *J Lipid Res*. 2008;49(5):1137-1146.

48. Pang Z, Chong J, Zhou G, et al. MetaboAnalyst 5 . 0 : narrowing the gap between raw spectra and functional insights. 2021;49:388-396.

49. Benkhalifa M, Ferreira YJ, Chahine H, et al. Mitochondria: Participation to infertility as source of energy and cause of senescence. *Int J Biochem Cell Biol*. 2014;55:60-64.

50. Liu L, Trimarchi JR, Smith PJS, Keefe DL. Mitochondrial dysfunction leads to telomere attrition and genomic instability. 2002;40-46.

51. Liu L, Trimarchi JR, Navarro P, Blasco MA, Keefe DL. Oxidative stress contributes to arsenic-induced telomere attrition, chromosome instability, and apoptosis. *J Biol Chem*. 2003;278(34):31998-32004.

52. Blasco MA, Partridge L, Serrano M, Kroemer G, Lo C. Review The Hallmarks of Aging. *Cell.* 2013.

53. Mari M, Morales A, Colell A, Garcia-Ruiz C, Fernandez-Checa JC. Mitochondrial glutathione, a key survival antioxidant. *Antioxidants Redox Signal*. 2009;11(11):2685-2700.

54. Meyer JN, Leung MCK, Rooney JP, et al. Mitochondria as a target of environmental toxicants. *Toxicol Sci*. 2013;134(1):1-17.

55. Igosheva N, Abramov AY, Poston L, et al. Maternal diet-induced obesity alters mitochondrial activity and redox status in mouse oocytes and zygotes. *PLoS One*. 2010;5(4):1-8.

56. Pawlak P, Malyszka N, Szczerbal I, Kolodziejski P. Fatty acid induced lipolysis influences embryo development, gene expression and lipid droplet formation in the porcine cumulus cells. *Biol Reprod*. 2020;103(1):36-48.

57. Dumollard R, Ward Z, Carroll J, Duchen MR. Regulation of redox metabolism in the mouse oocyte and embryo. *Development*. 2007;134(3):455-465.

58. Prasad S, Tiwari M, Pandey AN, Shrivastav TG, Chaube SK. Impact of stress on oocyte quality and reproductive outcome. *J Biomed Sci*. 2016;23(1):19-23.

59. Malott K, Luderer U. Toxicant effects on mammalian oocyte mitochondria. *Biol Reprod*. 2021:1-5.

60. Kasapoğlu I, Seli E. Mitochondrial dysfunction and ovarian aging. *Endocrinol*. 2020;161(2):1-11.

61. Chiaratti MR, Garcia BM, Carvalho KF, et al. Oocyte mitochondria: Role on fertility and disease transmission. *Anim Reprod*. 2018;15(3):231-238.

62. Wilding M, Dale B, Marino M, et al. Mitochondrial aggregation patterns and activity in human oocytes and preimplantation embryos. *Hum Reprod*. 2001;16(5):909-917.

63. Willems PHGM, Rossignol R, Dieteren CEJ, Murphy MP, Koopman WJH. Redox homeostasis and mitochondrial dynamics. *Cell Metab*. 2015;22(2):207-218.

64. Wai T, Langer T. Mitochondrial dynamics and metabolic regulation. *Trends Endocrinol Metab*. 2016;27(2):105-117.

65. Jamnongjit M, Hammes SR. Oocyte maturation: The coming of age of a germ cell. *Semin Reprod Med*. 2005;23(3):234-241.

66. Welte MA. Fat on the move: intracellular motion of lipid droplets. *Biochem Soc Trans*. 2009;37(5):991-996.

67. Goodman JM. The gregarious lipid droplet. *J Biol Chem*. 2008;283(42):28005-28009.

68. Li L, Zhu S, Shu W, et al. Characterization of metabolic patterns in mouse oocytes during meiotic maturation. *Mol Cell*. 2020;80(3):525-540.e9.

69. Prates EG, Nunes JT, Pereira RM. A role of lipid metabolism during cumulus-oocyte complex maturation: Impact of lipid modulators to improve embryo production. *Mediators Inflamm*. 2014;2014:1-11.

70. Baddela VS, Sharma A, Vanselow J. Non-esterified fatty acids in the ovary: Friends or foes? *Reprod Biol Endocrinol*. 2020;18(1):1-14.

71. Fayezi S, Leroy JLMR, Ghaffari Novin M, Darabi M. Oleic acid in the modulation of oocyte and preimplantation embryo development. *Zygote*. 2018;26(1):1-13.

72. Shaaker M, Rahimipour A, Nouri M, et al. Fatty acid composition of human follicular fluid phospholipids and fertilization rate in assisted reproductive techniques. *Iran Biomed J*. 2012;16(3):1-7.

73. Wakefield SL, Lane M, Schulz SJ, Hebart ML, Thompson JG, Mitchell M. Maternal supply of omega-3 polyunsaturated fatty acids alter mechanisms involved in oocyte and early embryo development in the mouse. *Am J Physiol - Endocrinol Metab*. 2008;294(2):425-434.

74. Mok HJ, Shin H, Lee JW, et al. Age-associated lipidome changes in metaphase II mouse oocytes. *PLoS One*. 2016;11(2):1-17.

75. Benador IY, Veliova M, Liesa M, Shirihai OS. Mitochondria bound to lipid droplets : Where mitochondrial dynamics regulate lipid storage and utilization. *Cell Metab*. 2019;29(4):827-835.

76. Benador IY, Veliova M, Mahdaviani K, et al. Mitochondria bound to lipid droplets have unique bioenergetics, composition, and dynamics that support lipid droplet expansion. *Cell Metab*. 2018;27(4):869-885.e6.

Chapter 5

5.1 Summary and Conclusions

PAHs are well-characterized ovotoxicants. BaP is a representative PAH that has been extensively studied and established as a reproductive toxicant. Our lab and others have demonstrated that exposure to BaP and other PAHs *in vitro* [87,88,95,101] and *in vivo* [83,84,86,92,93,98,109,117] induces germ cell death and is toxic to oocytes. PAHs are commonly found in PM2.5 resultant from incomplete combustion of organic materials and are known to mediate some of the toxicity of PM2.5 [7]. Exposure to PAHs is known to induce oxidative stress. GSH is an important antioxidant for reproductive health, and low GSH has been shown to shift the redox balance in the ovary, accelerating reproductive aging [49,54,55]. Oocytes derived from females of advanced maternal age are well-known to be of reduced developmental competence [58,66,118,119].

In this work, we assessed the impact of BaP exposure on embryonic ovary development. First, we exposed E13.5 ovaries to 0, 500, or 1000 ng/mL of BaP *in vitro* for 6 h to determine the mechanism of BaP-induced germ cell death. We observed that BaP exposure induced a significant increase in percentage of germ cells with DNA double strand breaks, measured using ɣH2AX immunostaining, and that this increase occurred primarily in cells in interphase of leptotene stage of prophase I of meiosis. We also measured expression of the proapoptotic BCL2 family protein PUMA in E13.5 ovaries and demonstrated that BaP exposure induced a modest, albeit not significant, increase in PUMA expression in E13.5 after 6 h. This is likely due to the fact that PUMA, an upstream regulator of BAX, is already highly expressed in the E13.5 ovary [120]. Previous work in this lab has shown that E13.5 ovaries exposed to BaP for 6 h have a significant increase in the percentage

of oocytes expressing BAX, and increased cleaved caspase-9 and -3 after 24 h of exposure [88]. In this work, we provide further evidence demonstrating that the mitochondrial apoptosis pathway plays a pivotal role in mediating BaP-induction of germ cell death in the E13.5 ovary. We observed that BaP exposure for 6 h significantly increased the percentage of oocytes in the ovary that were positive for cytochrome c release into the cytosol, in a dose-dependent manner, as measured using immunofluorescence and structured illumination microscopy.

Following the evidence of our *in vitro* paradigm, we demonstrated that *in utero* exposure to BaP hastened onset of puberty in F1 females and led to equivalent significant depletion of the ovarian reserve when fetuses were exposed from E6.5-11.5 or E12.5-17.5 in F1 pubertal females. Exposure in these windows also led to an equivalent significant increase in whole ovarian lipid peroxidation levels, as measured by 4-HNE concentration, across both exposure windows. Interestingly, we observed that BaP exposure resulted in a significant decrease in DNA DSBs, measured using γH2AX staining, in primordial and primary oocytes. We suspect that this unexpected result could be attributed to the induction of increased ROS and DNA damage earlier in pre-pubertal life and induced activation of DNA repair mechanisms in the ovary [99].

Further, we assessed the developmental competence of pubertal F1-derived oocytes that survive *in utero* BaP exposure from E6.5-11.5. We observed that BaP exposure significantly increased mitochondrial superoxide production in ovulated oocytes, while decreasing oocyte $\Delta\Psi m$ – indicative of persistent oxidative stress. This was further evidenced by mitochondrial clustering analysis, which showed that BaP6.5 oocytes had a borderline significant increase in subcortical mitochondrial clustering, suggesting the need

for conservation of bioenergetic resources [121]. We did not, however, observe any differences in whole oocyte GSH, measured by monochlorobimane fluorescence; or oocyte lipid peroxidation, measured by BODIPY 581/591 fluorescence. We hypothesized that the lack of increased lipid peroxidation may have been related to the LD content in BaP6.5 oocytes. Using BODIPY 493/503, we observed a significant decrease in the average volume of LDs in the whole oocyte and those colocalized with mitochondria. We observed a borderline significant decrease in the percentage of mitochondria colocalized with LDs. Collectively, these data demonstrated for the first time that *in utero* BaP exposure resulted in persistent oxidative stress in the F1 pubertal ovary and oocyte, resulting in compromised oocyte developmental competence.

Given that inhalation is another important route of human exposure to PAHs, we exposed female mice to concentrated air particulates at 2.5 μm or less in aerodynamic diameter using a Versatile Air Concentration Enrichment System (VACES) for 6 h/ day, 5 days/ week, for 12 weeks. For my part in this project I, with the help of our collaborators, developed and validated an extraction and HPLC-MS/MS method for measuring ovarian 17β-estradiol concentrations in exposed and unexposed mice, which were sacrificed on proestrus of the estrous cycle, when 17β-estradiol levels are highest, following 14 days of vaginal lavage to measure estrous cyclicity. We observed that mice exposed to PM2.5 were statistically significantly more likely to have irregular estrous cycles compared with filtered air controls, having significantly fewer leukocytic (metestrus and diestrus) days and significantly more cornified (estrus) days [122]. Consistent with our previous findings and supportive of our *in utero* data, the females exposed to PM2.5 had significantly fewer primordial, primary, and secondary ovarian follicles. But, we observed no differences in

healthy or atretic antral follicles [122]. The ovarian concentrations of 17β-estradiol did not differ among exposure groups; however, interestingly, the 17β-estradiol content of ovaries from wild-type, unexposed mice were significantly higher than that of either exposure group of the transgenic mouse model (*Apoe* -/-) that were used in this study [122]. Together these data demonstrate that *in vivo* exposure to a complex mixture, which contains BaP and other PAHs, results in depletion of the ovarian reserve similar to the effect of BaP alone. Further they support that *Apoe* plays a role in ovarian estradiol production.

To specifically understand how dysregulation of redox homeostasis alter oocyte developmental competence we used a transgenic mouse model, deleting the modifier subunit of the rate-limiting enzyme in GSH synthesis, glutamate cysteine ligase (*Gclm*). Mice with this deletion possess about 10-20% of normal GSH levels [44], live relatively healthy lives and are fertile, but produce fewer pups [49]. Using this mouse model, we demonstrated that *Gclm -/-* females ovulate equivalent numbers of oocytes when compared to *Gclm +/-* and *Gclm +/+.* But these knockout oocytes have increased levels of ROS and mitochondrial superoxide compared with wildtype and heterozygous oocytes [123]. *Gclm -/-* oocytes also had decreased oocyte ΔΨm and decreased volume of subcortical mitochondrial clustering [123]. However, we observed no differences among the genotypes in lipid peroxidation levels, measured with BODIPY 581/591. We attribute this to decreased LD content and significantly decreased average volume of individual LDs observed in *Gclm -/-* oocytes, further supported by serum lipidomics that confirmed significantly different serum lipid populations in superovulated *Gclm -/-* females [123].

Together these data demonstrate that BaP, a component of PM2.5 and other complex mixtures produced during incomplete combustion, is a potent transplacental ovotoxicant,

causing significant depletion of the ovarian reserve in F1 ovaries, driven by the mitochondrial apoptosis pathway. E13.5 ovaries had a significantly increased percentage of oocytes with evidence of DNA DSBs and cytochrome c release in the cytosol following *in vitro* BaP exposure. Ovaries from pubertal F1 females had significantly fewer primordial, primary, and secondary follicles; and increased persistent oxidative stress following *in utero* BaP exposure. *In utero* BaP exposure resulted in decreased oocyte competence through increased oxidative stress and depleted LD content. *Gclm -/-* mice serve as a model for accelerated reproductive aging [54]. Oocytes from *Gclm -/-* females were similar to the BaP exposed oocytes, including increased levels of mitochondrial superoxide, decreased oocyte ΔΨm and LD content. However, BaP-exposed oocytes had a marginally significant decrease in the percentage of mitochondria colocalized with LDs compared with oil controls while we observed no such effect when comparing *Gclm -/-, Gclm +/-,* and *Gclm +/+* oocytes.

5.2 Future research on gestational BaP exposure, oxidative stress, and the effect on oocyte competence

To our knowledge, this is the first time F1 oocyte developmental competence has been assessed following *in utero* BaP exposure. We know that oocytes exposed to BaP *in vitro* and *in vivo* have reduced developmental competence and preimplantation development success rates [101,109,124]. This work presents evidence to support that F1 oocytes exposed to BaP *in utero* would also have reduced preimplantation development success rates. We have published that F1 females exposed to BaP from E6.5-15.5 have decreased fertility [92] but have yet to confirm the mechanism by which this reduced fertility is mediated. Experiments to explore this mechanism could include *in utero* exposure to BaP

from E6.5-17.5 and the following assessments in F1 females, *in vitro* fertilization (IVF) rate and *in vitro* maturation (IVM) rate, as well as a breeding study and assessment of uterine implantation sites.

Should these studies yield results supporting the hypothesis that *in utero* BaP exposure reduced success of preimplantation development, further exploration of the mechanism underlying the reduction in oocyte developmental competence should be performed. Our data in this body of work, suggests interdependent mechanisms- energy production, redox homeostasis, and lipogenesis/ lipid consumption. The first line of inquiry should be measurement of ATP production in mature, superovulated oocytes using an ATP chemiluminescence assay. Concurrently, oxygen consumption rate and fatty acid β-oxidation should be explored. The mature, healthy, oocyte's primary sources of energy are fatty acids and pyruvate [31,36,125–128]; therefore, these three assays in tandem will provide a wealth of evidence to support whether there is, in fact, an effect directly on the mitochondria or if the data presented in this body of work is the result of aberrant redox homeostasis. Other lines of inquiry could specifically address lipogenesis in oocytes following *in utero* BaP exposure. Recently published work demonstrates that MII oocytes have the ability to activate *de novo* lipogenesis following de-lipidation and that this process is essential for oocyte competence [42]. Using a similar delipidation technique, one could interrogate if BaP disrupts lipogenesis in exposed oocytes.

Further, although this work did not observe a difference in the whole oocyte GSH between BaP and control oocytes, it is possible that there may still be an effect at the subcellular level. Mitochondria possess their own pool of GSH [129], and given the parallels observed between the *Gclm -/-* oocytes and BaP6.5 oocytes, especially in the mitochondria,

mitochondrial redox homeostasis may be worth exploring. This could be done using a similar *in utero* exposure paradigm and assessing F1 oocyte endpoints used in this body of work and suggested in the preceding paragraph. Instead of using wild type mice, employing the *Gclm* transgenic mouse line to directly assess treatment and genotype effects may be informative in distinguishing the weight of the role that redox homeostasis plays in determining oocyte competence.

This body of work has laid a groundwork for understanding how redox homeostasis and the interaction between oocyte mitochondria and LDs could play a larger role in determining the quality of an ovulated oocyte and potential for preimplantation development success rates. Further, it has demonstrated that *in utero* exposure to BaP, a key component of air pollution, can result in persistent F1 oxidative damage in the ovary and oocyte contributing to decreased fertility in subsequent generations. However, many questions still must be answered to uncover the underlying mechanisms.

References

1. Coulam CB, Adamson SC, Annegers JF. Incidence of premature ovarian failure. *Obstet Gynecol*. 1986;67(4):604-606.

2. Okoth K, Chandan JS, Marshall T, et al. Association between the reproductive health of young women and cardiovascular disease in later life: Umbrella review. *BMJ*. 2020;371. doi:10.1136/bmj.m3502

3. Mahalingaiah S, Hart JE, Laden F, et al. Adult air pollution exposure and risk of infertility in the Nurses' Health Study II. *Hum Reprod*. 2016;31(3):638-647. doi:10.1093/humrep/dev330

4. Conforti A, Mascia M, Cioffi G, et al. Air pollution and female fertility: A systematic review of literature. *Reprod Biol Endocrinol*. 2018;16(1):1-9. doi:10.1186/s12958-018-0433-z

5. Carré J, Gatimel N, Moreau J, Parinaud J, Léandri R. Does air pollution play a role in infertility?: A systematic review. *Environ Heal A Glob Access Sci Source*. 2017;16(1):1-16. doi:10.1186/s12940-017-0291-8

6. Nieuwenhuijsen MJ, Basagaña X, Dadvand P, et al. Air pollution and human fertility rates. *Environ Int*. 2014;70:9-14. doi:10.1016/j.envint.2014.05.005

7. ATSDR. Toxicological Profile for Polycyclic Aromatic Hydrocarbons. *ATSDR's Toxicol Profiles*. 1995;18(2):141-147. doi:10.3109/15569529909037564

8. Ambroz A, Vlkova V, Rossner P, et al. Impact of air pollution on oxidative DNA damage and lipid peroxidation in mothers and their newborns. *Int J Hyg Environ Health*. 2016;219(6):545-556. doi:10.1016/j.ijheh.2016.05.010

9. Ye X, Skjaerven R, Basso O, et al. In utero exposure to tobacco smoke and subsequent reduced fertility in females. *Hum Reprod*. 2010;25(11):2901-2906. doi:10.1093/humrep/deq235

10. Weinberg CR, Wilcox AJ, Baird DD. Reduced Fecundability in Women with Prenatal Exposure to Cigarette Smoking. *Am J Epidemiol*. 1989;129(5):1072-1078.

11. Jensen TK, Henriksen TB, Hjollund NHI, et al. Adult and prenatal exposures to tobacco smoke as risk indicators of fertility among 430 Danish couples. *Am J Epidemiol*. 1998;148(10):992-997. doi:10.1093/oxfordjournals.aje.a009576

12. Zhang B, Shi H, Wang Q, Zhang Z, Li M. Maternal passive smoking during pregnancy and age of menarche in daughters: A study of elementary and middle school students in Shanghai. *Asia-Pacific J Public Heal*. 2015;27:14S-20S. doi:10.1177/1010539515571581

13. Houghton LC, Goldberg M, Wei Y, et al. Why do studies show different associations between intrauterine exposure to maternal smoking and age at menarche? *Ann Epidemiol*. 2018;28(3):197-203. doi:10.1016/j.annepidem.2018.01.004

14. Shuster LT, Rhodes DJ, Gostout BS, Grossardt BR, Rocca WA. Premature menopause or early menopause: Long-term health consequences. *Maturitas*. 2010;65(2):161-166. doi:10.1016/j.maturitas.2009.08.003

15. Faubion SS, Kuhle CL, Shuster LT, et al. Menopause and Considerations for Management. 2016;18(4):483-491. doi:10.3109/13697137.2015.1020484.Long-term

16. Hamilton BE, Martin JA, Osterman MJK. Births: Provisional data for 2020. *NVSS Vital Stat Rapid Release*. 2021;(012):1-21. https://www.cdc.gov/nchs/data/vsrr/report002.pdf.

17. Zhang J, Li J, Wang P, et al. Estimating population exposure to ambient polycyclic aromatic hydrocarbon in the United States – Part I: Model development and evaluation. *Environ Int*. 2017;176(1):100–106. doi:10.1016/j.envint.2016.12.002.Estimating

18. IARC. Some Non-heterocyclic Polycyclic Aromatic Hydrocarbons and Some Related Exposures. *IARC Monogr Eval Carcinog Risks to Humans*. 2010;93:9-38. doi:10.1136/jcp.48.7.691-a

19. Xue W, Warshawsky D. Metabolic activation of polycyclic and heterocyclic aromatic hydrocarbons and DNA damage: A review. *Toxicol Appl Pharmacol*. 2005;206(1):73-93. doi:10.1016/j.taap.2004.11.006

20. Hankinson O. the Aryl Hydrocarbon Receptor Complex. *Annu Rev Pharmacol Toxicol*. 1995;35:307-340.

21. Miao W, Hu L, Scrivens PJ, Batist G. Transcriptional Regulation of NF-E2 p45-related Factor (NRF2) Expression by the Aryl Hydrocarbon Receptor-Xenobiotic Response Element Signaling Pathway. *J Biol Chem*. 2005;280(21):20340-20348. doi:10.1074/jbc.M412081200

22. Wear HM, McPike MJ, Watanabe KH. From primordial germ cells to primordial follicles: A review and visual representation of early ovarian development in mice. *J Ovarian Res*. 2016;9(1):1-11. doi:10.1186/s13048-016-0246-7

23. Sarraj MA, Drummond AE. Mammalian foetal ovarian development: Consequences for health and disease. *Reproduction*. 2012;143(2):151-163. doi:10.1530/REP-11-0247

24. Edson MA, Nagaraja AK, Matzuk MM. The mammalian ovary from genesis to revelation. *Endocr Rev*. 2009;30(6):624-712. doi:10.1210/er.2009-0012

25. Pepling ME, Spradling AC. Mouse ovarian germ cell cysts undergo programmed breakdown to form primordial follicles. *Dev Biol*. 2001;234(2):339-351. doi:10.1006/dbio.2001.0269

26. Hirshfield A. Overview of ovarian follicular development: considerations for the toxicologist. *Env Mol Mutagen*. 1997;29(1):10-15.

27. Ramalho-Santos J, Varum S, Amaral S, Mota PC, Sousa AP, Amaral A. Mitochondrial functionality in reproduction: From gonads and gametes to embryos and embryonic stem cells. *Hum Reprod Update*. 2009;15(5):553-572. doi:10.1093/humupd/dmp016

28. Brinster RL, Harstad H. Energy Metabolism in Primordial Germ Cells of the Mouse. *Exp Cell Res*. 1977;109:111-117.

29. Cinco R, Digman MA, Gratton E, Luderer U. Spatial Characterization of Bioenergetics and Metabolism of Primordial to Preovulatory Follicles in Whole Ex Vivo Murine Ovary. *Biol Reprod*. 2016;95(6):129-129. doi:10.1095/biolreprod.116.142141

30. Collado-Fernandez E, Picton HM, Dumollard Ré. Metabolism throughout follicle and oocyte development in mammals. *Int J Dev Biol*. 2012;56(10-12):799-808. doi:10.1387/ijdb.120140ec

31. Bradley J, Swann K. Mitochondria and lipid metabolism in mammalian oocytes and early embryos. *Int J Dev Biol*. 2019;63(3-4-5):93-103. doi:10.1387/ijdb.180355ks

32. Clarke HJ. Regulation of germ cell development by intercellular signaling in the mammalian ovarian follicle. *Wiley Interdiscip Rev Dev Biol*. 2018;7(1):1-22. doi:10.1002/wdev.294

33. Kidder GM, Mhawi AA. Gap junctions and ovarian folliculogenesis. *Reproduction*. 2002;123(5):613-620. doi:10.1530/rep.0.1230613

34. Chiaratti MR, Garcia BM, Carvalho KF, et al. Oocyte mitochondria: Role on fertility and disease transmission. *Anim Reprod*. 2018;15(3):231-238. doi:10.21451/1984-3143-AR2018-0069

35. Fujimoto T, Ohsaki Y, Cheng J, Suzuki M, Shinohara Y. Lipid droplets: A classic organelle with new outfits. *Histochem Cell Biol*. 2008;130(2):263-279. doi:10.1007/s00418-008-0449-0

36. Dumesic DA, Meldrum DR, Katz-Jaffe MG, Krisher RL, Schoolcraft WB. Oocyte environment: Follicular fluid and cumulus cells are critical for oocyte health. *Fertil Steril*. 2015;103(2):303-316.

doi:10.1016/j.fertnstert.2014.11.015

37. Zhang X, Wang T, Song J, Deng J, Sun Z. Study on follicular fluid metabolomics components at different ages based on lipid metabolism. *Reprod Biol Endocrinol*. 2020;18(1):1-8. doi:10.1186/s12958-020-00599-8

38. Prates EG, Nunes JT, Pereira RM. A role of lipid metabolism during cumulus-oocyte complex maturation: Impact of lipid modulators to improve embryo production. *Mediators Inflamm*. 2014;2014. doi:10.1155/2014/692067

39. Walther TC, Farese R V. The life of lipid droplets. *Biochim Biophys Acta - Mol Cell Biol Lipids*. 2009;1791(6):459-466. doi:10.1016/j.bbalip.2008.10.009

40. Walther TC, Farese R V. Lipid Droplets and Cellular Lipid Metabolism. *Annu Rev Biochem*. 2012;81(1):687-714. doi:10.1146/annurev-biochem-061009-102430

41. Jarc E, Petan T. Lipid droplets and the management of cellular stress. *Yale J Biol Med*. 2019;92(3):435-452.

42. Aizawa R, Ibayashi M, Tatsumi T, et al. Synthesis and maintenance of lipid droplets are essential for mouse preimplantation embryonic development. *Dev*. 2019;146(22). doi:10.1242/dev.181925

43. Dalton TP, Dieter MZ, Y Y, Shertzer HG, Nebert DW. Knockout of the mouse glutamate cysteine ligase catalytic subunit (Gclc) gene: embryonic lethal when homozygous, and proposed model for moderate glutathione deficiency when heterozygous. *Biochem Biophys Res Commun*. 2000;279(2):324-329. doi:15107237

44. Yang Y, Dieter MZ, Chen Y, Shertzer HG, Nebert DW, Dalton TP. Initial Characterization of the Glutamate-Cysteine Ligase Modifier Subunit Gclm (−/−) Knockout Mouse . *J Biol Chem*. 2002;277(51):49446-49452. doi:10.1074/jbc.m209372200

45. Calvin HI, Grosshans K, Blake EJ. Estimation and manipulation of glutathione levels in prepuberal mouse ovaries and ova:Relevance to sperm nucleus transformation in the fertilized egg. *Gamete Res*. 1986;14(3):265-275. doi:doi:10.1002/mrd.1120140310

46. Yoshida M, Ishigaki K, Nagai T, Chikyu M, Pursel VG. Glutathione Concentration during Maturation and after Fertilization in Pig Oocytes: Relevance to the Ability of Oocytes to Form Male Pronucleus1. *Biol Reprod*. 1993;49(1):89-94. doi:10.1095/biolreprod49.1.89

47. Perreault SD, Barbee RR, Slott VL. Importance of glutathione in the acquisition and maintenance of sperm nuclear decondensing activity in maturing hamster oocytes. *Dev Biol*. 1988;125(1):181-186. doi:10.1016/0012-1606(88)90070-x

48. Gardiner CS, Reed DJ. Status of Glutathione during Oxidant-Induced Oxidative Stress in the Preimplantation Mouse Embryo1. *Biol Reprod*. 1994;51(6):1307-1314. doi:10.1095/biolreprod51.6.1307

49. Nakamura BN, Fielder TJ, Hoang YD, et al. Lack of maternal glutamate cysteine ligase modifier subunit (Gclm) decreases oocyte glutathione concentrations and disrupts preimplantation development in mice. *Endocrinology*. 2011;152(7):2806-2815. doi:10.1210/en.2011-0207

50. Shelling AN. Premature ovarian failure. *Reproduction*. 2010;140(5):633-641. doi:10.1530/REP-09-0567

51. Sklar CA, Mertens AC, Mitby P, et al. Premature Menopause in Survivors of Childhood Cancer : 2006;98(13). doi:10.1093/jnci/djj243

52. Nippita TA, Baber RJ. Premature ovarian failure: A review. *Climacteric*. 2007;10(1):11-22. doi:10.1080/13697130601135672

53. Lopez-Otin C, Blasco MA, Partridge L, Serrano M, Kroemer G, Lo C. The Hallmarks of Aging. *Cell.* 2013; 153:1194-1217. doi:10.1016/j.cell.2013.05.039

54. Lim J, Nakamura BN, Mohar I, Kavanagh TJ, Luderer U. Glutamate cysteine ligase modifier subunit (Gclm) null mice have increased ovarian oxidative stress and accelerated age-related ovarian failure. *Endocrinology*. 2015;156(9):3329-3343. doi:10.1210/en.2015-1206

55. Lim J, Ali S, Liao LS, et al. Antioxidant supplementation partially rescues accelerated ovarian follicle loss, but not oocyte quality, of glutathione-deficient mice. *Biol Reprod*. 2020;102(5):1065-1079. doi:10.1093/biolre/ioaa009

56. Guérin P, El Mouatassim S, Ménézo Y. Oxidative stress and protection against reactive oxygen species in the pre-implantation embryo and its surroundings. *Hum Reprod Update*. 2001;7(2):175-189. doi:10.1093/humupd/7.2.175

57. Peters AE, Mihalas BP, Bromfield EG, Roman SD, Nixon B, Sutherland JM. Autophagy in Female Fertility: A Role in Oxidative Stress and Aging. *Antioxidants Redox Signal*. 2020;32(8):550-568. doi:10.1089/ars.2019.7986

58. Cimadomo D, Fabozzi G, Vaiarelli A, Ubaldi N, Ubaldi FM, Rienzi L. Impact of Maternal Age on Oocyte and Embryo Competence. *Front Endocrinol*. 2018;9(June). doi:10.3389/fendo.2018.00327

59. Sasaki H, Hamatani T, Kamijo S, Iwai M, Kobanawa M. Impact of Oxidative Stress on Age-Associated Decline in Oocyte Developmental Competence. *Front Endocrinol*. 2019;10(November):1-7. doi:10.3389/fendo.2019.00811

60. Wilding M, Dale B, Marino M, et al. Mitochondrial aggregation patterns and activity in human oocytes and preimplantation embryos. *Hum Reprod*. 2001;16(5):909-917. doi:10.1093/humrep/16.5.909

61. Tarín JJ. Potential effects of age-associated oxidative stress on mammalian oocytes/embryos. *Mol Hum Reprod*. 1996;2(10):717-724. doi:10.1093/molehr/2.10.717

62. Eichenlaub-Ritter U, Wieczorek M, Lüke S, Seidel T. Age related changes in mitochondrial function and new approaches to study redox regulation in mammalian oocytes in response to age or maturation conditions. *Mitochondrion*. 2011;11(5):783-796. doi:10.1016/j.mito.2010.08.011

63. Chiang JL, Shukla P, Pagidas K, et al. Mitochondria in Ovarian Aging and Reproductive Longevity. *Ageing Res Rev*. 2020;63(September):101168. doi:10.1016/j.arr.2020.101168

64. Zhang M, Bener MB, Jiang Z, et al. Mitofusin 1 is required for female fertility and to maintain ovarian follicular reserve. *Cell Death Dis*. 2019;10(8). doi:10.1038/s41419-019-1799-3

65. Hamatani T, Falco G, Carter MG, et al. Age-associated alteration of gene expression patterns in mouse oocytes. *Hum Mol Genet*. 2004;13(19):2263-2278. doi:10.1093/hmg/ddh241

66. Pasquariello R, Ermisch AF, Silva E, et al. Alterations in oocyte mitochondrial number and function are related to spindle defects and occur with maternal aging in mice and humans. *Biol Reprod*. 2019;100(4):971-981. doi:10.1093/biolre/ioy248

67. Al-Zubaidi U, Adhikari D, Cinar O, et al. Mitochondria-targeted therapeutics, MitoQ and BGP-15, reverse aging-associated meiotic spindle defects in mouse and human oocytes. *Hum Reprod*. 2021;36(3):771-784. doi:10.1093/humrep/deaa300

68. de Diego I, Peleg S, Fuchs B. The role of lipids in aging-related metabolic changes. *Chem Phys Lipids*. 2019;222(May):59-69. doi:10.1016/j.chemphyslip.2019.05.005

69. Mishra B, Ortiz L, Luderer U. Charged iron particles , components of space radiation , destroy ovarian follicles. *Hum Reprod*. 2016;31(8):1816-1826. doi:10.1093/humrep/dew126

70. Mishra B, Ripperdan R, Ortiz L, Luderer U, Biology C, Sciences A. Very low doses of heavy oxygen ion

radiation induce premature ovarian failure. *Reproduction*. 2017;154(2):123-133. doi:10.1530/REP-17-0101.Very

71. Mihalas BP, De Iuliis GN, Redgrove KA, McLaughlin EA, Nixon B. The lipid peroxidation product 4-hydroxynonenal contributes to oxidative stress-mediated deterioration of the ageing oocyte. *Sci Rep*. 2017;7(1):1-18. doi:10.1038/s41598-017-06372-z

72. Sayre LM, Lin D, Yuan Q, Zhu X, Tang X. Protein adducts generated from products of lipid oxidation: focus on HNE and one. *Drug Metab Rev*. 2006;38(4):651-675. doi:10.1080/03602530600959508

73. Gulham I, Bozkaya G, Uyar I, Oztekin D, Pamuk BO, Dogan E. Serum lipid levels in women with premature ovarian failure. *Menopause*. 2012;19(11):1231-1234. doi:10.1097/gme.0b013e318254102b

74. Tehrani FR, Erfani H, Cheraghi L, Tohidi M, Azizi F. Lipid profiles and ovarian reserve status : a longitudinal study. *Hum Reprod*. 2014;29(11):2522-2529. doi:10.1093/humrep/deu249

75. Knauff EAH, Westerveld HE, Goverde AJ, et al. Lipid profile of women with premature ovarian failure. *Menopause*. 2008;15(5):919-923. doi:10.1097/gme.0b013e31816b4509

76. Cordeiro FB, Montani DA, Fraietta R, Guimaraes E, Turco L. Ovarian environment aging : follicular fluid lipidomic and related metabolic pathways. *J Assist Reprod Genet*. 2018;35:1385-1393.

77. Boulet SL, Zhou Y, Shriber J, Kissin DM, Strosnider H, Shin M. Ambient air pollution and in vitro fertilization treatment outcomes. *Hum Reprod*. 2019;34(10):2036-2043. doi:10.1093/humrep/dez128

78. Anderson RA, McIlwain L, Coutts S, Kinnell HL, Fowler PA, Childs AJ. Activation of the aryl hydrocarbon receptor by a component of cigarette smoke reduces germ cell proliferation in the human fetal ovary. *Mol Hum Reprod*. 2014;20(1):42-48. doi:10.1093/molehr/gat059

79. Fowler PA, Childs AJ, Mackenzie A, et al. In utero exposure to cigarette smoke dysregulates human fetal ovarian developmental signalling. 2014;29(7):1471-1489. doi:10.1093/humrep/deu117

80. Tuttle AM, Stämpfli M, Foster WG. Cigarette smoke causes follicle loss in mice ovaries at concentrations representative of human exposure. *Hum Reprod*. 2009;24(6):1452-1459. doi:10.1093/humrep/dep023

81. Gannon AM, Stämpfli MR, Foster WG. Cigarette smoke exposure elicits increased autophagy and dysregulation of mitochondrial dynamics in murine granulosa cells. *Biol Reprod*. 2013;88(3):1-11. doi:10.1095/biolreprod.112.106617

82. Sobinoff AP, Beckett EL, Jarnicki AG, et al. Scrambled and fried: Cigarette smoke exposure causes antral follicle destruction and oocyte dysfunction through oxidative stress. *Toxicol Appl Pharmacol*. 2013;271(2):156-167. doi:10.1016/j.taap.2013.05.009

83. Mattison DR, Thorgeirsson SS. Ovarian aryl hydrocarbon hydroxylase activity and primordial oocyte toxicity of polycyclic aromatic hydrocarbons in mice. *Cancer Res*. 1979;39(9):3471-3475.

84. Mattison DR. Morphology of oocyte and follicle destruction by polycyclic aromatic hydrocarbons in mice. *Toxicol Appl Pharmacol*. 1980;53(2):249-259. doi:10.1016/0041-008X(80)90424-X

85. Archibong AE, Ramesh A, Inyang F, Niaz MS, Hood DB, Kopsombut P. Endocrine Disruptive Actions of Inhaled Benzo(a)pyrene on Ovarian Function and Fetal Survival in Fisher F-344 Adult Rats. *Reprod Toxicol*. 2012;34(4):635-643. doi:10.1016/j.reprotox.2012.09.003.ENDOCRINE

86. Sobinoff AP, Pye V, Nixon B, Roman SD, McLaughlin EA. Jumping the gun: Smoking constituent BaP causes premature primordial follicle activation and impairs oocyte fusibility through oxidative stress. *Toxicol Appl Pharmacol*. 2012;260(1):70-80. doi:10.1016/j.taap.2012.01.028

87. Matikainen TM, Moriyama T, Morita Y, et al. Ligand activation of the aromatic hydrocarbon receptor

transcription factor drives Bax-dependent apoptosis in developing fetal ovarian germ cells. *Endocrinology*. 2002;143(2):615-620. doi:10.1210/endo.143.2.8624

88. Lim J, Kong W, Lu M, Luderer U. The mouse fetal ovary has greater sensitivity than the fetal testis to benzo[a]pyrene-induced germ cell death. *Toxicol Sci*. 2016;152(2):372-381. doi:10.1093/toxsci/kfw083

89. Lim J, Luderer U. Glutathione deficiency sensitizes cultured embryonic mouse ovaries to benzo[a]pyrene-induced germ cell apoptosis. *Toxicol Appl Pharmacol*. 2018;352(February):38-45. doi:10.1016/j.taap.2018.05.024

90. Santucci R, Sinibaldi F, Cozza P, Polticelli F, Fiorucci L. Cytochrome c: An extreme multifunctional protein with a key role in cell fate. *Int J Biol Macromol*. 2019;136:1237-1246. doi:10.1016/j.ijbiomac.2019.06.180

91. Mackenzie K, Angevine DM. Infertility in Mice Exposed in utero to Benzo(a)pyrene. *Biol Reprod*. 1981;24:183-191.

92. Lim J, Lawson GW, Nakamura BN, et al. Glutathione-deficient mice have increased sensitivity to transplacental benzo[a]pyrene-induced premature ovarian failure and ovarian tumorigenesis. *Cancer Res*. 2013;73(2):908-917. doi:10.1158/0008-5472.CAN-12-3636

93. Lim J, Ramesh A, Shioda T, Parada KL, Luderer U. Sex Differences in Embryonic Gonad Transcriptomes and Benzo [a] pyrene Metabolite Levels After Transplacental Exposure. 2022;163(1):1-17.

94. Li WD, Yu S, Luo SM, Shen W, Yin S, Sun QY. Melatonin defends mouse oocyte quality from benzo[ghi]perylene-induced deterioration. *J Cell Physiol*. 2019;234(5):6220-6229. doi:10.1002/jcp.27351

95. Guo J, Huang J, Zhang L, et al. Benzo[b]fluoranthene Impairs Mouse Oocyte Maturation via Inducing the Apoptosis. *Front Pharmacol*. 2020;11(August):1-9. doi:10.3389/fphar.2020.01226

96. Jo Y, Yoon S, Park B, et al. Particulate Matter Exposure During Oocyte Maturation : Cell Cycle Arrest , ROS Generation , and Early Apoptosis in Mice. *Front Cell Dev Biol*. 2020;8(November):1-14. doi:10.3389/fcell.2020.602097

97. Zhang M, Miao Y, Chen Q, et al. BaP exposure causes oocyte meiotic arrest and fertilization failure to weaken female fertility. *FASEB J*. 2018;32(1):342-352. doi:10.1096/fj.201700514R

98. Einaudi L, Courbiere B, Tassistro V, et al. In vivo exposure to benzo(a)pyrene induces significant DNA damage in mouse oocytes and cumulus cells. *Hum Reprod*. 2014;29(3):548-554. doi:10.1093/humrep/det439

99. Stringer JM, Winship A, Zerafa N, Wakefield M, Hutt K. Oocytes can efficiently repair DNA double-strand breaks to restore genetic integrity and protect offspring health. *Proc Natl Acad Sci U S A*. 2020;117(21):11513-11522. doi:10.1073/pnas.2001124117

100. Guo Y, Cao Z, Jiao X, et al. Pre-pregnancy exposure to fine particulate matter (PM2.5) increases reactive oxygen species production in oocytes and decrease litter size and weight in mice. *Environ Pollut*. 2021;268:115858. doi:10.1016/j.envpol.2020.115858

101. Zhan S, Zhang X, Cao S, Huang J. Benzo(a)pyrene disrupts mouse preimplantation embryo development. *Fertil Steril*. 2015;103(3):815-825. doi:10.1016/j.fertnstert.2014.11.013

102. Malott K, Luderer U. Toxicant Effects on Mammalian Oocyte Mitochondria. *Biol Reprod*. 2021:1-5.

103. Backer JM, Weinstein IB. Interaction of Benzo(a)pyrene and Its Dihydrodiol-Epoxide Derivative with Nuclear and Mitochondrial DNA in C3H10T/2 Cell Cultures. *Cancer Res*. 1982;42(7):2764-2769.

104. Wells PG, Mccallum GP, Chen CS, et al. Oxidative stress in developmental origins of disease:

Teratogenesis, neurodevelopmental deficits, and cancer. *Toxicol Sci*. 2009;108(1):4-18. doi:10.1093/toxsci/kfn263

105. Azzam EI, Jay-Gerin J-P, Pain D. Ionizing radiation-induced metabolic oxidative stress and prolonged cell injury. *Cancer Lett*. 2012;327(1):48-60. doi:10.1038/jid.2014.371

106. Kondraganti SR, Fernandez-Saluguero P, Gonzalez FJ, Ramos KS, Jiang W, Moorthy B. Polycyclic aromatic hydrocarbon-inducible DNA adducts: Evidence by 32P-postlabeling and use of knockout mice for AH receptor-independent mechanisms of metabolic activation in vivo. *Int J Cancer*. 2003;103(1):5-11. doi:10.1002/ijc.10784

107. Bansal S, Leu AN, Gonzalez FJ, et al. Mitochondrial targeting of cytochrome P450 (CYP)1B1 and its role in polycyclic aromatic hydrocarbon-induced mitochondrial dysfunction. *J Biol Chem*. 2014;289(14):9936-9951. doi:10.1074/jbc.M113.525659

108. Devine PJ, Perreault SD, Luderer U. Roles of Reactive Oxygen Species and Antioxidants in Ovarian Toxicity1. *Biol Reprod*. 2012;86(2):1-10. doi:10.1095/biolreprod.111.095224

109. Sui L, Nie J, Xiao P, et al. Maternal benzo[a]pyrene exposure is correlated with the meiotic arrest and quality deterioration of offspring oocytes in mice. *Reprod Toxicol*. 2020;93(July 2019):10-18. doi:10.1016/j.reprotox.2019.12.003

110. Luderer U, Myers MB, Banda M, McKim KL, Ortiz L, Parsons BL. Ovarian effects of prenatal exposure to benzo[a]pyrene: Roles of embryonic and maternal glutathione status. *Reprod Toxicol*. 2017;69:187-195. doi:10.1016/j.reprotox.2017.03.001

111. Lim J, Ramesh A, Shioda T, Parada KL, Luderer U. Sex Differences in Embryonic Gonad Transcriptomes and Benzo[a]pyrene Metabolite Levels After Transplacental Exposure. *Endocrinology*. 2022;163(1):1-17.

112. Polacek D, Beckmann MW, Schreiber JR. Rat ovarian apolipoprotein E: Localization and gonadotropic control of messenger RNA. *Biol Reprod*. 1992;46(1):65-72. doi:10.1095/biolreprod46.1.65

113. Nicosia M, Moger WH, Dyer CA, Prack MM, Williams DL. Apolipoprotein-E messenger RNA in rat ovary is expressed in theca and interstitial cells and presumptive macrophage, but not in granulosa cells. *Mol Endocrinol*. 1992;6(6):978-988. doi:10.1210/mend.6.6.1495495

114. Zhang T, Dai P, Cheng D, et al. Obesity occurring in apolipoprotein E-knockout mice has mild effects on fertility. *Reproduction*. 2014;147(2):141-151. doi:10.1530/REP-13-0470

115. Kendig EL, Chen Y, Krishan M, et al. Lipid Metabolism and body composition in Gclm(-/-) mice. *Toxicol Appl Pharmacol*. 2011;257(3):338-348. doi:10.1038/mp.2011.182.doi

116. Ortiz L, Nakamura B, Li X, Blumberg B, Luderer U. In Utero Exposure to Benzo[a]pyrene Increases Adiposity and Causes Hepatic Steatosis in Female Mice, and Glutathione Deficiency Is Protective. *Toxicol Lett*. 2013;223(2):1-7. doi:10.1038/jid.2014.371

117. Jurisicova A, Taniuchi A, Li H, et al. Maternal exposure to polycyclic aromatic hydrocarbons diminishes murine ovarian reserve via induction of Harakiri. 2007;117(12):3971-3978. doi:10.1172/JCI28493.ment

118. Kushnir VA, Ludaway T, Russ RB, Fields EJ, Koczor C, Lewis W. Reproductive aging is associated with decreased mitochondrial abundance and altered structure in murine oocytes. *J Assist Reprod Genet*. 2012;29(7):637-642. doi:10.1007/s10815-012-9771-5

119. Igarashi H, Takahashi T, Abe H, Nakano H, Nakajima O, Nagase S. Poor embryo development in post-ovulatory in vivo-aged mouse oocytes is associated with mitochondrial dysfunction, but mitochondrial transfer from somatic cells is not sufficient for rejuvenation. *Hum Reprod*. 2016;31(10):2331-2338. doi:10.1093/humrep/dew203

120. Myers M, Morgan FH, Liew SH, et al. PUMA regulates germ cell loss and primordial follicle endowment in mice. *Reproduction*. 2014;148(2):211-219. doi:10.1530/REP-13-0666

121. Liesa M, Shirihai OS. Mitochondrial dynamics in the regulation of nutrient utilization and energy expenditure. *Cell Metab*. 2013;17(4):491-506. doi:10.1016/j.cmet.2013.03.002

122. Luderer U, Lim J, Ortiz L, et al. Exposure to environmentally relevant concentrations of ambient fine particulate matter (PM2.5) depletes the ovarian follicle reserve and causes sex-dependent cardiovascular changes in apolipoprotein E null mice. *Part Fibre Toxicol*. 2022;19(1):1-21. doi:10.1186/s12989-021-00445-8

123. Malott KF, Reshel S, Ortiz L, Luderer U. Glutathione deficiency decreases lipid droplet stores and increases reactive oxygen species in mouse oocytes. *Biol Reprod*. 2022:1-14. doi:10.1093/biolre/ioac032

124. Zhang M, Miao Y, Chen Q, et al. BaP exposure causes oocyte meiotic arrest and fertilization failure to weaken female fertility. *FASEB J*. 2018;32(1):342-352. doi:10.1096/fj.201700514R

125. Dunning KR, Russell DL, Robker RL. Lipids and oocyte developmental competence: the role of fatty acids and β-oxidation. *Reproduction*. 2014;148(1):R15-R27. doi:10.1530/rep-13-0251

126. Dunning KR, Cashman K, Russell DL, Thompson JG, Norman RJ, Robker RL. Beta-Oxidation Is Essential for Mouse Oocyte Developmental Competence and Early Embryo Development1. *Biol Reprod*. 2010;83(6):909-918. doi:10.1095/biolreprod.110.084145

127. Harris SE, Leese HJ, Gosden RG, Picton HM. Pyruvate and oxygen consumption throughout the growth and development of murine oocytes. *Mol Reprod Dev*. 2009;76(3):231-238. doi:10.1002/mrd.20945

128. Dumollard R, Ward Z, Carroll J, Duchen MR. Regulation of redox metabolism in the mouse oocyte and embryo. *Development*. 2007;134(3):455-465. doi:10.1242/dev.02744

129. Ribas V, García-Ruiz C, Fernández-Checa JC. Glutathione and mitochondria. *Front Pharmacol*. 2014;5 (July):1-19. doi:10.3389/fphar.2014.00151